Ministério da
Ciência e Tecnologia

sid.inpe.br/mtc-m19/2011/01.26.18.00-TDI

ANALYTICAL ANALYSIS OF LIQUID FUEL COMBUSTION ESTABLISHED IN A LOW POROSITY MEDIUM

Max Akira Endo Kokubun

Master Thesis at Post-Graduation Course in Space Engineering and Technology/Combustion and Propulsion, advised by Dr. Fernando Fachini Filho, approved in February 23, 2011

URL of the original document:
<http://urlib.net/8JMKD3MGP7W/393Q562>

INPE
São José dos Campos
2011

PUBLISHED BY :

Instituto Nacional de Pesquisas Espaciais - INPE
Gabinete do Diretor (GB)
Serviço de Informação e Documentação (SID)
Caixa Postal 515 - CEP 12.245-970
São José dos Campos - SP - Brasil
Tel.:(012) 3208-6923/6921
Fax: (012) 3208-6919
E-mail: pubtc@sid.inpe.br

Ministério da
Ciência e Tecnologia

sid.inpe.br/mtc-m19/2011/01.26.18.00-TDI

ANALYTICAL ANALYSIS OF LIQUID FUEL COMBUSTION ESTABLISHED IN A LOW POROSITY MEDIUM

Max Akira Endo Kokubun

Master Thesis at Post-Graduation Course in Space Engineering and Technology/Combustion and Propulsion, advised by Dr. Fernando Fachini Filho, approved in February 23, 2011

URL of the original document:
<http://urlib.net/8JMKD3MGP7W/393Q562>

INPE
São José dos Campos
2011

Cataloging in Publication Data

Kokubun, Max Akira Endo.
K829a Analytical analysis of liquid fuel combustion established in a low porosity medium / Max Akira Endo Kokubun. – São José dos Campos : INPE, 2011.
xviii+117 p. ; (sid.inpe.br/mtc-m19/2011/01.26.18.00-TDI)

Dissertação (Mestrado Engenharia e Tecnologia Espaciais / Combustão e Propulsão) – Instituto Nacional de Pesquisas Espaciais, São José dos Campos, 2011.
Orientador : Dr. Fernando Fachini Filho.

1. Diffusion flame. 2. Liquid fuel. 3. Fluids mechanics. 4. Porous medium. I.Título.

CDU 662.75

Aprovado (a) pela Banca Examinadora em cumprimento ao requisito exigido para obtenção do Título de ***Mestre*** em

Engenharia e Tecnologia Espaciais/Combustão e Propulsão

Dr. Fernando Fachini Filho

Presidente / Orientador(a) / INPE / Cachoeira Paulista - SP

Dr. Jerônimo dos Santos Travelho

Membro da Banca / INPE / São José dos Campos - SP

Dr. Fernando Marcelo Pereira

Convidado(a) / UFRGS / Porto Alegre - RS

Aluno (a): ***Max Akira Endo Kokubun***

São José dos Campos, 23 de fevereiro de 2011

"When we are little kid, it seen that we are a little bit of everything: doctor, teacher, researcher... it feels that growing up is giving up on those things, one by one ".

Kevin Arnold

"It ain't about how hard you hit, it's about how hard you can get hit, and keep moving forward... It's how much you can take, and keep moving forward. That's how winning is done."

Rocky Balboa

ACKNOWLEDGEMENTS

Agradeço ao meu orientador, dr. Fachini, pela paciência e pelos conhecimentos passados e à Coordenação de Aperferfeiçoamento de Pessoal de Nível Superior (CAPES), pelo apoio financeiro durante os dois anos de desenvolvimento deste trabalho. Agradeço também ao Laboratório de Combustão e Propulsão (LCP) do Instituto Nacional de Pesquisas Espaciais (INPE), por toda a estrtutura disponibilizada para o desenvolvimento deste trabalho

ABSTRACT

In this work, an analytical analysis of the heat transfer, vaporization and burning of liquid fuels in porous media is performed. A low porosity inert medium, filled with a pool of a low volatile liquid fuel, was considered to be under the action of a hot oxidant stream. The main focus of this study is the fluid-dynamical aspects of the reacting flow in porous medium. Under such scope, the present dissertation was divided in three parts, with the aim of detailing the proposed problem. The first part consider a Hiemenz flow established inside a porous medium, under the hypothesis of intense interphase heat exchange: heat transfer regime. The heat provided to the system is delivered from a heated solid wall, located in the plane normal to the impinging flow. The second part consists in replacing the solid wall by a liquid surface that limits the semi-infinite porous medium filled with a low volatile liquid fuel from the semi-infinite porous medium filled with hot oxidant. Under the action of an impinging hot gas, an evaporative regime (heat transfer along with phase change) of the liquid fuel is established. The third and final part considers, after initiating the evaporative regime and providing flammability conditions, a stationary non-premixed combustion regime (diffusion flame) established inside the porous medium. The Schvab-Ze'ldovich formulation was performed in order to analyze the diffusion flame regime. In the three cases, the conservation equations were solved analytically by using the singular perturbation method. This method is based on the expansion of the solutions in terms of a small parameter, which arises from the existence of several characteristic length scales corresponding to several physical processes. The proposed analysis improved the physical understanding of the fluid-dynamical aspects of a reacting flow on the particular conditions of low porosity and low volatile liquid fuel taking place inside a porous inert medium. Besides, the results can be used as benchmark for direct numerical simulations of in-situ combustion and on the simplification of numerical codes.

ANÁLISE ANALÍTICA DA COMBUSTÃO DE COMBUSTÍVEIS LÍQUIDOS EM MEIOS DE BAIXA POROSIDADE

RESUMO

Neste trabalho é realizada uma análise analítica da transferência de calor, vaporização e queima de combustíveis líquidos em meios porosos. Um meio inerte de baixa porosidade, embebido por uma piscina de combustível líquido de baixa volatilidade é considerado sob a ação de jato de oxidante quente. O foco principal desse estudo são os aspectos fluido-dinâmicos do escoamento reativo dentro do meio poroso. Sob tal escopo, a presente dissertação foi dividida em três partes, com a finalidade de detalhar apropriadamente o problema proposto. Na primeira parte considera-se um escoamento de Hiemenz estabelecido dentro de um meio poroso, sob a hipótese da existência de uma intensa troca de calor inter-fásico: regime de transferência de calor. O calor fornecido ao sistema é proveniente de uma parede aquecida, localizada no plano normal ao jato impingente. Duas situações distintas foram analisadas: temperatura prescrita e um fluxo de calor prescrito. A segunda parte consistiu em substituir a parede sólida por uma superfície líquida, que limita o meio poroso semi-inifinito preenchido por um combustível líquido de baixa volatilidade do meio poroso semi-infinito preenchido pelo escoamento gasoso. Sob a ação do gás quente impingente, um regime de evaporação do combustível líquido (transferência de calor conjuntamente com mudança de fase) foi estabelecido. A terceira e última parte do trabalho foi considerar que após o regime de evaporação ser iniciado, e preenchida as condições de flamabilidade, um regime de chama difusiva estacionária foi estabelecido dentro do meio poroso inerte. A formulação de Schvab-Ze'ldovich foi conduzida para analizar o problema da chama difusiva. Nos três casos estudados, as equações de conservação foram resolvidas analiticamente por meio do método das perturbações singulares. Tal método é basedo na expansão das soluções em termos de um pequeno parâmetro, que emerge devido a existência de diferentes escalas espaciais características, correspondentes aos diferentes processos físicos que ocorrem no meio poroso. A análise proposta melhorou o entendimento físico dos aspectos fluido-dinâmicos de um escoamento reativo ocorrendo nas condições particulares de um meio de baixa porosidade e um combustível líquido de baixa volatilidade. Os resultados obtidos também podem ser usados como comparativos à simulações numéricas de processos de combustão *in-situ* e também na simplificação de códigos numéricos.

LIST OF FIGURES

Pág.

LIST OF SYMBOLS

Greek symbols

ρ	–	density
ε	–	solid phase porosity
$\bar{\lambda}$	–	thermal conductivity
μ	–	dynamic viscosity
ν	–	kinematic viscosity
θ	–	non-dimensional temperature
ϱ	–	non-dimensional density
κ	–	non-dimensional and modified permeability ($\equiv Ka/z_s^2$)
η	–	non-dimensional and modified spatial coordinate ($\equiv \varrho a^{1/2} z$)
Γ	–	thermal conductivities ratio ($\equiv \bar{\lambda}_s/\bar{\lambda}_g$)
β	–	permeability parameter of the order of unity
γ	–	porosity parameter ($\equiv (1-\varepsilon)/\varepsilon$)
Θ	–	temperature parameter ($\equiv \theta_0 - 1$)
τ	–	characteristic time

Latin symbols

F	–	Fuel
O	–	Oxidant
s	–	stoichiometric coefficient
P	–	combustion products
Q	–	heat (release or delivered)
$\bar{x}$	–	dimensional spatial coordinate
$\bar{z}$	–	dimensional spatial coordinate
$\bar{u}$	–	dimensional gas velocity
$\bar{v}$	–	dimensional velocity
$\bar{p}$	–	dimensional pressure
K	–	solid phase permeability
C_E	–	Ergun constant
Y	–	mass fraction
$\bar{D}$	–	mass diffusivity coefficient
$\bar{w}$	–	reaction rate
c_p	–	gas phase specific heat capacity
c_l	–	liquid phase specific heat capacity
T	–	temperature
h_g	–	gas-solid heat transfer coefficient
$\dot{q}_r$	–	radiant heat flux

$\dot{m}$	–	vaporization rate
h_l	–	liquid-solid heat transfer coefficient
$\bar{w}_F$	–	rate of conversion of fuel mass to product mass
z_s	–	characteristic length scale
L	–	liquid fuel latent heat of vaporization
$\bar{\dot{m}}$	–	liquid fuel vaporization rate
l	–	non-dimensional liquid fuel latent heat of vaporization
a	–	non-dimensional strain-rate
x	–	non-dimensional spatial coordinate
z	–	non-dimensional spatial coordinate
u	–	non-dimensional gas velocity
v	–	non-dimensional velocity
p	–	non-dimensional pressure
U	–	non-dimensional horizontal velocity
F	–	non-dimensional function of pressure gradient
f	–	non-dimensional and re-scaled vertical velocity/momentum
Pr	–	Prandtl number
Le	–	Lewis number
w	–	non-dimensional reaction rate
q	–	non-dimensional heat (released or delivered)
n	–	interphase heat transfer parameter of the order of unity
R	–	Gas specific constant

Subscripts

g	–	gas
l	–	liquid
s	–	solid
B	–	boiling
F	–	fuel
O	–	oxidant
∞	–	upper injection property
$-\infty$	–	lower injection property
0	–	property at the interface/wall
ts	–	thermal stagnation
f	–	flow
h	–	heat exchange

CONTENTS

Pág.

1 INTRODUCTION

In the present chapter, a brief overview of the main characteristics of combustion processes occurring inside a porous medium and some of its applications are exhibited. Then, the objectives of this work are stated and the structure of the dissertation is presented.

1.1 Combustion in porous medium: general properties and applications

Combustion phenomena established inside porous medium have been studied for decades (TAKENO; SATO, 1979; BEAR, 1988a; HANAMURA et al., 1993; HOWELL et al., 1996). Such interest may be explained by the large number of technologic and scientific problems which are still open in this area. The combustion process confined into a porous medium may be classified in three main types: (a) inert, (b) catalytic and (c) combustible (VAFAI, 2005). This classification, somewhat arbitrary, reflects the current potential of systems based in combustion in porous medium. The burning of wood, as in fire propagation in forests, is an example of combustible porous medium combustion, as the wood pyrolysis provides the required fuel, and the atmospheric air is the required oxidant. Chemical catalysts are used in thrusters, in order to achieve a more efficient burning of the propellant. Those catalysts are often used in packed beds geometries, in order to increase the superficial contact area with the injected propellant. Inert porous medium are very often utilized in the industry, also. As an example, it is possible to cite radiant porous burners. When hydrocarbons are burned inside a porous medium, the high temperature achieved, as a consequence of the exothermic chemical reaction, heats the solid matrix. The heated solid creates an intense radiative field.

Combustion processes confined in inert porous medium have some different characteristics than those observed in free combustion systems. These new characteristics are consequence of the combination of the thermophysical properties of the solid phase and gas/liquid phase found in porous systems: long range conduction, convection and radiation. The large contact area between solid and gas/liquid and the radiation field, created by the heated solid, contributes to improve the interphase heat transfer in these systems. Combustible gases flowing and reacting through the inert porous medium release heat. The amount of heat released is intimately coupled not only to the energy and mass transport in the gas phase but also to transport processes that occur in the solid phase. Under these new conditions, porous medium

flames exist far below the flammability limit for free flames (the term “free” is used to denote flames established outside of a porous medium).

One of the main features related to porous media confined combustion is the existence of a heat recirculation by the solid matrix from the hot region downstream to the cold region upstream the flame. This property is responsible for starting the heating process of the reactants prior to the their entrance in the gas-phase preheating zone (BARRA; ELLZEY, 2004; VAFAI, 2005; HANAMURA et al., 1993). The heat recirculation characteristic arise from the large value of heat conduction of solids, when compared to gases. It is worth to remark that the recirculation of heat provides an excess enthalpy at the flame, then, leading to a more efficient burning and even making it possible to burn very lean mixtures (LLOYD; WEINBERG, 1974; PEREIRA et al., 2010; TIERNEY et al., 2010). A schematic representation of the heat recirculation process in a premixed combustion is presented in Figure (1.1).

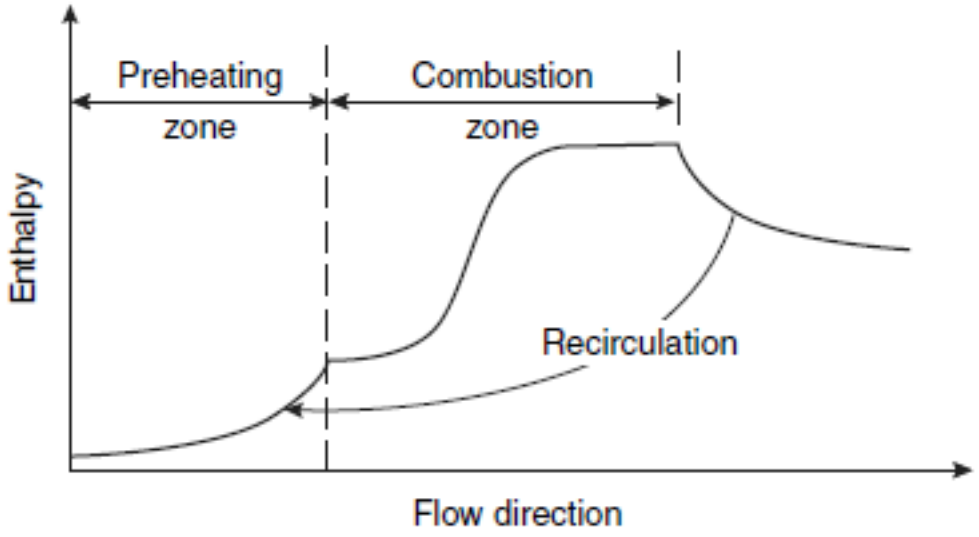

Figure 1.1 - Heat recirculation in combustion in porous medium
SOURCE: (VAFAI, 2005)

It is possible to visualize in Figure (1.1) the heat recirculated from the upstream to the downstream region of the flame, pre-heating the incoming fresh reactants. Heat

recirculation induced by the porous medium also may adds to the excess enthalpy released by the combustion, resulting in local temperatures higher than the adiabatic flame temperature. This process has been called superadiabatic combustion (ZHDANOK et al., 1995; PEREIRA et al., 2009).

Although the principle of heat recirculation is straightforward, the consequences of its application can be far reaching concerning the process efficiency, fuel conservation, combustion intensity, and pollutant emissions. Several studies in confined combustion have led to a series of technological development. Some examples are: compact industrial burners, radiant porous burners (for paper and wood drying, powder coating, plastic curing and forming and food baking (MUJEEBU et al., 2008; MUJEEBU et al., 2009; MUJEEBU et al., 2009; JUGJAI; PONGSAI, 2007)), lightning systems, and even fuel burners for a single piston internal combustion engine (OLIVEIRA; KAVIANY, 2001).

Not only restricted to industrial or fundamental issues, the study of porous medium combustion find a wide range of applications. The study of flammability limits and flame stability in forest fires are of great interest to society, for instance. Safety issues concerning the aerospace industry are of interest also, since solid propellants may also be studied under the scope of combustion in porous medium (TELENGATOR et al., 2006; TELENGATOR et al., 2000). If, by any reason, significant temperature changes occur during the storage of solid propellants, holes may develop due to the catalytic decomposition of the chemical compound. If the compounds reach ignition conditions, a deflagration wave, or, in limiting cases, even a detonation wave (BERNECKER; PRICE, 1982; KRIER; KEZERLE, 1979; BUTLER et al., 1982) may develop in the solid propellant.

Relevant studies and technological advances in the field of combustion in porous media are extensive and the reader may be referred to the literature in order to find specific analysis. Despite the examples described latter, the interest of this work is on the in-situ combustion applied to the heavy-oil thermal recovery (SARATHI, 1998; GOTTFRIED, 1968; BRANCH, 1979). In the next section this issue is presented.

1.2 In-situ combustion

Despite of the industrial use of combustion confined in man-manufactured porous media, the combustion can be observed in natural porous media. One with major

economic and strategic importance is the in-situ combustion used as an oil thermal recovery method. Petroleum is still the most important and utilized source of energy of the society. Since it is a non-renewable energy its exploration must be made the most efficient as possible. Analytical, numerical and experimental studies are necessary in order to fully understand the dynamics of this thermal recovery method, and hence, improve it. Heavy oils are hard to recover due to its high viscosity and, very often, high amount of impurities. In-situ combustion is the oil recovery method that consists in burning part of the fuel inside the well. The heat released by the exothermic reaction increases the temperature inside the well and the consequence is the diminishment of the oil viscosity. Also the heat released produces an increase of the pressure by the thermal expansion that, together with the reduction of the viscosity, augments the oil mobility which helps the extraction.

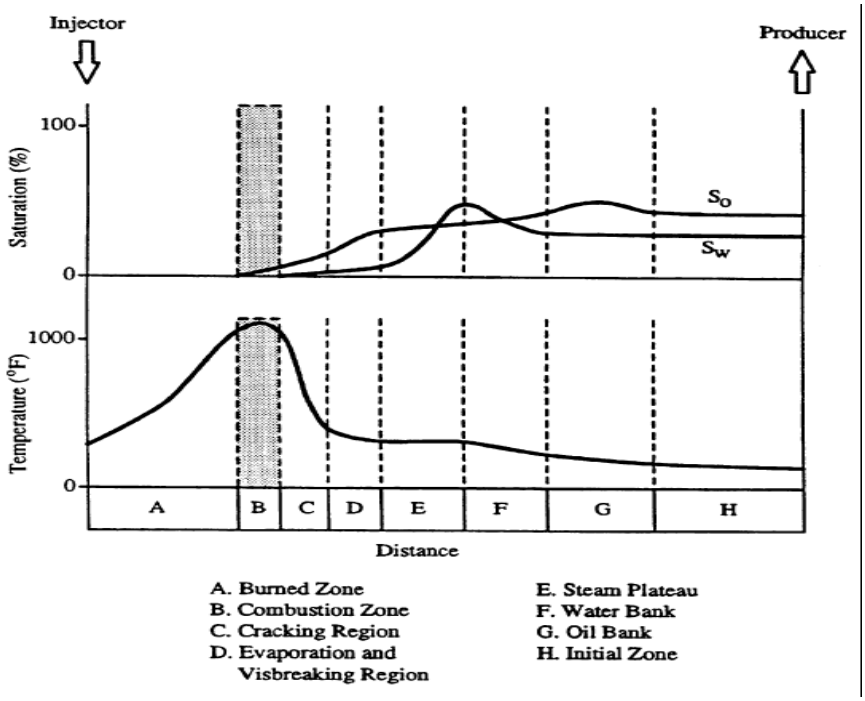

Figure 1.2 - Schematic diagram of forward in-situ combustion
SOURCE: (WU; FULTON, 1971)

Basically there are two types of in-situ combustion: dry, or wet. In the dry combustion, only the gaseous oxidant is injected in the well, while in the wet combustion, water is added within the oxidant stream. In the present work, only dry combustion

is considered. In this process, the gaseous oxidant (usually air) is pump into the well for a few days and ignites the fuel-oxidant mixture. When the combustion is established, it is sustained by a continuous oxidant flow. As the front propagates, one can find several zones between the injection site and the producer site, due to heat and mass transport and chemical reactions occurring in the process (CASTANIER; BRIGHAM, 2003). Ranging from the injection site to the producer site, it is possible to identify seven different zones: burned zone, combustion zone, cracking/vaporization and visbreaking (viscosity lowering) region, steam plateau, water bank, oil bank and initial zone. A schematic representation of these zones is shown in Figure (1.2), in which the temperature and fluid saturation distribution in each zone is shown. It is seen the locations of the various zones and temperature and fluid saturation distributions. In the field, there are transitions between zones, which are not exhibited in the idealized Figure (1.2).

The burned zone contains the already burned fuel. This region is filled with air and may contain small amounts of residual unburned organic solids. In this zone, there is no oil left. The combustion zone is the region of highest temperature, in which the oxidation (combustion) of the fuel takes place. The fuel is formed in the thermal cracking zone just ahead of the front and is the product of cracking and pyrolysis, which is deposited on the rock matrix. It must be noted that the burned fuel is the heaviest part of the oil. The cracking/vaporization zone is located downstream to the combustion front. The oil remaining in this zone is the residual oil left behind the steam plateau. The crude oil is modified in this zone by the high temperature of the combustion process. The light species vaporize and are transported downstream where they condense and mix with the original crude. The heavy species pyrolyse, resulting in hydrocarbon gases and solid organic fuel being deposited on the rock. The steam plateau is next downstream. Most of the oil is displaced ahead of the steam. The immobile oil undergoes steam distillation. Further downstream, in low temperature zone, some of the hydrocarbon vapors condense. At the leading edge of the steam plateau, the temperature is less than steam saturation temperature, and a water bank is formed that decreases in temperature and saturation as we look downstream, with a resulting increase in oil saturation. Beyond the water bank (zone) the oil bank zone is found, which contains most of the oil displaced from upstream, including most of the light ends that resulted from the thermal cracking upstream. Finally, after the oil bank zone, lays the undisturbed original reservoir. Gas saturation will only increase slightly in this region because of the high mobility

of combustion gases. The production mechanism in this region is gas drive from the combustion products.

The combustion front propagates in the well and the exothermic reaction is responsible for an increasing in the well temperature, hence, lowering the heavy-oil viscosity. There are others thermal recovery methods, such as steam injection (ARNOLD, 1989; BABADAGLI; AL-BEMANI, 2007; JABBOUR et al., 1996; PRATS, 2003), that also induces a lowering in the oil viscosity. However, the advantages of in-situ combustion relies mainly on the fact that the heat is generated inside the well, lowering heat losses to the well along the injection. The in-situ combustion process is complex and its understanding involves a series of concepts from different scientific areas, ranging from geology, hydrology, chemistry and thermal sciences, such as combustion. A deep understanding of the physical process for the the in-situ combustion recovery method is valuable not only for academia, but for the global economy, since the successful application of the in-situ combustion in a heavy-oil and already explored reservoirs will represent a new vision for the petroleum as a energy source.

Some effort has been made in order to study the structure of the propagating combustion front, specially when it comes to conditions to sustain the stable flame (AKKUTLU; YORTSOS, 2003). The usual approach of analysis is consider the large-scale well dimension processes, because the front inside the reservoir has the well dimension (CASTANIER; BRIGHAM, 2003), that may range from hundreds of meters to kilometers of extension. However, like free flames, they are also controlled by small-scale (porous dimension, gas heat transport length scale and solid heat transport length scale) processes. Therefore, the fully understanding of the effects of these small-scale processes on the in-situ combustion is vital not only for the fundamental knowledge but also to provide correct physical (sub-grid) models to be used in simulations of well conditions by numerical codes.

The in-situ combustion, as one can observe, is a complex phenomenon, and a complete description of the entire process is not the objective of this work. The present work intends to analyze the combustion front zone under simplifying assumptions that will be stated next.

1.3 Objectives

In order to analyze the small-scale processes for the combustion of a heavy liquid fuel inside a porous medium (with particular emphasis on the in-situ combustion), the present work extend the use of a turbulent combustion tool (flamelet) to study the propagation of a combustion front inside an oil reservoir. The flamelet theory was born in the context of the study of turbulent combustion, and basically consists in "breaking" the turbulent propagating flame into small pieces, and studying one of these small flame elements, and hence avoiding the complex geometry of the turbulent flame front (LIBBY; WILLIAMS, 1982; POINSOT; VEYNANTE, 2005). By utilizing the flamelet approach, it is possible to focus on the local flame state and also examine conditions to sustain the flame front. Figure (1.3) presents a representative scheme showing the idea behind the flamelet theory.

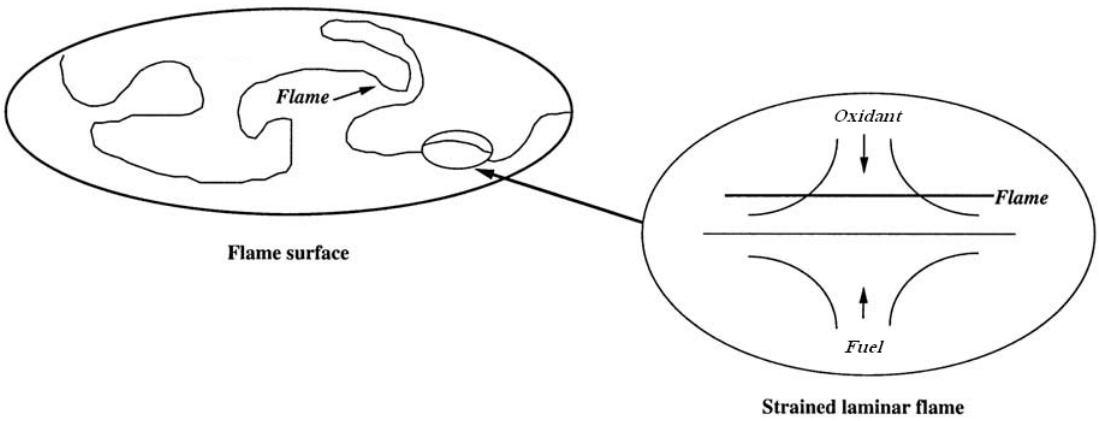

Figure 1.3 - Turbulent flame element
SOURCE: (VEYNANTE; VERVISCH, 2002)

Under the scope of the flamelet theory, the study of a turbulent flame summarizes into analyzing a simpler configuration, the counterflow flame. The counterflow flame structure was studied initially by Liñan (LIÑAN, 1974) and extended by Peters (PETERS, 1984), who utilized the asymptotic theory in order to analyze the structure

of a diffusion flame under the flamelet approach and analyzing the fluid-dynamical aspects of the combustion process.

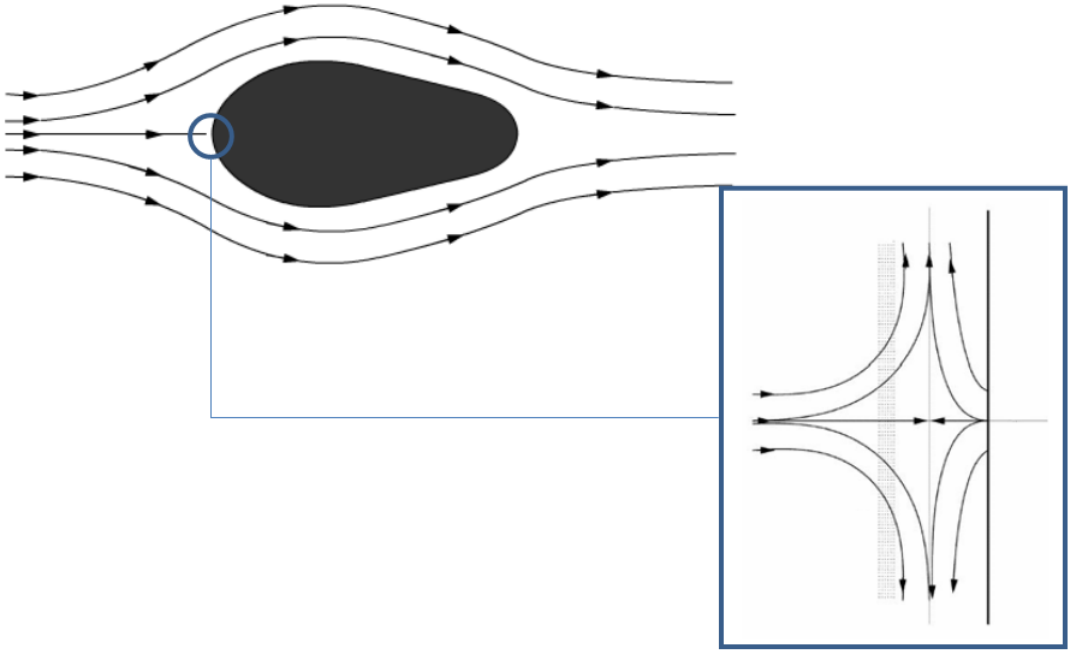

Figure 1.4 - Local analysis of an oil well

It is possible to apply the idea of the flamelet analysis in order to study the combustion front inside a oil reservoir (or, more generically, inside a porous medium). When the injected oxidant encounter a heavy-oil pool inside the well, a local (flamelet) analysis may be performed at the vicinity of the stagnation-point. The proposed analysis is presented schematically in Figure (1.4).

The study of the stagnation-point region is important, since ignition and extinction of the flame occur firstly in this region (NIIOKA; WILLIAMS, 1977; KRISHNAMURTHY, 1976; CHAO et al., 1996; ALKIDAS; DURBETAKI, 1973; SHARMA; SIRIGNANO, 1969).

The study of the proposed geometry provides a starting-point for a throughout analysis of the features of the liquid fuel combustion inside a porous medium, with a primary focus on the in-situ combustion process.

In order to perform an detailed analysis for the problem, the present work is di-

vided in three parts. In the first part, it is analyzed a Hiemenz flow (HIEMENZ, 1911) established inside a porous medium with a heated wall at the stagnation point. In the second one, a stream of a hot oxidant impinging into a pool of liquid fuel (Hiemenz flow with phase change) is studied. In this situation, an evaporative regime is established inside the porous medium. The third and final part consider the establishment of the diffusion flame itself, in the Burke-Schumann limit, such that the reaction rate is considered infinitely fast. The proposed approach of dividing the problem into three parts is made in order to obtain a greater level of detail of such system. In addition, the understanding and solution of the first part help the understanding and solution of the second part and also to the third, the most complex part, as will be seen next.

2 GENERAL MATHEMATICAL FORMULATION

The mathematical formulation of the proposed problem is presented in this chapter. It must be pointed that the mathematical formulations for the three related cases studied are very similar, differing mainly on (but not restricted to) the boundary conditions.

The homogeneous combustion is an exothermic reaction flow. The chemical reactions take place in the gas phase, between a fuel and an oxidant, in the interior of the flow. They are result from the inelastic collisions between the reactant molecules. If the fuel is in a liquid phase (or in a solid phase), the chemical reaction must be preceded by the vaporization of the fuel (or gasification, in the solid fuel case). After the vaporization takes place, the gaseous fuel mixes with the gaseous oxidant by means of molecular diffusion, intensified by convection. The thermal energy generated during the chemical reaction is transported through convection, conduction and radiation, from the reaction zone to the whole flow field. It is worth to mention the case in which the chemical reactions proceed between one reactant in gaseous phase and another reactant in solid phase, the solid burning, namely heterogeneous combustion

The present work analyzes the problem of the combustion of heavy liquid fuel inside a low porosity medium under the scope of the fluid-dynamical aspects. The reacting flow conservation equations - continuity, Navier-Stokes, energy and species conservation equations - are utilized, considering the energy source and the mass sink terms in the governing equations. An excellent review about the importance of the fluid-dynamical analysis for the combustion science may be found somewhere (LIÑAN, 1991).

It must be observed that the proposed study is a coupled three-phase problem, such that the interactions between gas-solid phases and liquid-solid phases must be considered in the mathematical formulation. The considered geometry is established by an impinging flow, as given by Figure (2.1). An infinite solid matrix is considered in order to avoid boundary effects. Injection conditions are then considered from far upstream and far downstream from the gas-liquid interface. The proposed geometry gives to the analysis of the problem a local character. The local analysis focuses on the region close to the stagnation-point of the impinging flow. Figure (2.1) represents schematically the combustion problem of an oil pool close to the stagnation-point: flamelet.

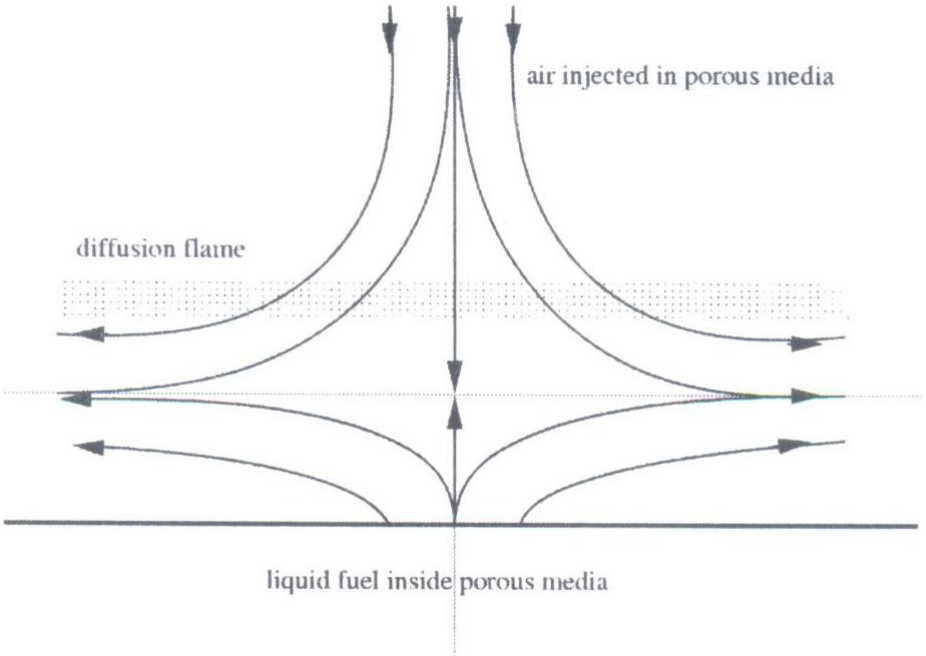

Figure 2.1 - Liquid fuel combustion in porous medium.

Based on Hiemenz's pioneer work on the stagnation-point flow (HIEMENZ, 1911), a non-dimensionalization procedure is performed, followed by a variable transformation, in order to transform the partial differential equations into ordinary differential equations.

The combustion process is accounted in the model as a single-step global chemical reaction, following the general formula:

$$F + sO \rightarrow (1+s)P + Q\,(\equiv \text{heat released}) \tag{2.1}$$

in which s mass unities of oxidant (O) are consumed for each mass unity of fuel (F), generating $(1+s)$ mass unities of products (P) and releasing an amount (Q) of heat in the exothermic process.

2.1 Governing equations

As mentioned previously, the proposed problem is a three-phases coupled analysis. The analyzed geometry is an impinging flow, such that the problem is divided in two main regions, separated by the gas-liquid interface: gas (oxidant + fuel) filling

the porous (gas-solid region) and liquid (fuel) filling the porous (liquid-solid region). Two spatial coordinates are considered, $\bar{x}$ as the coordinate tangential to the liquid surface, and $\bar{z}$ as the coordinate normal to the liquid interface. The coordinate system is chosen in such a way that the gas-liquid interface is located at $\bar{z} = 0$. The boundary-layer approximation is utilized, leading to variables that depend only on $\bar{z}$ coordinate. This approximation arises from the assumption that variations normal to the interface are more intense than variations tangential to the interface.

The assumptions made in order to build the mathematical model for the proposed problem are the following:

- Stationary flow;
- 1D flow in the liquid-solid region;
- 2D flow in the gas-solid region;
- Body forces neglected;
- Low porosity and inert solid matrix;
- Intense interphase heat transfer;
- Low volatile fuel;
- Negligible gas thermal expansion;
- Constant thermal-physical properties;

The conservation equations are volume-averaged over a representative elementary volume (BEAR, 1988b). This volume-averaging procedure is necessary in order to avoid statistical fluctuations resultant from a pore-scale analysis.

The governing equations for the gas phase, above $\bar{z} = 0$, are presented in the following in their differential form. The volume average notation is neglected in order to simplify the equations.

First, the mass conservation equation:

$$\rho\frac{\partial\bar{u}}{\partial\bar{x}} + \rho\frac{\partial\bar{v}}{\partial\bar{z}} = 0, \tag{2.2}$$

The momentum conservation equation must take into account some effects of the porous medium and it has several different versions, depending on the authors and assumptions made. The version utilized in the present work follows the work of Vafai

and Tien (VAFAI; TIEN, 1981) (in its stationary form and neglecting the body forces term), as:

$$\frac{\rho}{\varepsilon}\vec{u}.\nabla\vec{u} = -\nabla p + \underbrace{\frac{\mu}{\varepsilon}\nabla^2\vec{u}} - \underbrace{\frac{\mu}{K}\vec{u}} - \underbrace{\frac{C_E}{K^{1/2}}\rho|\vec{u}|\vec{u}} \tag{2.3}$$

in which the terms highlighted are, respectively, the Brinkman term (takes into account the macroscopic shear-stress diffusion), the Darcy term (takes into account the microscopic shear-stress) and the Ergun term (takes into account the microscopic inertial forces, C_E is a constant). The Ergun term may be viewed as a correction of the order of $K^{1/2}$ of the Darcy term, and in the present work will be neglected.

Hence, the two conservation equations for the momentum are given by:

$$\rho\bar{u}\frac{\partial\bar{u}}{\partial\bar{x}} + \rho\bar{v}\frac{\partial\bar{u}}{\partial\bar{z}} = -\varepsilon\frac{\partial\bar{p}}{\partial\bar{x}} + \bar{\mu}\frac{\partial^2\bar{u}}{\partial\bar{z}^2} - \varepsilon\bar{\mu}\frac{\bar{u}}{K}, \tag{2.4}$$

$$\rho\bar{u}\frac{\partial\bar{v}}{\partial\bar{x}} + \rho\bar{v}\frac{\partial\bar{v}}{\partial\bar{z}} = -\varepsilon\frac{\partial\bar{p}}{\partial\bar{z}} + \bar{\mu}\frac{\partial^2\bar{v}}{\partial\bar{z}^2} - \varepsilon\bar{\mu}\frac{\bar{v}}{K}, \tag{2.5}$$

in which ε is the solid matrix porosity, and it is given by the volume occupied by the pores divided by the total volume (pores + solid matrix). It ranges from 0 to 1 and it can be thought as the "void" volume.

The Darcy term, that appears in the two above equations, takes into account the resistance against the flow due to the existence of the tortuous channels of the porous matrix.

The species conservation equations (for gaseous fuel and oxidant, respectively) are given by:

$$\varepsilon\rho\bar{v}\frac{\partial Y_F}{\partial\bar{z}} = \varepsilon\rho\bar{D}_F\frac{\partial^2 Y_F}{\partial\bar{z}^2} - \varepsilon\bar{w}_F, \tag{2.6}$$

$$\varepsilon\rho\bar{v}\frac{\partial Y_O}{\partial\bar{z}} = \varepsilon\rho\bar{D}_O\frac{\partial^2 Y_O}{\partial\bar{z}^2} - \varepsilon s\bar{w}_F. \tag{2.7}$$

It is possible to observe a mass sink term for both species, arising from the strong non-linear reaction rate term, $\bar{w}_F$, that measures the consumption/production of species at the flame. The chemical reaction is performed stoichiometrically, for each unity of fuel mass consumed, s unities of oxidant mass are consumed, according to Equation (2.1). Such term follows the Arrhenius type reaction term and it is not detailed, because in the process of solving such equations it will be eliminated through the Schvab-Ze'ldovich procedure (FACHINI, 2007; FACHINI, 1999; LIÑAN;

WILLIAMS, 1993).

The energy conservation for the gas phase is given by:

$$\varepsilon\rho\bar{v}c_p\frac{\partial T_g}{\partial \bar{z}} = \varepsilon\bar{\lambda}_g\frac{\partial^2 T_g}{\partial \bar{z}^2} + \varepsilon Q\bar{w}_F + h_g(T_s - T_g), \tag{2.8}$$

from which is possible to note the existence of a heat source due to the exothermic chemical reaction between gaseous fuel and hot oxidant. The combustion process releases a amount Q of heat in the ambient, as given by Equation (2.1).

In the gas-solid region (in which the gas flow fills the semi-infinite porous medium), the energy conservation for the solid matrix is governed by the following differential equation:

$$0 = (1-\varepsilon)\bar{\lambda}_s\frac{d^2 T_s}{d\bar{z}^2} - h_g(T_s - T_g) \tag{2.9}$$

It is worth to note that the two-phase energy problem is coupled through the interphase heat transfer, due to temperature differences between gas and solid. This heat transfer, assumed to be intense, is quantified by the volumetric convection heat transfer coefficient, h_g, and it is directly proportional to the temperature difference between phases.

It must be noted that since the considered problem deals with thermal non-equilibrium, there may be temperature differences between phases. When a solid is heated, the radiation field must be considered, since it reaches longer distances when compared to heat diffusion in the solid matrix. In a rigorous way, this term should be included by a radiant heat flux, $\dot{q}_r$. Note that under such assumption, the solid matrix becomes a participating medium, absorbing and scattering radiation. However, when an optically thick medium is considered (usually for small pores mediums, which is the case of the proposed problem), a diffusion approximation can be used. In this approximation, namely the Rosseland approximation (SIEGEL; HOWELL, 1992; KAVIANY; SINGH, 1993), the radiant heat flux is assumed to be dependent on the local temperature gradient only, in such a way it is possible to obtain an effective radiant conductivity of the solid-phase, hence, the radiant heat flux is absorbed as an improved thermal conductivity.

Below the gas-liquid interface, $\bar{z} = 0$ the porous medium is filled with the low volatile liquid fuel. The governing equations for the liquid fuel in this region are given by:

$$\rho_l \bar{v}_l = \bar{\dot{m}}, \tag{2.10}$$

$$\varepsilon \rho_l \bar{v}_l c_l \frac{dT_l}{d\bar{z}} = \varepsilon \bar{\lambda}_l \frac{d^2 T_l}{d\bar{z}^2} + h_l (T_s - T_l), \tag{2.11}$$

in which $\bar{\dot{m}}$ is the vaporization rate, considered to be independent on the spatial coordinates.

The energy conservation for the solid matrix below $\bar{z} = 0$ follows energy conservation by means of the differential equation given by:

$$0 = (1 - \varepsilon) \bar{\lambda}_s \frac{d^2 T_s}{d\bar{z}^2} - h_l (T_s - T_l), \tag{2.12}$$

The temperature difference between phases (last term in the right side) couples the liquid-solid problem by the interphase heat transfer coefficient, h_l, that is assumed to be constant and intense.

The presented set of governing equations provide the basis for the mathematical model for the combustion of the heavy liquid fuel inside the low porosity inert medium.

2.2 Length scales

It must be pointed out that the solid matrix interacts directly with the combustion process. The flame is a heat source, that provides energy to the gas flow and also to the porous medium. The provided heat is transported to both streams, of the incoming oxidant and gaseous fuel and also to the liquid fuel. The solid matrix is able to "carry" the heat farther than the gas, due to its high thermal conductivity. By considering the effective solid thermal conductivity (the Rosseland approximation) the heat transport reaches a region whose thickness is several orders of magnitude larger than that controlled by the gas heat transfer. As a result, it is observed effects that occur in the length scale of the solid phase heat conduction, and effects that occur in the length scale of the gas phase heat conduction.

The existence of physical processes occurring at different length scales requires a care in order to perform a proper analysis of the system.

2.3 Non-dimensionalization and variable change

The provided set of governing equations in Section (2.1) is the basis of the mathematical model for the proposed problem. In order to perform an universal analysis, the variables are made non-dimensional, and then, in order to transform the partial differential equations into ordinary differential equations, easier to handle, a variable transformation is proposed (SCHLICHTING, 1968; FACHINI, 2007), following the original work by Hiemenz (HIEMENZ, 1911), but with modifications that deals with the existence of the porous matrix.

2.3.1 Non-dimensional variables

The following non-dimensional variables: $u \equiv \bar{u}/\bar{v}_\infty$, $v \equiv \bar{v}/\bar{v}_\infty$,$v_l \equiv \bar{v}_l/\bar{v}_\infty$, $\varrho \equiv \rho/\rho_\infty$, $\varrho_l \equiv \rho_l/\rho_\infty$, $p \equiv \bar{p}/(\rho_\infty v_\infty^2)$, $x \equiv \bar{x}/z_s$, $z \equiv \bar{z}/z_s$, $\theta_g \equiv T_g/T_\infty$, $\theta_s \equiv T_s/T_\infty$, $\theta_l \equiv T_l/T_\infty$, $y_O \equiv Y_O/Y_{O\infty}$ and $y_F \equiv Y_F$ are used in this work. The non-dimensional strain-rate is defined as: $a \equiv (z_s/\bar{v}_\infty)d\bar{u}/d\bar{x}|_\infty$. The strain-rate is the gradient of the incoming horizontal velocity component. Close to the stagnation point the gradient of the velocity component is large indicating that the flow is deflecting.

It must be noted that all spatial variables are normalized by a characteristic length scale defined as $z_s \equiv \bar{\lambda}_s/(\rho_\infty c_p \bar{v}_\infty)$. Such length scale may be referred as a characteristic solid conduction length, relating to the solid matrix thermal conductivity.

2.3.2 Variable change: local analysis

The idea of the proposed problem is to study the impinging flow configuration at the vicinity of the stagnation-point. In order to perform such local analysis, a variable change is chosen following Hiemenz's work on the study of the stagnation-point flow (HIEMENZ, 1911). However, the transformations are modified in order to assimilate the existence of the porous medium.

The transformations are given by (SCHLICHTING, 1968; FACHINI, 2007):

$$u = a\ x\ U(z), \quad \varrho\ v = -a^{1/2} f,$$
$$p_0 - p = \frac{1}{2} Pr\ a^2 \left(1 + \frac{1}{\kappa\Gamma}\right)\left[x^2 + \frac{2F(z)}{a}\right], \quad \eta = a^{1/2}\varrho\ z \tag{2.13}$$

in which $Pr \equiv \nu/\alpha$ is the Prandtl number, $\kappa \equiv aK/z_s^2$ is the porous medium non-

dimensional permeability and $\Gamma \equiv \bar{\lambda}_s/\bar{\lambda}_g$ is the ratio between solid and gas thermal conductivities. This ratio is high, such that the condition $\Gamma \gg 1$ is satisfied.

It also must be remembered that the boundary-layer approximation is applied to all dependent variables, in such a way that the variations in $\bar{z}$ are much more significant than the variations in $\bar{x}$.

The pressure expression was modified from the classical Hiemenz's transformations (HIEMENZ, 1911) in such a way that for low porosities media ($\varepsilon \ll 1$ and $\kappa \sim 0$) the non-dimensional Darcy equation is obtained, while for high porosities media ($\varepsilon \sim 1$ and $\kappa \to +\infty$), the original equation obtained by Hiemenz is recovered (HIEMENZ, 1911). The proposed transformations decouple the dependence of the variables on the $\bar{x}$ and $\bar{z}$ spatial coordinates.

2.4 Non-dimensional equations, parameters and mathematical method

The non-dimensional equations for the gas-solid region are given by:

$$U = \frac{df}{d\eta}, \tag{2.14}$$

$$\frac{Pr}{\Gamma}\frac{d^3f}{d\eta^3} + f\frac{df^2}{d\eta^2} - \left(\frac{df}{d\eta}\right)^2 - \varepsilon Pr\frac{1}{\kappa\Gamma}\frac{df}{d\eta} = -\varepsilon Pr\left(1 + \frac{1}{\kappa\Gamma}\right), \tag{2.15}$$

$$\frac{Pr}{\Gamma}\frac{d^2f}{d\eta^2} + f\frac{df}{d\eta} - \Gamma\varepsilon\beta Prf = \varepsilon Pr\left(1 + \beta\Gamma\right)\frac{dF}{d\eta}, \tag{2.16}$$

$$\frac{1}{\Gamma}\frac{d^2y_f}{d\eta^2} + Le_F f\frac{dy_f}{d\eta} = Le_F\frac{w_F}{a}, \tag{2.17}$$

$$\frac{1}{\Gamma}\frac{d^2y_O}{d\eta^2} + Le_O f\frac{dy_O}{d\eta} = S\ Le_F\frac{w_F}{a}, \tag{2.18}$$

$$0 = \frac{\varepsilon}{\Gamma}\frac{d^2\theta_g}{d\eta^2} + \varepsilon f\frac{d\theta_g}{d\eta} + \varepsilon q\frac{w_F}{a} + N_g(\theta_s - \theta_g), \tag{2.19}$$

$$0 = (1-\varepsilon)\frac{d^2\theta_s}{d\eta^2} - N_g(\theta_s - \theta_g), \tag{2.20}$$

in which $Pr \equiv \nu/\alpha_g$ is the Prandtl number, $Le_i \equiv \alpha_g/D_i$ is the $i-$specie Lewis number, $w_F \equiv \bar{w}_F z_s/\left(\rho_\infty \bar{v}_\infty\right)$ is the non-dimensional reaction rate, $S \equiv \left(s/Y_{O\infty}\right) Le_O/Le_F$ is the stoichiometric coefficient and $q \equiv Q/(c_p T_\infty)$ is the non-dimensional heat released.

While for the liquid-solid region the conservation equations are:

$$\varrho_l v_l = \dot{m} \tag{2.21}$$

$$\varepsilon J \frac{d^2\theta_l}{dz^2} - \varepsilon M \frac{d\theta_l}{dz} = -N_l(\theta_s - \theta_l), \tag{2.22}$$

$$(1-\varepsilon)\frac{d^2\theta_s}{dz^2} = N_l(\theta_s - \theta_l), \tag{2.23}$$

in which $\dot{m} \equiv \bar{\dot{m}}/\left(\rho_\infty \bar{v}_\infty\right)$, $M \equiv \dot{m}(c_l/c_p)$ and $J \equiv \bar{\lambda}_l/\bar{\lambda}_s$.

The idea of turning the governing equations into their non-dimensional form is made in order to universalize the analysis. The price to be paid is the appearing of some non-dimensional parameters. For instance, the Reynolds number emerges from the non-dimensional form of the Navier-Stokes equation, and its magnitude is related to the determination if a flow is viscous or non-viscous.

In the present work, five non-dimensional parameters arises from the non-dimensionalization procedure: κ, the non-dimensional and transformed medium permeability, that compares two distinct boundary layers, as will be seen in Chapter (3), N_g, the non-dimensional form of h_g (heat transfer coefficient between gas and solid), N_l, the non-dimensional form of h_l (heat transfer coefficient between liquid and solid), Γ, the ratio between solid and gas phase thermal conductivities, and l, the non-dimensional liquid fuel latent heat of vaporization (not shown yet). The first three parameters depend on the geometric properties of the porous matrix and on the interactions between solid and gas phase and solid and liquid fuel, while the fourth is dependent on the ratio between solid and gas thermal conductivities and l is dependent on the liquid fuel thermal-physical properties. Even though the five of them are not fixed, Γ is known to be high and, hence, it appears as a large parameter in the governing equations. This fact ($\Gamma \gg 1$) motivates to seek solutions by means of the singular perturbation method (HOLMES, 1995; NAYFEH, 1981).

Motivated by the fact that the order of magnitude of Γ is known, the other four parameters are chosen to be proportional to it, with the aim of analyzing the distinguished limit of $\Gamma \gg 1$. Under such hypothesis, they are expressed as:

$$\frac{N_g}{a} = O(\Gamma) \Rightarrow \frac{N_g}{a} = n_g\,\Gamma, \quad N_l = O(\Gamma^2) \Rightarrow N_l = n_l\,\Gamma^2,$$

$$\kappa = O(\Gamma^{-2}) \Rightarrow \kappa = \beta^{-1}\Gamma^{-2}, \quad l = O(\Gamma) \Rightarrow l = \tilde{l}\,\Gamma, \tag{2.24}$$

in which β, n_l, n_g and $\tilde{l}$ are parameters of the order of unity. It can be noted that N_g, N_l and l are chosen to be high, while the permeability κ is chosen to be low, since $\Gamma \gg 1$, in such a way that the assumptions made in the beginning of this chapter are promptly respected (high rates of interphase heat transfer, low porosity medium, and consequently low permeability medium, and low-volatile liquid fuel).

Under those assumptions, the non-dimensional equations will present the large parameter Γ in their formulation. This will allow us to perform the perturbation method in order to seek solutions for the desired variables.

It is worth to note that the choices of $N_g = O(\Gamma)$, $N_l = O(\Gamma^2)$ and $\kappa = O(\Gamma^{-2})$, are not restricted to, respectively, high rates of interphase heat transfer and low permeability medium. These non-dimensional parameters are given by:

$$N_g \equiv \frac{\bar{\lambda}_s h_g}{\left(\rho_\infty c_p \bar{v}_\infty\right)^2}\ , \quad N_l \equiv \frac{\bar{\lambda}_s h_l}{\left(\rho_\infty c_p \bar{v}_\infty\right)^2}\ , \quad \kappa \equiv \frac{aK}{z_s^2} = K\frac{a\left(\rho_\infty c_p \bar{v}_\infty\right)}{\bar{\lambda}_s^2}. \tag{2.25}$$

Even though N_g, N_l and κ are directly proportional to the gas-solid heat transfer, liquid-solid heat transfer and solid matrix permeability, respectively, their order of magnitude, as assumed in this work, can be accomplished by choosing, for example, a low velocity of oxidant injection ($\bar{v}_\infty$).

Another interesting feature is the non-dimensional parameter κ. This parameter, that emerges from the non-dimensional procedure, gathers information from the transport phenomena in gas and solid phases, as seen in Equation (2.25). It also determines the flow field, as will be seen in Chapter (3).

3 HIEMENZ FLOW IN POROUS MEDIUM WITH HEAT EXCHANGE

In this chapter, a Hiemenz flow established inside a semi-infinite low porosity medium with heat exchange is analyzed analytically. Heat is supplied to the system through two different wall conditions: a constant wall temperature, and a constant wall heat flux. Local thermal non-equilibrium is considered, and the two-equation model is used to consider heat exchange between gas and solid phases. The flow is analyzed through a non-Darcian model, in which viscous and convective terms are considered in the Darcy pressure equation. An extension of the pressure expression on the classical variable change is chosen in a such way that for a very large permeability the model is able to recover the equations for the Hiemenz flow, and for the particular case of a very small permeability, as described by the Darcy flow. Then, the perturbation method is used, and one is able to obtain an approximate analytical temperature and velocity profiles for the flowing gas, and temperature profile for the porous medium. Two distinct length scales are recognized: one corresponding to the porous medium thermal conductivity and the other one corresponding to the gas thermal conductivity. In this analysis, only the case of a low porosity medium is studied, but a wide range of the space parameter can be explored. The results obtained point out the importance of the inner zone (close to the wall) analysis in the case of a constant wall heat flux. From the analysis, a new dimensionless parameter, κ, emerges, which gathers information of the transport phenomena in gas and solid phases, and it is responsible to determine the flow field. The results also show that, although the porous medium is the main agent responsible for removing conductively the heat from the wall, the gas flow plays convectively an important role in the heat dissipation.

3.1 Introduction

The interest on flows inside porous media has grown considerably in the last decades, since this geometry arises in many different systems, ranging from natural to man-manufactured technological ones. Oil wells, underground aquifers, chemical catalysts and wood are some examples of porous media (BEAR, 1988a; OLIVEIRA; KAVIANY, 2001). Therefore, the fluid flow and heat transfer study in those systems is a subject of great interest in many branches of engineering and science. The governing equations of a fluid flow in a porous medium are non-linear and difficult to handle analytically. So, problems concerning flows in porous medium are usually solved by

numerical methods.

Many numerical analysis related to isothermal flows in porous media have been conducted. Nevertheless, analytical analysis dealing with such problems are not extensive in the current literature. Siddiqui *et al.* (SIDDIQUI et al., 2006) used inverse methods to obtain exact solutions of several types of two-dimensional steady, viscous and incompressible fluid flows through porous medium. They compared the obtained solutions with known solutions in the absence of the porous medium. Wu *et al.* (WU et al., 2005) studied an impinging flow configuration to analyze transition in flow behavior, from the classical Hiemenz flow to the local solution of the Brinkman equation (BRINKMAN, 1947). Also, by considering small permeability values, Wu *et al.* (WU et al., 2005) utilized the perturbation technique to obtain asymptotic solutions for velocity and pressure fields. They found a new dimensionless parameter relating the square of two lengths, the classical boundary layer thickness for a high Reynolds number flow and the boundary layer thickness associated with the viscous attachment at the pore size. Kumaran *et al.* (KUMARAN et al., 2009) also analyzed an impinging flow. By using an implicit perturbation technique, they extended Wu *et al.* (WU et al., 2005) previous analytic results by considering large permeability.

Heat transfer in porous media has also been a subject of interest. The large contact surface between solid and fluid phases enhances considerably the heat transfer. Under the consideration of heat transfer, numerical studies are vastly found in the literature. Attia (ATTIA, 2007) studied the effect of the porosity in a stagnation-point flow impinging on a permeable surface by using a porosity parameter (inversely proportional to the porosity). Results indicated that by increasing the porosity parameter, and hence, reducing the medium porosity, causes a decrease on the thickness of both thermal and velocity layers and an increasing in the heat transfer at the permeable surface. Jiang and Ren (JIANG; REN, 2001) numerically investigated the forced convection heat transfer inside a porous medium by considering a thermal non-equilibrium model, known as two-equations model. They also analyzed the effects of viscous dissipation, appropriate boundary conditions, thermal dispersion and geometric properties of the medium, and compared the results with experimental data. The analysis showed that it is possible to predict numerically the convection heat transfer in porous medium by using the thermal non-equilibrium model with the ideal constant wall heat flux as a boundary condition. Jiang and Lu (JIANG; LU, 2007) analyzed thermal boundary characteristics at the contact interface between

a porous medium and an impermeable wall subject to a constant heat flux on the upper surface, with and without the consideration of a thermal contact resistance. They considered both a finite-thickness and a zero-thickness wall. Alazmi and Vafai (ALAZMI; VAFAI, 2002) investigated different forms of the constant wall heat flux boundary conditions. Effects of variable porosity and thermal dispersion were also studied. A comparison between different models of heat transfer at the wall was performed by the authors. The cooling of heated elements in a parallel-plate channel with porous inserts at the adiabatic walls (upper and lower plates) and under a laminar forced convection flow was studied numerically by Yucel and Guven (YUCEL; GUVEN, 2007). Their results showed that heat transfer can be enhanced by using high-thermal-conductivity porous inserts and that the insertion of heated elements and a porous matrix cause a rapid increase in the pressure drop along the channel with increasing the Reynolds number.

Numerical studies on stagnation-point flow in porous medium are also found extensively in the literature. Jeng and Tzeng (JENG; TZENG, 2005) investigated numerically the impinging cooling of porous metallic foam heat sink. Their simulation results revealed that when the Reynolds number is low, the maximum Nusselt number occurs at the stagnation point. However, when the Reynolds number increases, the maximum Nusselt number moves downward, to the narrowest part between the recirculation zone and the heating surface. Calculations were performed for a highly porous medium. Dórea and de Lemos (DóREA; LEMOS, 2010) performed simulations of a laminar jet impinging on a flat plate covered by a porous layer at the wall. They considered two macroscopic models for analyzing energy conservation, the one-energy equation model, which considers a local thermal equilibrium hypothesis, and the two-energy equation model, where distinct conservation equations for the fluid phase and for the porous matrix follow the local non-thermal equilibrium assumption. Thermal physical properties were varied and their influences on the energy transport were obtained. The results showed that for low porosities (low permeabilities), for thin porous layers and for high values of solid-to-fluid thermal conductivity ratio, a different distribution of local Nusselt number at the wall is calculated depending on the energy model applied.

Differently from numerical studies, analytical results concerning heat transfer are scarce in the open literature. Lee and Vafai (LEE; VAFAI, 1999) provided an extensive analytical characterization of forced convective flow through a channel filled with a

porous material. A heated wall was considered to provide heat flux transversely to the flow. They obtained exact solutions for the temperature profiles of solid and fluid phases, and classified heat transfer characteristics into three regimes, each of them dominated by a physical heat transfer mechanism: fluid conduction, solid conduction and internal heat exchange between solid and fluid phases.

In the present work chapter, an analytical study is performed on a stagnation-point flow inside a porous medium with heat exchange between phases and with heat provided by the wall at the stagnation-point. Heat supply is considered in two similar situations: a prescribed wall temperature, and a prescribed constant wall heat flux. A procedure using asymptotic theory is proposed in order to solve the problem by assuming a very large value for the interphase heat exchange and a low porosity medium. Under these assumptions, the problem presents two different length scales, z_s and z_g, associated with solid and gas phase thermal conductivities, respectively. These characteristic length scales are identified (PEREIRA et al., 2009; PEREIRA et al., 2010) and the results for temperatures and flow field are obtained for each scale, providing an analytical solutions for the problem.

3.2 Mathematical formulation

An impinging flow configuration inside a porous medium is assumed for the studied system in this chapter, considering $\bar{z}$ the normal coordinate and $\bar{x}$ the tangential coordinate to the wall. An schematic illustration is shown in Figure (3.1).

The steady-state volume-averaged mass, momentum and energy conservation equations under the above assumptions are given by:

$$\rho\frac{\partial\bar{u}}{\partial\bar{x}}+\rho\frac{\partial\bar{v}}{\partial\bar{z}}=0 \tag{3.1}$$

$$\rho\bar{u}\frac{\partial\bar{u}}{\partial\bar{x}}+\rho\bar{v}\frac{\partial\bar{u}}{\partial\bar{z}}=-\varepsilon\frac{\partial\bar{p}}{\partial\bar{x}}+\bar{\mu}\frac{\partial^2\bar{u}}{\partial\bar{z}^2}-\varepsilon\bar{\mu}\frac{\bar{u}}{K} \tag{3.2}$$

$$\rho\bar{u}\frac{\partial\bar{v}}{\partial\bar{x}}+\rho\bar{v}\frac{\partial\bar{v}}{\partial\bar{z}}=-\varepsilon\frac{\partial\bar{p}}{\partial\bar{z}}+\bar{\mu}\frac{\partial^2\bar{v}}{\partial\bar{z}^2}-\varepsilon\bar{\mu}\frac{\bar{v}}{K} \tag{3.3}$$

$$\varepsilon\rho\bar{v}c_p\frac{\partial T_g}{\partial\bar{z}}=\varepsilon\bar{\lambda}_g\frac{\partial^2T_g}{\partial\bar{z}^2}+h_v(T_s-T_g) \tag{3.4}$$

$$0=(1-\varepsilon)\bar{\lambda}_s\frac{d^2T_s}{d\bar{z}^2}-h_v(T_s-T_g) \tag{3.5}$$

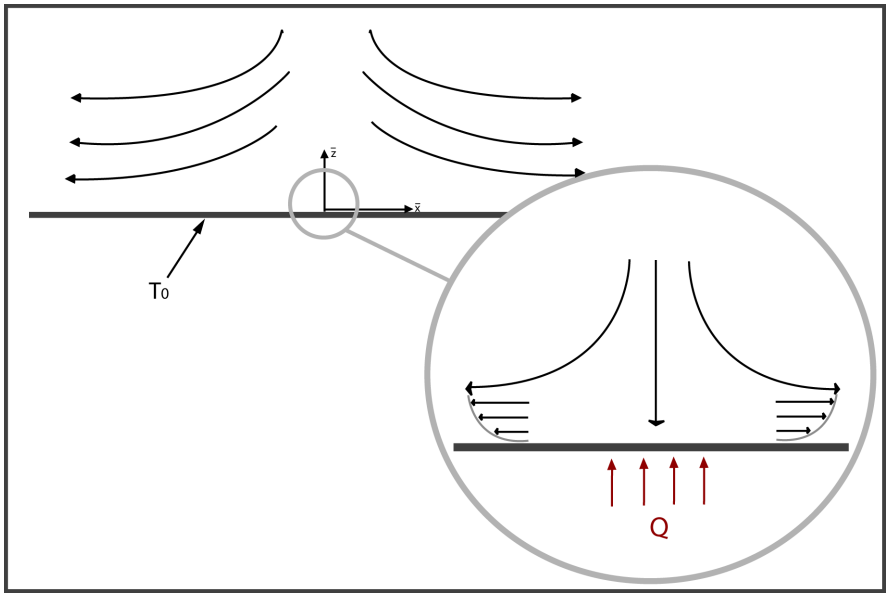

Figure 3.1 - Schematic diagram at the vicinity of the stagnation-point.

The boundary conditions far from the wall ($\bar{z} \to \infty$) are given by:

$$\bar{v} = \bar{v}_\infty, \quad \bar{u} = \bar{x} \left.\frac{d\bar{u}}{d\bar{x}}\right|_\infty, \quad T_g = T_s = T_\infty, \tag{3.6}$$

and at the wall, $\bar{z} = 0$, are given by:

$$\bar{v} = \bar{u} = 0, \quad \bar{p} = \bar{p}_0, \quad T_g = T_s = T_0. \tag{3.7}$$

The condition at the wall ($\bar{z} = 0$) for the energy problem depends on whether one considers a constant wall temperature or a constant wall heat flux.

3.2.1 Non-dimensional equations

The governing equations are made non-dimensional and transformed by means of the non-dimensional variables and variable transformations defined in Chapter (2). Equations (3.1) to (3.5) become:

$$U = \frac{df}{d\eta} \tag{3.8}$$

$$\frac{Pr}{\Gamma}\frac{d^3 f}{d\eta^3} + f\frac{d^2 f}{d\eta^2} - \left(\frac{df}{d\eta}\right)^2 - \Gamma\varepsilon\beta Pr\frac{df}{d\eta} = -\varepsilon Pr\,(1 + \beta\Gamma) \tag{3.9}$$

$$\frac{Pr}{\Gamma}\frac{d^2f}{d\eta^2} + f\frac{df}{d\eta} - \Gamma\varepsilon\beta Prf = \varepsilon Pr\left(1+\beta\Gamma\right)\frac{dF}{d\eta} \tag{3.10}$$

$$\frac{\varepsilon}{\Gamma}\frac{d^2\theta_g}{d\eta^2} + \varepsilon f\frac{d\theta_g}{d\eta} = -\Gamma n_g(\theta_s - \theta_g) \tag{3.11}$$

$$(1-\varepsilon)\frac{d^2\theta_s}{d\eta^2} = \Gamma n_g(\theta_s - \theta_g) \tag{3.12}$$

The boundary conditions are $\theta_s = \theta_g = 1$ and $df/d\eta = U_\infty$ for $\eta \to \infty$, and $f = df/d\eta = 0$ at $\eta = 0$. Two different energy boundary conditions at the wall are analyzed: a constant wall temperature and a constant wall heat flux.

In a region of the order of unity, corresponding to z_s, the viscous effects and the thermal non-equilibrium among flowing gas and porous medium are not observed. These effects occur only in a region of order Γ^{-1} near the wall, corresponding to z_g, and a boundary-layer expansion is necessary in order to describe them.

It is important to point that the studied system present three different boundary layers: one due to viscous attachment of the flow at the impermeable wall, one due to the attachment of the flow at the porous walls and a thermal boundary layer. The first boundary layer is the classical viscous boundary layer, and its effects are accounted by the first term in the left side of Equations (3.9) and (3.10). It has an order of magnitude of Γ^{-1}, as pointed by Equations (3.9) and (3.10). The second boundary layer is related to the fluid attachment at the porous wall, and its effect are accounted by the choice of κ. The thickness of the thermal boundary layer is determined by the order of Γ^{-1}.

At the same time that the viscous and thermal boundary layers are considered, it is necessary to take into account the thermal equilibrium or thermal non-equilibrium between the gas and solid phases. The thermal condition between the phases is controlled by the parameter N_g. The choice of N_g determines the thickness of the thermal equilibrium and non-equilibrium zones. In the present study, the non-dimensional parameters κ and N_g are chosen in such a way that the three distinct boundary layers and the thermal non-equilibrium zone have the same thickness, Γ^{-1}, hence, these effects are coupled in the inner zone.

If a lower porosity medium was considered, by using, for instance, $\kappa = O(\Gamma^{-3})$ the Darcy flow would be observed practically in the whole inner zone. Therefore, the

(impermeable wall) viscous boundary layer would not have the same thickness of the thermal boundary layer (inner zone). The viscous effects of the porous medium internal area would not permit the establishment of the (impermeable wall) viscous boundary layer in the inner zone (thickness of order of the Γ^{-1}). The viscous boundary layer would occur in a zone of order of the $\Gamma^{-3/2}$ attached to the impermeable wall. If, on the other hand, a higher porosity medium was considered, by using $\kappa = O(\Gamma^{-1})$, the flow in the outer zone would be governed by the Darcy equation with the inertia terms. In this situation, the porous-fluid viscous interaction would be minimized, and in the scale of Γ^{-1} the viscous boundary-layer due to the impermeable wall would be observed. The choice of the value of κ (a non-dimensional parameter that relates the permeability of the medium with the thermal-physical properties of gas and solid phases) determines the length scale of the viscous boundary-layers.

3.3 The constant wall temperature case

If a wall with a prescribed temperature θ_0 is considered, the energy equations must obey a boundary condition given by $\theta_s = \theta_g = \theta_0$ at $\eta = 0$, together with the boundary conditions mentioned in the previous section. The problem of unitary order, corresponding to the solid-phase thermal diffusivity length scale, is described first, then the problem of order Γ^{-1}, corresponding to the gas thermal diffusivity length scale.

3.3.1 Outer zone: problem of the order of unity

In the outer zone, corresponding to the solid-phase thermal diffusivity, the flow is basically governed by the pressure gradient (Darcy flow).

The equations to be analyzed to obtain the momentum variations and the pressure field in this region are given by:

$$\frac{Pr}{\Gamma}\frac{d^3f}{d\eta^3} + f\frac{d^2f}{d\eta^2} - \left(\frac{df}{d\eta}\right)^2 - \Gamma\varepsilon\beta Pr\frac{df}{d\eta} = -\varepsilon Pr\,(1+\beta\Gamma) \tag{3.13}$$

$$\frac{Pr}{\Gamma}\frac{d^2f}{d\eta^2} + f\frac{df}{d\eta} - \Gamma\varepsilon\beta Prf = \varepsilon Pr\,(1+\beta\Gamma)\,\frac{dF}{d\eta} \tag{3.14}$$

The solution for the momentum function f is obtained from Equation (3.13) and may be expressed as $f = f_{(0)} + \Gamma^{-1}f_{(1)} + O(\Gamma^{-2})$. Substituting it in Equation (3.13) and collecting similar powers of Γ, two differential equations are found for the first

two terms:

$$f'_{(0)} = 1 \tag{3.15}$$

$$\varepsilon\beta Pr\ f'_{(1)} = \varepsilon Pr + f_{(0)} f''_{(0)} - \left(f'_{(0)}\right)^2 \tag{3.16}$$

in which the prime denotes differentiation with respect to η. The boundary conditions are given by $f_{(0)} = f_{(1)} = 0$, at $\eta = 0$, and $f'_{(0)} = 1$ and $f'_{(1)} = U_1$ for $\eta \to \infty$. The value U_1 comes from the expansion $U_\infty = 1 + \Gamma^{-1} U_1 + O(\Gamma^{-2})$.

Solving Equations (3.15) and (3.16) with the appropriate boundary conditions, the momentum expression in the outer zone is obtained as:

$$f(\eta) = \eta - \Gamma^{-1} \frac{1 - \varepsilon Pr}{\varepsilon\beta Pr} \eta + O\left(\Gamma^{-2}\right) \tag{3.17}$$

If one evaluates all terms of the proposed series solution of Equation (3.17), then it will be seen that all of them have a linear form, and hence, the first and the second terms in the left side of Equation (3.13) are null for every evaluation performed. If one notes that those terms are the viscous terms, then the analysis of the problem in the outer zone is conducted to the Darcy equation with corrections given by the third term on the left side of Equation (3.13).

The horizontal component of the velocity in the outer zone is given by U, and is obtained by deriving Equation (3.17) with respect to η:

$$U(\eta) = 1 - \Gamma^{-1} \frac{1 - \varepsilon Pr}{\varepsilon\beta Pr} + O\left(\Gamma^{-2}\right) \tag{3.18}$$

The result exhibited by Equation (3.18) points out to a constant value of U in the whole region of order of unity (solid phase characteristic length scale) as shown in Figure (3.2). This value is below one, since $U_1 = -(1 - \varepsilon Pr)/(\varepsilon\beta Pr) < 0$, which indicates the influence of the solid-phase on the strain-rate of the flow. Most of the analysis on impinging flow configurations established in porous media usually considers $f'|_{+\infty} = 1$ as a boundary condition. This condition comes from the classical Hiemenz solution of an impinging flow without the porous medium. However, if one considers the porous medium, the resistance exerted by the tortuous channels requires a correction term in velocity fields, as pointed by Equations (3.17) and (3.18).

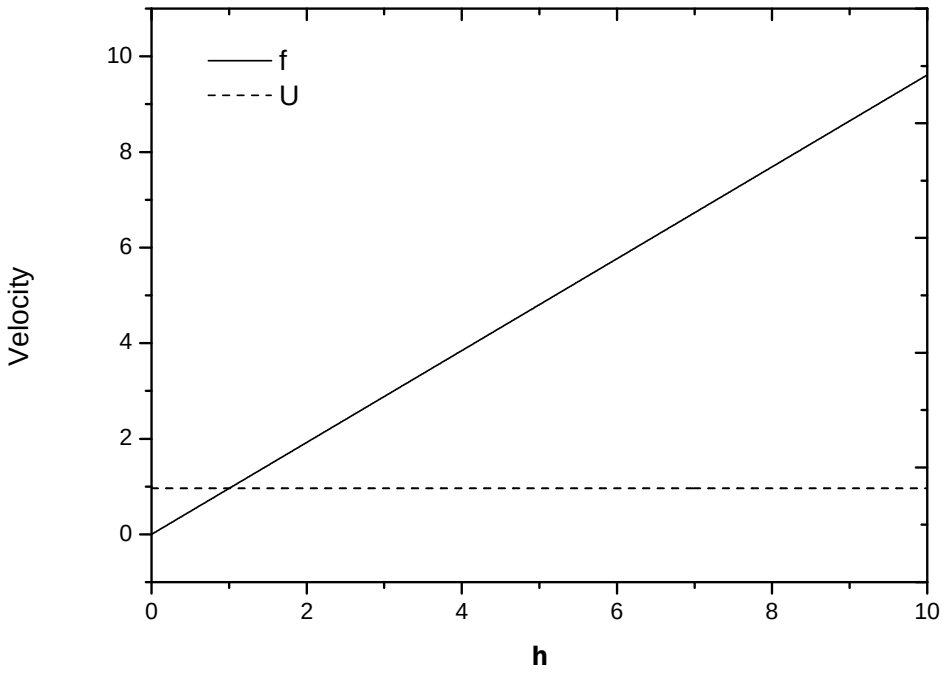

Figure 3.2 - Velocity in the outer zone, $\varepsilon = 0.3$, $\beta = Pr = 1.0$.

The pressure field is obtained from Equation(3.14) and its solution is considered to be expressed as $F(\eta) = F_{(0)} + \Gamma^{-1}F_{(1)} + O(\Gamma^{-2})$. Substituting the proposed solution in Equation (3.14) and collecting similar powers of Γ, two differential equations are found for the first two terms:

$$F'_{(0)} = -f_{(0)}, \tag{3.19}$$

$$F'_{(1)} = \frac{f_{(0)}f'_{(0)}}{\varepsilon\beta Pr} - f_{(1)} - \frac{F'_{(0)}}{\beta} \tag{3.20}$$

which must satisfy the boundary conditions $F_{(0)} = F_{(1)} = 0$ at $\eta = 0$.

The solutions of Equations (3.19) and (3.20) give the pressure field in the outer zone as:

$$F(\eta) = -\frac{\eta^2}{2} + \Gamma^{-1}\frac{\eta^2}{\varepsilon\beta Pr} + O(\Gamma^{-2}) \tag{3.21}$$

In the outer zone, gas phase and solid phase are in thermal equilibrium due to the high value of the interphase heat exchange. Under this condition, it is assumed $\theta_g = \theta_s = \theta$ in this region, and one must solve the following equation:

$$\frac{1}{\Gamma}\frac{d^2\theta}{d\eta^2} + \gamma\frac{d^2\theta}{d\eta^2} + f\frac{d\theta}{d\eta} = 0 \tag{3.22}$$

which was obtained by summing Equations (3.11) and (3.12) and using the definition $\gamma \equiv (1-\varepsilon)/\varepsilon$. If one express the solution as $\theta = \theta_{(0)} + \Gamma^{-1}\theta_{(1)} + O(\Gamma^{-2})$, the two following differential equations are obtained, when similar powers of Γ are collected:

$$\gamma\theta''_{(0)} + f_{(0)}\theta'_{(0)} = 0, \tag{3.23}$$

$$\gamma\theta''_{(1)} + f_{(0)}\theta'_{(1)} = -\theta''_{(0)} - f_{(1)}\theta'_{(0)} \tag{3.24}$$

which must satisfy the boundary conditions $\theta_{(0)} = \theta_0$ and $\theta_{(1)} = 0$, at $\eta = 0$, and $\theta_{(0)} = 1$ and $\theta_{(1)} = 0$ for $\eta \to \infty$. The solutions of Equations (3.23) and (3.24) gives the temperature expression in the outer zone as:

$$\theta(\eta) = \theta_0 - \Theta\ erf\left(\frac{\eta}{\sqrt{2\gamma}}\right) + \Gamma^{-1}\frac{\Theta}{2\gamma}\sqrt{\frac{2}{\pi\gamma}}\left(1 + \frac{1-\varepsilon Pr}{\varepsilon\beta Pr}\gamma\right)\ \eta\ e^{-\eta^2/2\gamma} + O\left(\Gamma^{-2}\right) \tag{3.25}$$

in which for the sake of compactness it was defined $\Theta \equiv (\theta_0 - 1) > 0$.

In the outer zone, both gas and solid phases experience an exponential increase in the temperature, due to the heated wall. Since the interphase heat exchange is assumed to be high, thermal equilibrium is observed in the outer zone. In the present case, the temperature in the wall is assumed to be known. Plots for three different temperatures in the wall are presented in Figure (3.3). The exponential increase in the temperature downward to the wall is clearly observed.

The analysis of the limit cases: of a very high porosity medium ($\gamma \ll 1$) and of a very low one ($\gamma \gg 1$) for the leading order term of Equation (3.25) shows:

$$\theta(\eta) = \begin{cases} 1, & \text{for } \gamma \ll 1, \\ \theta_0, & \text{for } \gamma \gg 1. \end{cases}$$

The first solution represents the limit in which the porous medium is eliminated. In this limit, $\gamma \ll 1$, the temperature in the outer zone is the same as the temperature far from the wall. The temperature variations will occur only in the inner zone (gas

phase characteristic length scale, z_g). The second solution corresponds to the limit $\gamma \gg 1$, a solid with no void spaces, the temperature is of that of the wall, θ_0. The analyzed cases in the present study are not in these limits, i.e., γ is of the order of unity.

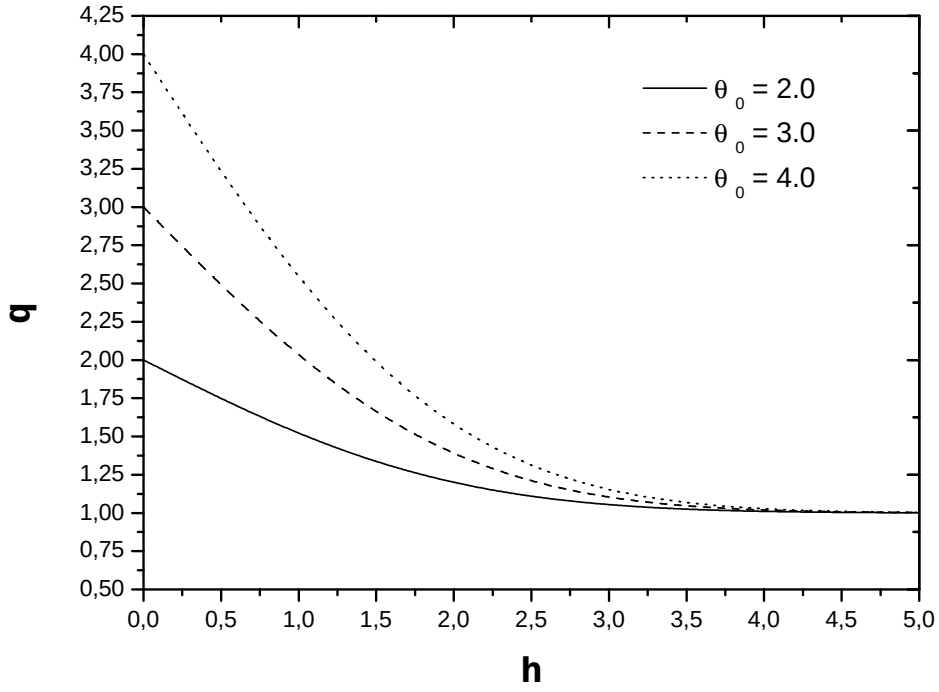

Figure 3.3 - Temperature in the outer zone, $\varepsilon = 0.3$, $\beta = Pr = 1.0$.

3.3.2 Inner zone: problem of the order of Γ^{-1}

In this region, due to viscous effects, variations in the momentum are of order of Γ^{-1}, as already pointed by Equation (3.17) with $\eta \sim \Gamma^{-1}$. Then, to capture those variations it is necessary to re-scale $\tilde{f} = \Gamma f$ and also to express it as $\tilde{f} = \tilde{f}_{(0)} + \Gamma^{-1}\tilde{f}_{(1)} + O(\Gamma^{-2})$.

With this in mind, after performing a boundary-layer expansion in the spatial coordinate, $\tilde{\eta} = \Gamma\eta$, the first two governing equations for the momentum are:

$$\tilde{f}'''_{(0)} - \varepsilon\beta\left(\tilde{f}'_{(0)} - 1\right) = 0 \tag{3.26}$$

$$Pr\tilde{f}'''_{(1)} + \tilde{f}_{(0)}\tilde{f}''_{(0)} - \left(\tilde{f}'_{(0)}\right)^2 - \varepsilon\beta Pr\tilde{f}'_{(1)} = -\varepsilon Pr \tag{3.27}$$

in which the prime now denotes differentiation with respect to $\tilde{\eta}$. The boundary conditions are given by $\tilde{f}_{(0)} = d\tilde{f}_{(0)}/d\tilde{\eta} = \tilde{f}_{(1)} = d\tilde{f}_{(1)}/d\tilde{\eta} = 0$ at $\tilde{\eta} = 0$, and account for the non-slip condition at the wall for both vertical and horizontal velocities. The remaining boundary conditions are given by matching this solution with the solution provided by the outer zone analysis:

$$\left.\frac{d\tilde{f}_{(0)}}{d\tilde{\eta}}\right|_{\infty} = \left.\frac{df_{(0)}}{d\eta}\right|_{0} = 1 \tag{3.28}$$

$$\left.\frac{d\tilde{f}_{(1)}}{d\tilde{\eta}}\right|_{\infty} = \left.\frac{df_{(1)}}{d\eta}\right|_{0} = -\frac{1-\varepsilon Pr}{\varepsilon\beta Pr} \tag{3.29}$$

Solving Equations (3.26) and (3.27) with the appropriate boundary and matching conditions, the momentum in the inner zone is obtained as:

$$\tilde{f}(\tilde{\eta}) = \tilde{\eta} + \frac{1}{\sqrt{\varepsilon\beta}}\left(e^{-\sqrt{\varepsilon\beta}\tilde{\eta}} - 1\right) - \Gamma^{-1}\left[\frac{1-\varepsilon Pr}{\varepsilon\beta Pr}\tilde{\eta} + e^{-\sqrt{\varepsilon\beta}\tilde{\eta}}\left(\frac{10\tilde{\eta} + 2\sqrt{\varepsilon\beta}\tilde{\eta}^2}{8\varepsilon\beta Pr}\right) + \frac{\left(e^{-\sqrt{\varepsilon\beta}\tilde{\eta}} - 1\right)}{8\varepsilon\beta Pr}.\frac{(18 - 8\varepsilon Pr)}{\sqrt{\varepsilon\beta}}\right] + O\left(\Gamma^{-2}\right) \tag{3.30}$$

In the inner zone, the decrease in the momentum variable is no longer linear, as in the outer zone, but exponential, pointing to the viscous effects due to the wall.

From the derivative of Equation (3.30), the horizontal velocity profile for the inner zone is obtained as:

$$\tilde{U}(\tilde{\eta}) = 1 - e^{-\sqrt{\varepsilon\beta}\tilde{\eta}} - \Gamma^{-1}\left[\frac{1-\varepsilon Pr}{\varepsilon\beta Pr} - \frac{e^{-\sqrt{\varepsilon\beta}\tilde{\eta}}}{8\sqrt{\varepsilon\beta}Pr}\left(10\tilde{\eta} + 2\sqrt{\varepsilon\beta}\tilde{\eta}^2\right) + \frac{e^{-\sqrt{\varepsilon\beta}\tilde{\eta}}}{8\varepsilon\beta Pr}\left(4\sqrt{\varepsilon\beta}\tilde{\eta} - 8(1-\varepsilon Pr)\right)\right] + O\left(\Gamma^{-2}\right) \tag{3.31}$$

In the inner zone, the macroscopic viscous effects become relevant due to the fluid viscous attachment at the wall.

Such behavior is observed in Figure (3.4).

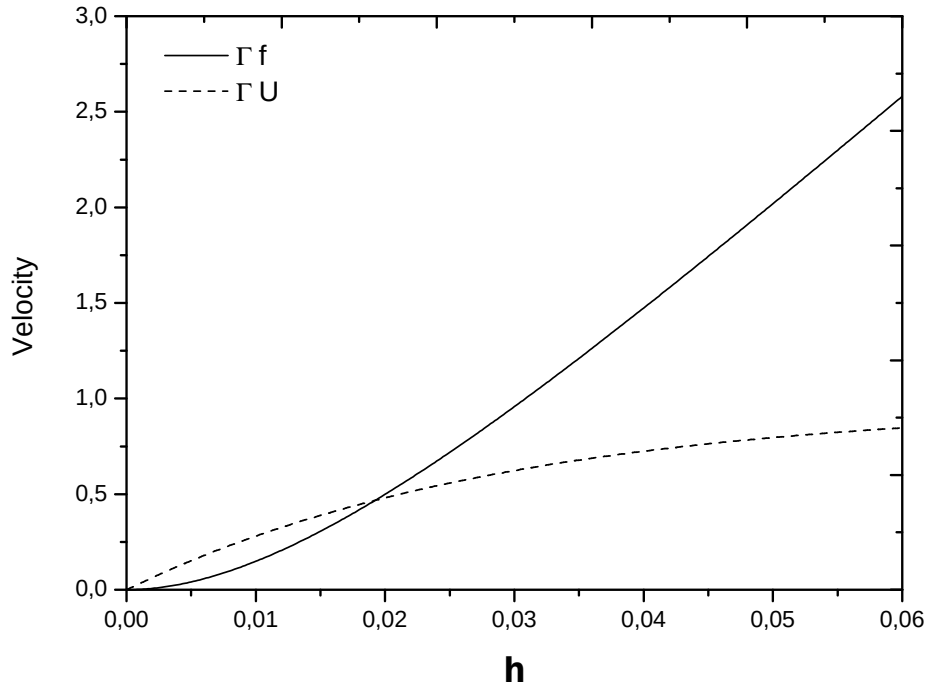

Figure 3.4 - Velocity in the inner zone, $\varepsilon = 0.3$, $\beta = Pr = 1.0$.

The pressure field is described by the same transformation, given by $\tilde{F} = \Gamma F = \tilde{F}_{(0)} + \Gamma^{-1}\tilde{F}_{(1)} + O(\Gamma^{-2})$. Performing the same spatial coordinate change used before for the momentum, and after collecting similar powers of Γ, Equation (3.10) provides the following differential equations:

$$\tilde{F}'_{(0)} = 0 \tag{3.32}$$

$$\tilde{F}'_{(1)} = \frac{\tilde{f}''_{(0)}}{\varepsilon\beta} - \tilde{f}_{(0)} \tag{3.33}$$

When Equations (3.32) and (3.33) with boundary conditions given by $\tilde{F}_{(0)} = \tilde{F}_{(1)} = 0$ at $\eta = 0$ are solved, the pressure field in the inner zone is found:

$$\tilde{F}(\tilde{\eta}) = \Gamma^{-1}\left(\frac{\tilde{\eta}}{\sqrt{\varepsilon\beta}} - \frac{\tilde{\eta}^2}{2}\right) + O(\Gamma^{-2}) \tag{3.34}$$

In the inner zone, the problem analyzed is in a region very near the stagnation-point. As a result, the variable $\tilde{F}$ is nearly null, because the pressure is very close to that of stagnation, and variations in $\tilde{F}$ become relevant only in higher order terms. It is possible to write Equation (3.34) as:

$$\tilde{F}(\tilde{\eta}) = -\Gamma^{-1}\frac{\tilde{\eta}^2}{2}\left(1 - \frac{2}{\tilde{\eta}\sqrt{\varepsilon\beta}}\right) + O(\Gamma^{-2}). \tag{3.35}$$

If the limit $\tilde{\eta} \to \infty$ is taken, the pressure field in the inner zone is given by:

$$\tilde{F}(\tilde{\eta} \to \infty) \sim -\Gamma^{-1}\frac{\tilde{\eta}^2}{2} \tag{3.36}$$

Equation (3.36) has to be compared with Equation (3.21), written in terms of $\tilde{F}$, which leads to:

$$\tilde{F}(\eta \to \Gamma^{-1}) = -\Gamma^{-1}\frac{\tilde{\eta}^2}{2} + O(\Gamma^{-2}). \tag{3.37}$$

Note that taking appropriate limits, the coupling between Equations (3.21) and (3.34) is obeyed.

In the inner zone the gas phase and solid phase temperature profiles detach one from another because the thermal equilibrium is no longer satisfied. Then, the governing equations must be analyzed separately. The energy flux from the outer zone must match the energy flux from the inner zone in all orders, a condition that accounts for the continuity of the first derivative (physically speaking, it accounts for the continuity of the heat flux). This mandatory matching conditions is expressed by:

$$\left.\frac{d\theta}{d\eta}\right|_0 = \Gamma \left.\frac{d\theta_g}{d\tilde{\eta}}\right|_{+\infty} = \Gamma \left.\frac{d\theta_s}{d\tilde{\eta}}\right|_{+\infty}. \tag{3.38}$$

The temperature variation are not abrupt in the inner zone, unlike those in combustion problems (PEREIRA et al., 2009; PEREIRA et al., 2010). Then, differently from the momentum variable f, in the inner zone, one does not re-scale the temperature variables θ_s and θ_g. Both temperature solutions are expressed in a general form as

$\theta = \theta_{(0)} + \Gamma^{-1}\theta_{(1)} + O(\Gamma^{-2})$, but to respect the magnitude order in the matching condition given by Equation (3.38), the conditions $d\theta_{g(0)}/d\tilde{\eta} = d\theta_{s(0)}/d\tilde{\eta} = 0$ for $\tilde{\eta} \to +\infty$ must be imposed. From the boundary condition $\theta_{g(0)} = \theta_{s(0)} = \theta_0$ at $\tilde{\eta} = 0$, $\theta_{g(0)} = \theta_{s(0)} = \theta_0$, for every $\tilde{\eta}$, is obtained. Hence, the temperature solutions in the inner zone are expressed as:

$$\begin{cases} \theta_g = \theta_0 + \Gamma^{-1}\theta_{g(1)} + \Gamma^{-2}\theta_{g(2)} + O(\Gamma^{-3}), \\ \theta_s = \theta_0 + \Gamma^{-1}\theta_{s(1)} + \Gamma^{-2}\theta_{s(2)} + O(\Gamma^{-3}). \end{cases} \tag{3.39}$$

Substituting these expressions in Equations (3.11) and (3.12) with the re-scaled spatial coordinate $\tilde{\eta} = \Gamma\eta$ and collecting equal powers of Γ, a set of governing equations is obtained as:

$$\varepsilon\theta''_{g(1)} = -n_g\left(\theta_{s(1)} - \theta_{g(1)}\right), \tag{3.40}$$

$$\varepsilon\theta''_{g(2)} + \varepsilon\tilde{f}_{(0)}\theta'_{g(1)} = -n_g\left(\theta_{s(2)} - \theta_{g(2)}\right), \tag{3.41}$$

$$(1-\varepsilon)\theta''_{s(1)} = 0, \tag{3.42}$$

$$(1-\varepsilon)\theta''_{s(2)} = n_g\left(\theta_{s(1)} - \theta_{g(1)}\right). \tag{3.43}$$

The boundary conditions are $\theta_{g(1)} = \theta_{s(1)} = \theta_{g(2)} = \theta_{s(2)} = 0$ at $\tilde{\eta} = 0$. Equations (3.40) to (3.43) must match the temperature solution from the outer zone as given by Equation (3.38), thus the following conditions must be obeyed:

$$\left.\frac{d\theta_{g(1)}}{d\tilde{\eta}}\right|_{+\infty} = \left.\frac{d\theta_{s(1)}}{d\tilde{\eta}}\right|_{+\infty} = \left.\frac{d\theta_{(0)}}{d\eta}\right|_{0} = -\Theta\sqrt{\frac{2}{\pi\gamma}}, \tag{3.44}$$

$$\left.\frac{d\theta_{g(2)}}{d\tilde{\eta}}\right|_{+\infty} = \left.\frac{d\theta_{s(2)}}{d\tilde{\eta}}\right|_{+\infty} = \left.\frac{d\theta_{(1)}}{d\eta}\right|_{0} = \frac{\Theta}{2\gamma}\sqrt{\frac{2}{\pi\gamma}}\left(1 + \frac{1-\varepsilon Pr}{\varepsilon\beta Pr}\gamma\right). \tag{3.45}$$

If Equations (3.40) and (3.43) are solved, then the solid phase temperature in the inner zone is obtained:

$$\theta_s(\tilde{\eta}) = \theta_0 - \Gamma^{-1}\Theta\sqrt{\frac{2}{\pi\gamma}}\tilde{\eta} + \Gamma^{-2}\frac{\Theta}{2\gamma}\sqrt{\frac{2}{\pi\gamma}}\left(1 + \frac{1-\varepsilon Pr}{\varepsilon\beta Pr}\gamma\right)\tilde{\eta} + O\left(\Gamma^{-3}\right). \tag{3.46}$$

The gas phase temperature in the inner zone is given by solving Equations (3.40) and (3.41). In the process of solving Equation (3.41) it is assumed that $\varepsilon^2 \ll 1$, so one treats a simplified form of such equation when all variables are substituted in

Equation (3.41). Details on the solving procedure are found in the Appendix (A). Under such conditions, the gas phase temperature profile in the inner zone is given by:

$$\theta_g(\tilde{\eta}) = \theta_0 - \Gamma^{-1}\Theta\sqrt{\frac{2}{\pi\gamma}}\tilde{\eta} + \Gamma^{-2}\left[\Theta\sqrt{\frac{2\varepsilon}{\pi\gamma\beta}}\frac{1}{n_g} + \sqrt{\frac{2}{\pi\gamma}}\frac{\Theta}{2\gamma}\left(1 + \frac{1-\varepsilon Pr}{\varepsilon\beta Pr}\gamma\right)\tilde{\eta} + \right.$$

$$\left.\Theta\sqrt{\frac{2}{\pi\gamma\varepsilon\beta}}\left(\frac{\varepsilon}{\varepsilon^2\beta - n_g}\right)e^{-\sqrt{\varepsilon\beta}\tilde{\eta}} - \Theta\sqrt{\frac{2\varepsilon\beta}{\pi\gamma}}\frac{\varepsilon^2}{n_g\left(\varepsilon^2\beta - n_g\right)}e^{-\sqrt{\frac{n_g}{\varepsilon}}\tilde{\eta}}\right] + O\left(\Gamma^{-3}\right). \quad (3.47)$$

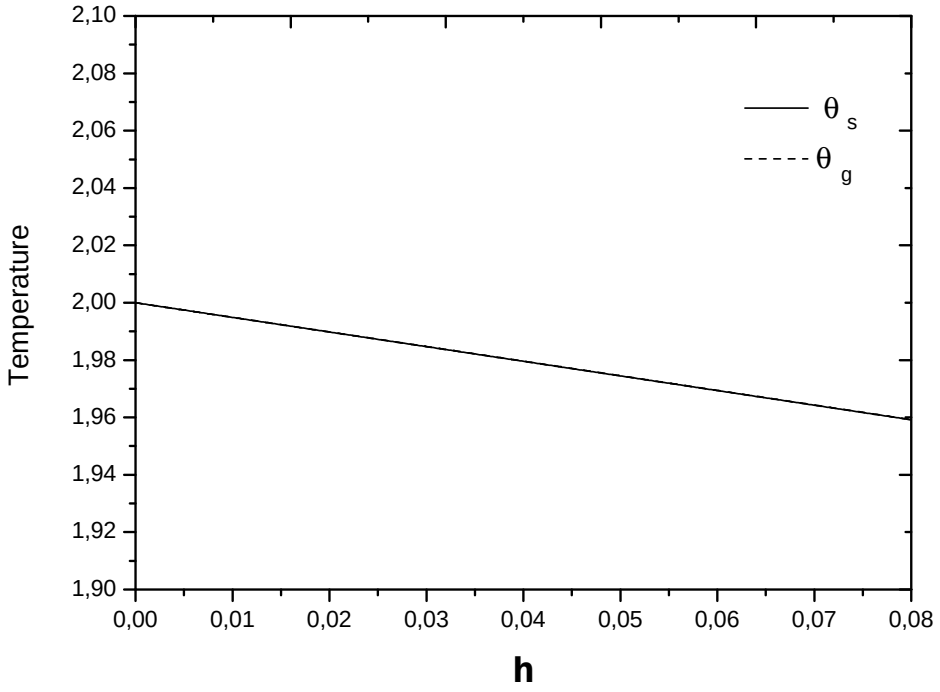

Figure 3.5 - Temperature in the inner zone, $\varepsilon = 0.3$, $\beta = Pr = n_g = 1.0$, $\theta_0 = 2.0$,

In the inner zone, temperature profiles detach one from another due to the difference in solid phase and gas phase thermal conductivities. However, in the inner zone one is analyzing a region very near the stagnation-point, such that the velocity field

is near zero - from the re-scaling of f, the velocity field in the inner zone is of order Γ^{-1}. Because of the very low velocity of the gas, there is enough time to solid phase and gas phase to reach an equilibrium temperature in higher orders, and the thermal non-equilibrium is only observed in the terms of order Γ^{-2}, as can be seen from Equations (3.47) and (3.46). It is possible to observe such nearly-equilibrium situation in Figure (3.5). In Figure (3.6) the corrections of order Γ^{-2} are presented. The thermal non-equilibrium between solid and gas phase appears only on this order and higher.

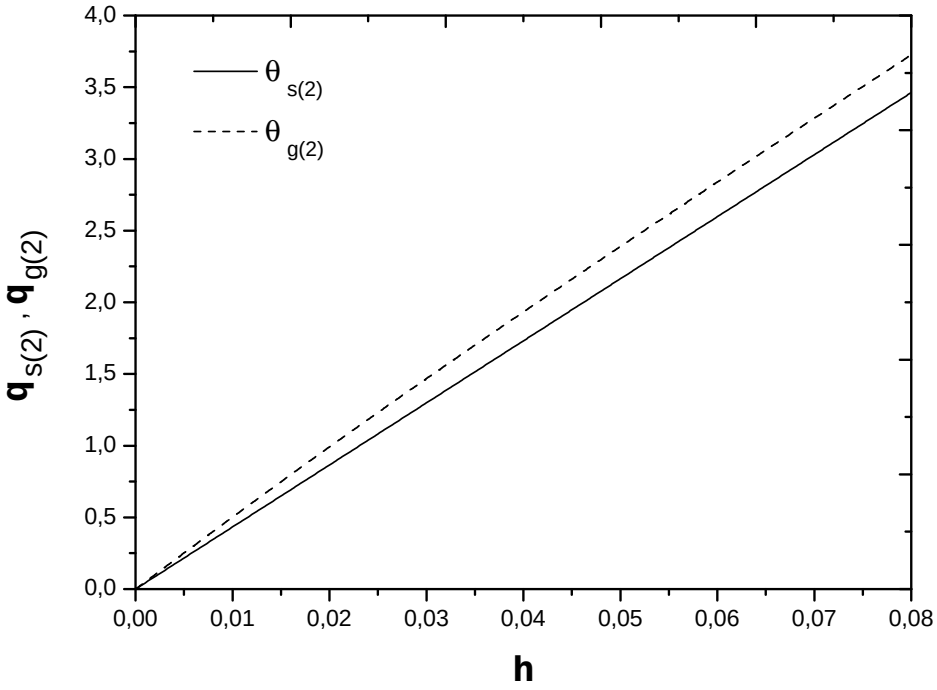

Figure 3.6 - Corrections of temperatures, $\varepsilon = 0.3$, $\beta = Pr = n_g = 1.0$, $\theta_0 = 2.0$.

The convective heat transport is a process that occurs in the outer zone, while the heat removal, mainly by the solid phase conductive heat transport, is a process that occurs in the inner zone if the heat flux is not too high. If the convective heat transport is balanced with the conductive heat transport, a plane of thermal stagnation is found. An estimative of the position of this plane may be performed, by balancing the convective heat transport from the outer zone, with the solid phase

conductive heat transport, from the inner zone. In a non-dimensional form, the following approximated relation for the position of the plane of thermal stagnation is found:

$$-\varepsilon f\ \theta|_{\eta_{ts}} \sim \Gamma(1-\varepsilon)\ \left.\frac{d\theta_s}{d\tilde{\eta}}\right|_{\tilde{\eta}_{ts}}, \tag{3.48}$$

in which η_{ts} and $\tilde{\eta}_{ts}$ are the position of the thermal stagnation plane observed from the outer zone and from the inner zone, respectively. Collecting similar power terms:

$$\varepsilon f_{(0)}\ \theta_{(0)}\big|_{\eta_{ts}} \sim (1-\varepsilon)\ \left.\frac{d\theta_{s(1)}}{d\tilde{\eta}}\right|_{\tilde{\eta}_{ts}}. \tag{3.49}$$

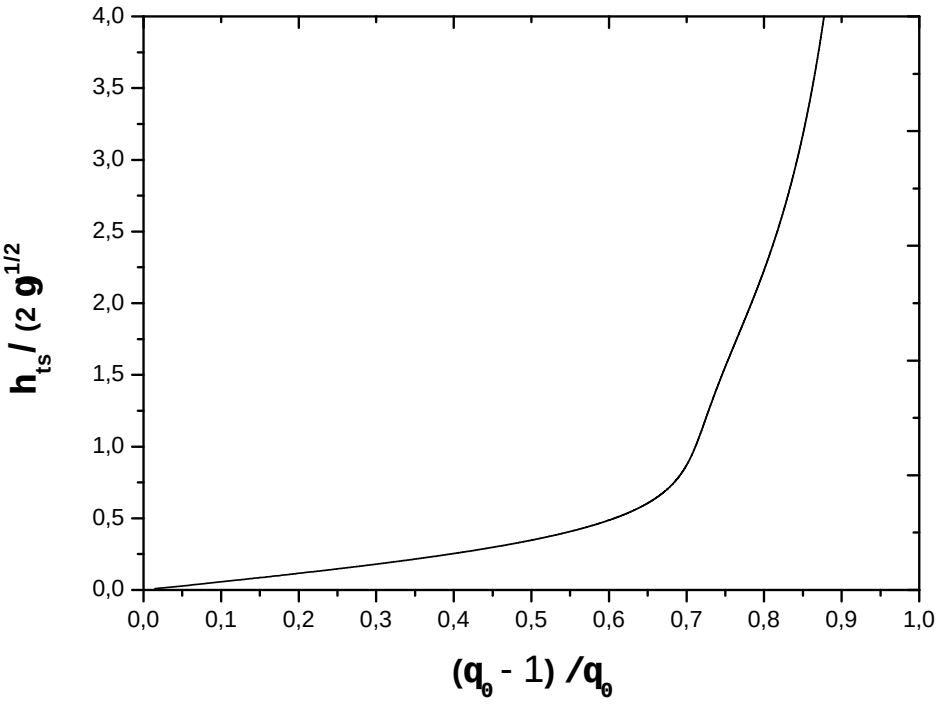

Figure 3.7 - Position of the thermal stagnation plane

.

From Equation (3.49) the position of the thermal stagnation plane is found by solving

the following transcendental expression for η_{ts}:

$$\frac{\eta_{ts}}{\sqrt{2\gamma}}\left[1-\frac{(\theta_0-1)}{\theta_0}erf\left(\frac{\eta_{ts}}{\sqrt{2\gamma}}\right)\right]\sim\frac{(\theta_0-1)}{\theta_0}\frac{1}{\sqrt{\pi}}. \tag{3.50}$$

Even though Equation (3.50) is an approximation, some features can be observed from it. It is possible to observe that as the wall temperature increases, the thermal stagnation plane goes farther from the wall. Since the inner zone is a very small region, if the wall temperature is high enough (if compared to the injection temperature), the heat flux is high, leading the heat removal from the wall to be a process that occur in the outer zone. Hence, the thermal stagnation plane goes far from the wall, as shown by $\eta_{ts}/\sqrt{2\gamma}\sim\pi^{-1/2}/[1-erf(\eta_{ts}/\sqrt{2\gamma})]$ for $(\theta_0-1)/\theta_0\to 1$. Contrarily, if the wall temperature is close to the air injected temperature, the thermal stagnation plane is close to the wall, according to $\eta_{ts}/\sqrt{2\gamma}\sim\pi^{-1/2}(\theta_0-1)/\theta_0$ for $(\theta_0-1)/\theta_0\to 0$.

Figure (3.7) presents the position of the thermal stagnation plane as a function of the wall temperature. The horizontal axis have been normalized and the vertical axis have been re-scaled.

3.4 The constant wall heat flux case

If the interest relies not on a prescribed temperature at $\bar{z}=0$, but instead on removing an amount Q of heat through the wall, the development considered before may be performed by only changing the boundary condition at $\bar{z}=0$ to:

$$(1-\varepsilon)\,\bar{\lambda}_s\frac{dT_s}{d\bar{z}}\bigg|_0+\varepsilon\bar{\lambda}_g\,\frac{dT_g}{d\bar{z}}\bigg|_0=-Q \tag{3.51}$$

or, in its non-dimensional form, at $\eta=0$:

$$(1-\varepsilon)\,\frac{d\theta_s}{d\eta}\bigg|_0+\frac{\varepsilon}{\Gamma}\,\frac{d\theta_g}{d\eta}\bigg|_0=-q \tag{3.52}$$

in which is considered that $q\equiv[Q/(c_pT_\infty)]\,[1/(\rho_\infty\bar{v}_\infty)]\left[1/a^{1/2}\right]$, the non-dimensional heat flux, is of the order of unity.

The problem in the outer zone is described first. Then the problem in the inner zone is described. In both regions, solutions will be obtained using the perturbation method, as in the previous case. The velocities and the pressure fields will be the

same as those obtained for the case considering a constant wall temperature, but expressions for the temperature profiles will be different.

3.4.1 Outer zone: problem of the order of unity

In the outer zone, velocity and pressure fields are given by Equations (3.17) and (3.21), and energy conservation is given by Equation (3.22). The same type of solution for θ is performed as before, and then one must solve the already obtained set of two equations given by Equations (3.23) and (3.24).

The boundary condition at $\eta = 0$, when observed from the outer zone, is a temperature θ_0 and its correction of the order of Γ^{-1} given by θ_1, but, differently from the previous case, this temperature is unknown and dependent on the value of the heat flux q. Boundary conditions for Equations (3.23) and (3.24) are then $\theta_{(0)} = \theta_0$ and $\theta_{(1)} = \theta_1$ for $\eta = 0$, and $\theta_{(0)} = 1$ and $\theta_{(1)} = 0$ for $\eta \to \infty$.

The thermal solution in the outer zone is then given by solving Equations (3.23) and (3.24) with the appropriate boundary conditions, obtaining:

$$\theta(\eta) = \theta_0 - (\theta_0 - 1)erf\left(\frac{\eta}{\sqrt{2\gamma}}\right) + \Gamma^{-1}\left[\theta_1 + \frac{\theta_0 - 1}{2\gamma}\sqrt{\frac{2}{\pi\gamma}}\left(1 + \frac{1 - \varepsilon Pr}{\varepsilon\beta Pr}\gamma\right)\eta\, e^{-\frac{\eta^2}{2\gamma}} - \theta_1\, erf\left(\frac{\eta}{\sqrt{2\gamma}}\right)\right] + O(\Gamma^{-2}). \tag{3.53}$$

As expected, the expression for the temperature in the outer zone in the constant wall heat flux case is similar to the expression for the temperature in the constant wall temperature case. Such similarity may be exhibited if Equation (3.53) is written as:

$$\theta(\eta) = \text{Equation (3.25)} + \Gamma^{-1}\theta_1\left[1 - erf\left(\frac{\eta}{\sqrt{2\gamma}}\right)\right] \tag{3.54}$$

The extra term is a fluctuation in the wall temperature, that in the present case (constant wall heat flux) becomes an unknown value.

3.4.2 Inner zone: problem of the order of Γ^{-1}

The same re-scaling performed previously is made, and velocities and pressure fields are also the same as those obtained for the case of a constant wall temperature,

and are given by Equations (3.30) and (3.34), respectively. Considerations made previously about matching the heat flux from the outer zone with the inner zone are also valid in the present case. The difference appears on the boundary condition at $\tilde{\eta} = 0$, that now is given by:

$$\Gamma(1-\varepsilon)\left.\frac{d\theta_s}{d\tilde{\eta}}\right|_0 + \varepsilon\left.\frac{d\theta_g}{d\tilde{\eta}}\right|_0 = -q. \tag{3.55}$$

Expressing temperature profiles as before one must solve the same set of equations obtained previously, given by Equations (3.40) to (3.43), and imposing the boundary conditions given by $\theta_{s(1)} = \theta_{g(1)} = \theta_1$, $\theta_{s(2)} = \theta_{g(2)} = \theta_2$, $d\theta_{s(1)}/d\tilde{\eta} = -Q/(1-\varepsilon)$ and $(1-\varepsilon)d\theta_{s(2)}/d\tilde{\eta} + \varepsilon d\theta_{g(1)}/d\tilde{\eta} = 0$, at $\tilde{\eta} = 0$. The matching conditions impose that:

$$\left.\frac{d\theta_{g(1)}}{d\tilde{\eta}}\right|_{+\infty} = \left.\frac{d\theta_{s(1)}}{d\tilde{\eta}}\right|_{+\infty} = \left.\frac{d\theta_{(0)}}{d\eta}\right|_0 = -(\theta_0 - 1)\sqrt{\frac{2}{\pi\gamma}}, \tag{3.56}$$

$$\left.\frac{d\theta_{g(2)}}{d\tilde{\eta}}\right|_{+\infty} = \left.\frac{d\theta_{s(2)}}{d\tilde{\eta}}\right|_{+\infty} = \left.\frac{d\theta_{(1)}}{d\eta}\right|_0 =$$

$$\frac{\theta_0 - 1}{2\gamma}\sqrt{\frac{2}{\pi\gamma}}\left(1 + \frac{1-\varepsilon Pr}{\varepsilon\beta Pr}\gamma\right) + \theta_1\left(\frac{\sqrt{\pi\gamma} - \sqrt{2}}{\sqrt{\pi\gamma}}\right). \tag{3.57}$$

It is worth to note that, since the heat removed from the wall is assumed to be of the order of unity, the leading order term for the temperature expressions must be a constant value. This condition reinforces the consistence of the proposed model.

Solid phase temperature profile is obtained solving Equations (3.42) and (3.43) with boundary and heat flux matching conditions. The result is:

$$\theta_s(\tilde{\eta}) = \theta_0 + \Gamma^{-1}\left(\theta_1 - \frac{q}{1-\varepsilon}\tilde{\eta}\right) + \Gamma^{-2}\left[\theta_2 + \left(\frac{\theta_0 - 1}{2\gamma}\sqrt{\frac{2}{\pi\gamma}}\left(1 + \frac{1-\varepsilon Pr}{\varepsilon\beta Pr}\gamma\right) + \right.\right.$$

$$\left.\left.\theta_1\left(\frac{\sqrt{\pi\gamma} - \sqrt{2}}{\sqrt{\pi\gamma}}\right)\right)\tilde{\eta}\right] + O(\Gamma^{-3}). \tag{3.58}$$

The same simplifying assumption made before, $\varepsilon^2 \ll 1$, is performed here, and similarly from the previous case, a simplified form of Equation (3.41) is solved,

obtaining a gas phase temperature solution in the inner zone given by:

$$\theta_g(\tilde{\eta}) = \theta_0 + \Gamma^{-1}\left(\theta_1 - \frac{q}{1-\varepsilon}\tilde{\eta}\right) + \Gamma^{-2}\left[-\left(\theta_2 + \frac{q}{\gamma}\frac{\varepsilon}{n_g}\frac{\sqrt{\varepsilon}}{\varepsilon^2\beta - n_g}\right)e^{-\sqrt{\frac{n_g}{\varepsilon}}\tilde{\eta}} + \right.$$

$$\theta_2 + \frac{q}{\gamma}\frac{1}{n_g\sqrt{\varepsilon\beta}} + \left(\frac{q}{\gamma}\frac{1}{2(1-\varepsilon)}\left(1 + \frac{1-\varepsilon Pr}{\varepsilon\beta Pr}\gamma\right) + \theta_1\left(\frac{\sqrt{\pi\gamma}-\sqrt{2}}{\sqrt{\pi\gamma}}\right)\right)\tilde{\eta} +$$

$$\left.\frac{q}{\gamma}\frac{e^{-\sqrt{\varepsilon\beta}\tilde{\eta}}}{\sqrt{\varepsilon\beta}\,(\varepsilon^2\beta - n_g)}\right] + O(\Gamma^{-3}). \tag{3.59}$$

From the matching conditions expressed by Equations (3.56) and (3.57) the temperature at the stagnation-point and its correction, as a function of the removed heat q, are obtained:

$$\theta_0 = 1 + q\sqrt{\frac{\pi}{2\varepsilon(1-\varepsilon)}}, \tag{3.60}$$

$$\theta_1 = \frac{q}{2\varepsilon}\left(\frac{\varepsilon}{1-\varepsilon}\right)^2\frac{\sqrt{\pi\gamma}}{\sqrt{\pi\gamma}-\sqrt{2}}\left(1 - \frac{1-\varepsilon Pr}{\varepsilon\beta Pr}\gamma\right). \tag{3.61}$$

Equation (3.60) points that the temperature at the stagnation-point increases as the heat flux from the wall to the system increases. It also points out an increase temperature at the wall by reducing the medium porosity. Lowering the porosity of the medium, the volume of solid increases - the solid fills the volume given by $(1-\varepsilon)$ -, and consequently the gas phase convective heat transfer decreases. The result is that the heat transfer becomes predominantly conductive by the solid phase. Since the length of the porous material is considered semi-infinite with a prescribed temperature on one "side", and a heat flux on the other side, the stationary solution for this material leads to an infinite temperature at the wall as $\varepsilon \to 0$. This behavior is captured by Equations (3.60) and (3.61). Equation (3.60) also shows that the temperature at the wall increases, as the porosity increases. This behavior is not physically correct. As the porosity is made large, the heat transfer becomes predominantly convective and conductive through the gas phase. Then, under this condition, the wall temperature does not go to infinite. This happens because the model is not valid for high porosities. The limit of this model can be roughly estimated by the

temperature correction θ_1, as will be seen subsequently.

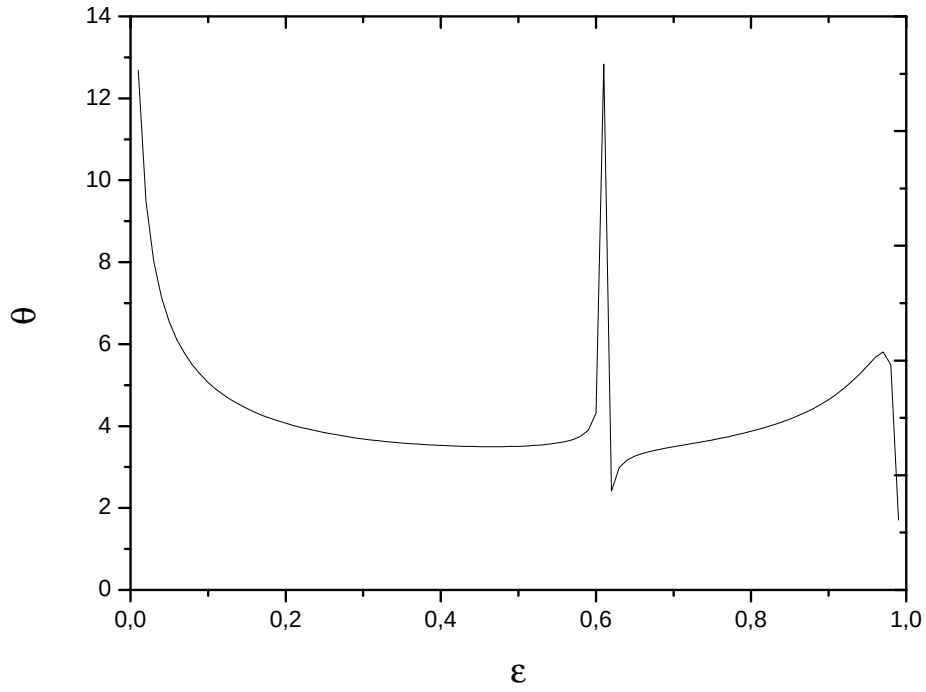

Figure 3.8 - Temperature at the wall $\times$ Porosity, $q = \beta = Pr = 1.0$.

The first correction to the stagnation-point temperature is given by Equation (3.61), and one must note that θ_1 is negative, since the last term in the parentheses is larger than one. The heat flux from the wall appears as a boundary condition, as can be seen in Equation (3.55), and its value q is assumed to be of the order of unity and having none corrections, since its value is assumed to be known. Under this feature, one observes that Equation (3.55) points out that all heat provided by the wall goes to the solid phase, in a first approximation. In this scenario, we are overestimating the temperature at the stagnation-point, since we are not considering the existence of a small heat flux from the wall to the gas phase, in a first approximation. The negative value for θ_1 compensates this fact. Equation (3.61) is a correction of order Γ^{-1} for Equation (3.60), except in the limits of $\varepsilon \sim 1$, $\varepsilon \sim 0$ and $\sqrt{\pi\gamma} \sim \sqrt{2}$. At these limits, θ_1 diverges and becomes as significant as the leading order term θ_0. The first two limits are compatible with the limits presented before for the leading order

term θ_0, but the third is not. With the condition $\sqrt{\pi\gamma} \sim \sqrt{2}$ it is possible to obtain an estimative for the porosity value at which the proposed model fails. This limit leads to an estimated limiting value of porosity, given by $\varepsilon < \pi/(2+\pi) \sim 0.6$, at which the proposed model is valid. The dependence of the temperature with porosity is presented in Figure (3.8).

In order to obtain the value for θ_2, appearing in Equations (3.58) and (3.59), one must evaluate the temperature solution of the order of Γ^{-3}. This procedure results in a new constant θ_3. This constant is obtained by the term of order Γ^{-4}, and so on. The main goal in this analysis was to show that the non-equilibrium between solid phase and gas phase occurs only in higher order terms. In face of that, the constant θ_2 will not be obtained, although we reinforce that if one wishes to obtain it, one should evaluate the result for $\theta_{s(3)}$ and $\theta_{g(3)}$ and apply the boundary condition for the heat flux at the wall in these lower order terms.

3.5 Conclusions

A Hiemenz flow established inside a low porosity medium with high heat exchange between phases was analyzed in this chapter. Solutions for temperature, momentum and pressure fields were obtained analytically. When one considers the existence of a heat exchange between phases, the parameter $\Gamma = \bar{\lambda}_s/\bar{\lambda}_g$ emerges. Two different regions must be considered in this situation: an outer zone and an inner zone. Since the value of Γ is high, the perturbation method is applied to detail profiles in both zones. The large value of the parameter Γ points to physical processes occurring in different length scales, hence, the need to analyze two different zones.

The model studied in this chapter may be thought as a porous heat dissipator for cooling devices, e.g. electronic components. Two boundary condition cases are analyzed: a constant wall temperature and a constant wall heat flux. The first case is useful if the electronic component have a maximum operating temperature, and the second is useful when one is interested on removing a certain amount of heat from the components. The present results show that the porous medium is the main responsible from removing heat from the heated components, as pointed out by Equation (3.55), but it is also shown that the flowing gas have a key role in dissipating the removed heat. It is also shown that since in the inner zone $f \to 0$, the solution in the outer zone is sufficient to describe the problem considering a prescribed wall temperature. However, when one considers a constant wall heat

flux, it is necessary to treat the thermal process in the inner zone, since heat release occurs in this small region.

Calculations were performed assuming a low porosity medium and a high value for the interphase heat flux. The modeling fails when one increases the medium porosity, close to $\varepsilon < \pi/(2+\pi)$, but the proposed model opened an opportunity to explore a wider range of the space parameter by only modifying the order of magnitude of the parameter κ. The analysis presents a modification to include the Darcy term on the classical pressure expression that is able to describe the influence of the linear Darcy term. It is shown the importance of the description of the inner zone process for systems in which the heat flux at the wall is known.

It must be pointed that if one wishes to analyze a gas cooling system by means of a porous matrix, would only be necessary to change the sign of the term in the right-side in Equation (3.51).

4 EVAPORATION OF LOW-VOLATILE LIQUID FUEL INSIDE A POROUS MEDIUM

In the present chapter, the features of a liquid fuel evaporation inside a low porosity medium subjected to an impinging stream of hot oxidant is investigated using the asymptotic expansion method. A low volatile liquid fuel is assumed, hence a low vaporization regime is studied. High rates of heat transfer between liquid and solid, and between gas and solid, are also assumed. The problem is divided in two regions: a region of the porous matrix filled by gas flow, defined here as gas-solid region, and a region of the porous matrix filled by the low volatile liquid fuel, defined here as liquid-solid region. In the gas-solid region, two characteristic zones must be analyzed, an outer zone (correspondent to the solid thermal diffusivity) and an inner zone (correspondent to the gas thermal diffusivity), near the gas-liquid interface. In the outer zone, gas and solid phases are in thermal equilibrium due to the high rate of heat transfer between them, and a single equation may be assumed for the energy conservation. As the flow approaches the gas-liquid interface, the temperature profiles for both phases must be analyzed separately; and a two-equation model is required. In the liquid-solid region, two zones are also observed. In most part below the interface, liquid and solid phases are in thermal equilibrium, due to the high rate of heat transfer between them. The one-equation model is used to describe the gas and solid temperatures. Close to the liquid-gas interface there is a boiling zone in the liquid-solid region. In this zone the liquid fuel is at an approximately constant temperature and all the heat transferred to this region results in phase change. Since the solid does not have the constant temperature constraint, the thermal equilibrium between phases is not observed. Under this condition, a two-equation model is required.

When the conservation equation for the mass fraction is solved, an intermediary zone (between the outer and the inner zone) is required, in order that the matching procedure is accomplished. This intermediary zone is necessary only for the fuel mass fraction variable.

The results for the interface point out for a solid phase temperature higher than the liquid fuel temperature. As known, the vaporization rate is determined by the energy balance at the liquid-gas interface. Also, the results show the vaporization rate to be mainly controlled by the heat exchange between solid and liquid phases in the boiling zone.

Liquid fuel vaporization in free conditions is a non-efficient process, because it depends on heat transfer from the gas phase to the gas-liquid surface. But if a porous matrix is added to this system, the liquid fuel vaporization becomes an efficient process, because it will depends on the heat transfer from the solid phase, which is almost two orders of magnitude higher than that promoted by the gas phase.

4.1 Mathematical formulation

A stream of hot oxidant impinging on the surface of a liquid fuel pool is considered in this analysis. The proposed problem is divided in two regions: a region of the solid matrix filled by the gas, gas-solid region, and a region of the solid matrix filled by the liquid, liquid-solid region. Two spatial coordinates are considered for the model: $\bar{z}$, the spatial coordinate normal to the liquid surface, and $\bar{x}$, the spatial coordinate tangential to the liquid surface. The gas-liquid interface is located in the plane determined by $\bar{z} = 0$. An schematic representation of the analyzed geometry is given by Figure (4.1) (in which the inner and boiling zones are presented in the detail).

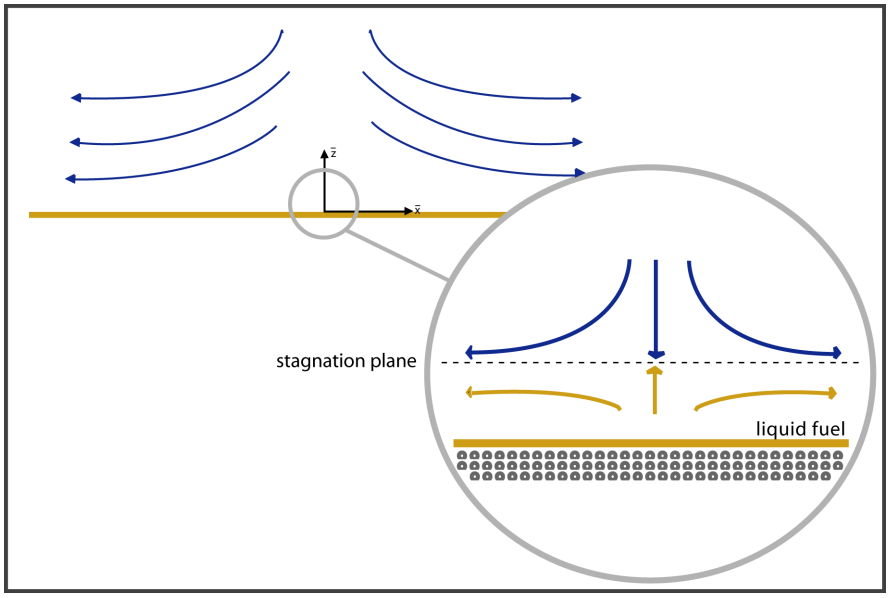

Figure 4.1 - Schematic diagram of the evaporation regime.

For the gas-solid region, the conservation equations are given by:

$$\frac{\partial \bar{u}}{\partial \bar{x}} + \frac{\partial \bar{v}}{\partial \bar{z}} = 0, \tag{4.1}$$

$$\rho \bar{u} \frac{\partial \bar{u}}{\partial \bar{x}} + \rho \bar{v} \frac{\partial \bar{u}}{\partial \bar{z}} = -\varepsilon \frac{\partial \bar{p}}{\partial \bar{x}} + \bar{\mu} \frac{\partial^2 \bar{u}}{\partial \bar{z}^2} - \varepsilon \bar{\mu} \frac{\bar{u}}{K}, \tag{4.2}$$

$$\varepsilon \rho \bar{v} \frac{dY_F}{d\bar{z}} = \varepsilon \rho \bar{D}_F \frac{d^2 Y_F}{d\bar{z}^2}, \tag{4.3}$$

$$\varepsilon \rho \bar{v} c_p \frac{dT_g}{d\bar{z}} = \varepsilon \bar{\lambda}_g \frac{d^2 T_g}{d\bar{z}^2} + h_v (T_s - T_g), \tag{4.4}$$

$$0 = (1 - \varepsilon) \bar{\lambda}_s \frac{d^2 T_s}{d\bar{z}^2} - h_v (T_s - T_g). \tag{4.5}$$

The boundary conditions far from the interface ($\bar{z} \to +\infty$) are given by:

$$\bar{v} = \bar{v}_\infty, \quad \bar{u} = \bar{x} \left. \frac{d\bar{u}}{d\bar{x}} \right|_\infty, \quad T_g = T_s = T_\infty, \quad Y_F = 0, \tag{4.6}$$

and at the interface, at $\bar{z} = 0$, are given by:

$$\bar{v} = \bar{v}_0, \quad T_g = T_0, \quad T_s = T_{s0}, \quad Y_F = Y_{F0}. \tag{4.7}$$

The boundary conditions at the interface, $\bar{v}_0$, T_{s0} and Y_{F0} are unknown values of the problem, and are specified from the coupling of the solutions for the gas-solid region and for the liquid-solid region, at the interface $\bar{z} = 0$. The interface $\bar{z} = 0$ separates the liquid fuel, at $\bar{z} < 0$, from the gaseous fuel, at $\bar{z} > 0$. At the interface, liquid and gaseous fuel are approximately in equilibrium at the boiling temperature, T_B. Therefore, it is possible to consider $T_0 = T_B$, in which T_0 is the gaseous fuel temperature at $\bar{z} = 0^+$.

The velocity of the gas at the liquid surface, $\bar{v}_{0^+}$, is related with the vaporization rate, $\bar{\dot{m}}$, through:

$$\rho . \bar{v}_{0^+} = \rho_l . \bar{v}_{l0^-} = \bar{\dot{m}}, \tag{4.8}$$

in which the velocities $\bar{v}_{l0^-}$ and $\bar{v}_{0^+}$ represent the velocities of the liquid fuel and vapor fuel at the interface, respectively.

In the liquid-solid region, below $\bar{z} = 0$, the conservation equations are given by:

$$\rho_l \bar{v}_l = \dot{\bar{m}} \tag{4.9}$$

$$\varepsilon \rho_l \bar{v}_l c_l \frac{dT_l}{d\bar{z}} = \varepsilon \bar{\lambda}_l \frac{d^2 T_l}{d\bar{z}^2} + h_l (T_s - T_l) \tag{4.10}$$

$$0 = (1 - \varepsilon) \bar{\lambda}_s \frac{d^2 T_s}{d\bar{z}^2} - h_l (T_s - T_l) \tag{4.11}$$

The boundary conditions far below the interface, for $\bar{z} \to -\infty$ are given by:

$$T_l = T_s = T_{-\infty}, \quad \bar{v}_l = \bar{v}_{l-\infty}, \tag{4.12}$$

in which the injection velocity, $\bar{v}_{l-\infty}$, is such that the gas-liquid interface remains stationary at $\bar{z} = 0$.

At the interface, mass and energy conservation must be imposed, which are expressed respectively by:

$$\rho \bar{D}_F \frac{\partial Y_F}{\partial \bar{z}}\bigg|_{\bar{z}=0} = -(1 - Y_{F0})\, \rho \bar{v}|_{\bar{z}=0^+}\,, \tag{4.13a}$$

$$\varepsilon \bar{\lambda}_g \frac{dT_g}{d\bar{z}}\bigg|_{\bar{z}=0^+} = \rho \bar{v}|_{\bar{z}=0^+} L + \varepsilon\, \bar{\lambda}_l \frac{dT_l}{d\bar{z}}\bigg|_{\bar{z}=-\bar{z}_b} - h_l \int_{-\bar{z}_b}^{0^-} (T_s - T_l) d\bar{z}. \tag{4.13b}$$

From Equation (4.13b), it is possible to observe the existence of a region of thickness $\bar{z}_b$, just below the interface. In this region, phase change of the liquid occurs. The vaporization rate of the liquid is calculated from Equation (4.13b). The last term in the right-side of this equation accounts for the heat exchange between solid matrix and liquid in the phase change (boiling) zone of thickness $\bar{z}_b$. This heat exchange is the main responsible for the liquid phase change, as will be seen in the next sections.

4.1.1 Non-dimensional formulation

The governing equations are made non-dimensional according to definitions given in Chapter (2).

Performing the changes and transformations presented in Chapter (2) in Equations (4.1) - (4.5), and considering the hypotheses presented in Chapter (2) for the model,

the following set of equations for the gas-solid region are found:

$$U = \frac{df}{d\eta} \tag{4.14}$$

$$\frac{Pr}{\Gamma}\frac{d^3f}{d\eta^3} + f\frac{df^2}{d\eta^2} - \left(\frac{df}{d\eta}\right)^2 - \Gamma\varepsilon\beta Pr\frac{df}{d\eta} = -\varepsilon Pr\,(1+\beta\Gamma) \tag{4.15}$$

$$\frac{1}{\Gamma}\frac{d^2y_f}{d\eta^2} + Le_F f\frac{dy_f}{d\eta} = 0 \tag{4.16}$$

$$-\varepsilon f\frac{d\theta_g}{d\eta} = \frac{\varepsilon}{\Gamma}\frac{d^2\theta_g}{d\eta^2} + \Gamma\ n_g(\theta_s - \theta_g) \tag{4.17}$$

$$0 = (1-\varepsilon)\frac{d^2\theta_s}{d\eta^2} - \Gamma\ n_g(\theta_s - \theta_g) \tag{4.18}$$

in which Le_F is the Lewis number, defined by $Le_F \equiv \alpha_g/D_F$, a ratio between the thermal diffusivity and mass diffusivity.

The boundary conditions far above the interface, at $\eta \to \infty$ are given by:

$$\left.\frac{df}{d\eta}\right|_{+\infty} = U_\infty, \quad \theta_s = \theta_g = 1, \quad y_F = 0, \tag{4.19}$$

and at the interface, at $\eta = 0$:

$$\left.\frac{df}{d\eta}\right|_0 = f - f_0 = 0, \quad \theta_s - \theta_{s0} = \theta_g - \theta_0 = 0, \quad y_F = y_{F0}. \tag{4.20}$$

The injection condition $df/d\eta|_{+\infty} = U_\infty$ represent the initial resistance suffered by the horizontal component of the velocity field.

Performing the same variable changes in Equations (4.9) - (4.11), the following conservation equations for the liquid-solid region are obtained:

$$\varrho_l v_l = \dot{m} \tag{4.21}$$

$$\varepsilon J\frac{d^2\theta_l}{dz^2} - \varepsilon M\frac{d\theta_l}{dz} = -\Gamma^2\ n_l(\theta_s - \theta_l) \tag{4.22}$$

$$(1-\varepsilon)\frac{d^2\theta_s}{dz^2} = \Gamma^2\ n_l(\theta_s - \theta_l) \tag{4.23}$$

in which $\dot{m} \equiv \bar{\dot{m}}/\left(\rho_\infty \bar{v}_\infty\right)$, $M \equiv \dot{m}(c_l/c_p)$ and $J \equiv \bar{\lambda}_l/\bar{\lambda}_s$. The parameter J is the

ratio between the liquid fuel and the solid matrix thermal conductivities, and it is of the order of unity. It must be pointed out that since the liquid is considered to be low volatile, the evaporative regime is determined by a low vaporization rate. As a consequence of this feature, it will be seen that $M = O(\Gamma^{-1})$.

The boundary conditions far below the interface, for $z \to -\infty$, are given by:

$$\theta_l = \theta_s = \theta_{-\infty}. \tag{4.24}$$

Mass and energy conservation at the interface are expressed by:

$$\frac{1}{\Gamma}\frac{1}{Le_F}\left.\frac{dy_F}{d\eta}\right|_{\eta=0^+} = (1 - y_{F0})\, f|_0\,, \tag{4.25a}$$

$$\frac{\varepsilon}{\Gamma}\left.\frac{d\theta_g}{d\eta}\right|_{\eta=0^+} = -l\, f|_0 + \varepsilon\frac{J}{a^{1/2}}\left.\frac{d\theta_l}{dz}\right|_{z=-z_b} - \frac{N_l}{a^{1/2}}\int_{-z_b}^{0}(\theta_s - \theta_l)dz. \tag{4.25b}$$

Since $\Gamma \gg 1$, and knowing that $l = O(\Gamma)$, $J = O(1)$ and $N_l = O(\Gamma)$ (from the hypotheses assumed in Chapter (2)), a quick analysis in Equation (4.25b) reveals that the the solid matrix is the main responsible for providing heat to the liquid fuel. This characteristic indicates that the inclusion of a porous matrix into the system leads to an enhancement on the vaporization rate.

The vaporization rate is related to f_0 by:

$$-\,a^{1/2}\, f|_0 = \dot{m} \tag{4.26}$$

In the proposed model, the boundary values at the interface, θ_{s0}, $f|_0$ and y_{F0}, are unknown values of the problem. The main goal of the present analysis is to calculate the vaporization rate and to exhibit the influence of the porous medium in the heavy liquid evaporation.

4.2 Gas-solid region

Above the interface, $\eta > 0$, a gas flow is considered. The analysis presented here is similar to the analysis presented in Chapter (3).

Far above the interface the velocity field is imposed only by the hot oxidant stream,

but close to the gas-liquid interface, the velocity field is imposed uniquely by a plane-normal, low-rate vaporization. Two zones must be analyzed separately: one denoted as the outer zone, related to the solid phase thermal diffusivity, and one denoted the inner zone, related to the gas phase thermal diffusivity, that is close to the gas-liquid interface. In the outer zone, of unitary order (since the spatial scale was non-dimensionalized with respect to the solid phase thermal diffusivity length scale), gas and solid phase are in thermal equilibrium due to the high value of the interphase heat transfer (as can be seen from $N_g = O(\Gamma)$), and the macroscopic viscous effects due to the liquid-gas interaction are not observed (similar to the case studied in Chapter (3)). Because of the thermal equilibrium, a one-equation model for energy conservation is used. In the inner zone, of the order Γ^{-1} and close to the interface, the thermal equilibrium is no longer satisfied, and the macroscopic viscous effects become relevant. In this zone, a two-equation model for the energy conservation is required, in order to account for the thermal non-equilibrium between gas and solid phases. In order to analyze the inner zone, a boundary-layer expansion must be performed for the η spatial variable.

Solutions for both regions are obtained by utilizing the singular perturbation method (NAYFEH, 1981; HOLMES, 1995), and the matching between inner zone and outer zone profiles is imposed.

4.2.1 Outer zone: problem of the order of unity

In a region of the order of unity above the gas-liquid interface, momentum and temperature profiles are obtained from Equations (4.15) - (4.18) . Summing Equations (4.17) and (4.18) and substituting $\theta_s = \theta_g = \theta$, since thermal equilibrium is assumed in the outer zone, a single equation for the energy conservation is obtained:

$$\Gamma^{-1}\theta'' + \gamma\theta'' + f\theta' = 0 \tag{4.27}$$

where for the sake of compactness was defined $\gamma = (1-\varepsilon)/\varepsilon$ as the porosity parameter, and the prime denotes differentiation with respect to η.

Solutions for momentum and energy are expressed as:

$$\left.\begin{aligned} f &= f_{(0)} + \Gamma^{-1} f_{(1)} + O(\Gamma^{-2}), \\ \theta &= \theta_{(0)} + \Gamma^{-1}\theta_{(1)} + O(\Gamma^{-2}). \end{aligned}\right\} \tag{4.28}$$

Substituting the proposed solutions in Equations (4.15) and (4.27), and collecting terms of the same power of Γ, the following set of equations for the first two components of the momentum and the temperature are obtained:

$$f'_{(0)} = 1 \tag{4.29a}$$

$$f_{(0)} f''_{(0)} - \left(f'_{(0)}\right)^2 - \varepsilon Pr \beta f'_{(1)} = -\varepsilon Pr \tag{4.29b}$$

$$\gamma \theta''_{(0)} + f_{(0)} \theta'_{(0)} = 0 \tag{4.29c}$$

$$\gamma \theta''_{(1)} + f_{(0)} \theta'_{(1)} + \theta''_{(0)} + f_{(1)} \theta'_{(0)} = 0 \tag{4.29d}$$

The boundary conditions far from the interface, for $\eta \to \infty$, are given by:

$$f'_{(0)} - 1 = f'_{(1)} - U_1 = 0, \quad \theta_{(0)} - 1 = \theta_{(1)} = 0, \tag{4.30}$$

and the boundary conditions at the interface, $\eta = 0$, analyzing from the outer zone, are given by:

$$f_{(0)} = f_{(1)} = 0, \quad \theta_{(0)} - \theta_{s0} = \theta_{(1)} = 0 \tag{4.31}$$

In the outer zone, the effect of the low vaporization can not be observed on the flow field, since it occurs in the inner zone and is of the order of Γ^{-1}. In this zone, the solid phase is the main responsible for the heat transport, and hence, when the flow observes the inner zone, from the outer zone, the solid phase temperature at the interface is observed (together with its correction θ_{s1}). The boundary values of f' for $\eta \to \infty$ are found by substituting the expansion of f in Equation (4.14) and applying the limit $\eta \to \infty$, obtaining, hence, $f' = 1 + \Gamma^{-1} U_1 + O(\Gamma^{-2})$ at $\eta \to \infty$. The first term of such expansion, 1, represents the classical Hiemenz flow boundary condition, while the second indicates the influence of the solid matrix on the strain-rate (the same as seen in Chapter (3)).

Solving the above set of equations with the boundary conditions given by Equations (4.30) and (4.31), momentum and temperature profiles in the outer zone are determined as:

$$f(\eta) = \eta - \Gamma^{-1} \frac{1 - \varepsilon Pr}{\varepsilon \beta Pr} \eta + O(\Gamma^{-2}) \tag{4.32a}$$

$$\theta(\eta) = \theta_{s0} + (1 - \theta_{s0}) erf\left(\frac{\eta}{\sqrt{2\gamma}}\right) - \Gamma^{-1} \left[\frac{(1 - \theta_{s0})}{2\gamma} \sqrt{\frac{2}{\pi\gamma}} \left(1 + \frac{1 - \varepsilon Pr}{\varepsilon \beta Pr} \gamma\right) \eta \, e^{-\eta^2/2\gamma} +\right]$$

$$O(\Gamma^{-2}) \tag{4.32b}$$

The value of θ_{s0} will be calculated from the solid phase heat flux continuity condition at the gas-liquid interface. It is important to emphasize that from the outer zone the evaporating effects are not captured, as exhibited by the boundary conditions expressed in Equation (4.31). This feature, as explained before, is due to the fact that in the proposed problem a low-vaporization regime is established, as a result of the assumption of a low-volatile liquid fuel, confining the evaporating effects to the inner zone.

The profile for the temperature in the outer zone is presented in Figure (4.2). The solid phase temperature at the interface is found through the condition of continuity of the heat flux at the interface, and it is used to present the figures in the following, although such temperature is only to be obtained at the end of the calculations. The reader is referred to the Section (4.5) in order to obtain the solid phase temperature at the interface.The momentum profile is exactly the same as the one obtained in Chapter (3) and presented in Figure (3.2).

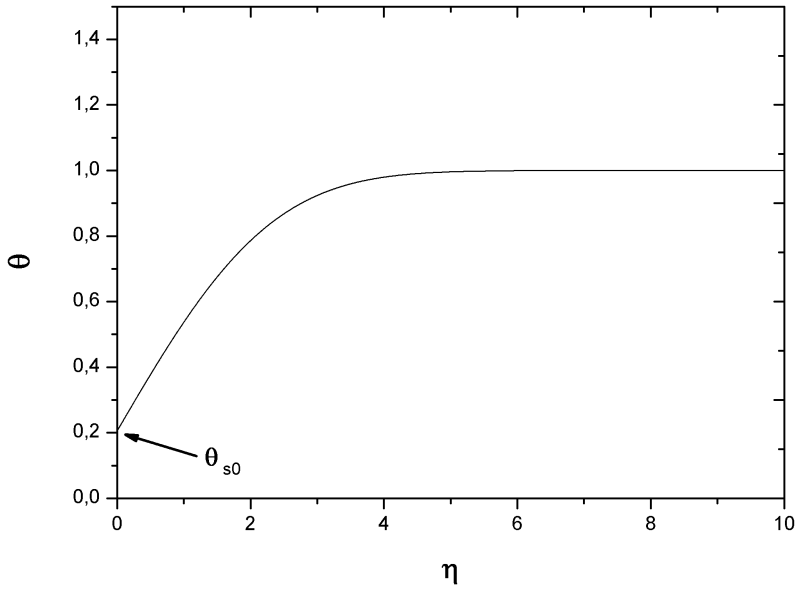

Figure 4.2 - Temperature in the outer zone, $\theta_{s0} \simeq 0.206$, $\varepsilon = 0.3$, $Pr = \beta = 1.0$.

In the outer zone, thermal equilibrium between solid and gas is observed. Both phases sense an exponential decrease in its temperature, as pointed by Equation (4.32b) and Figure (4.2), since heat is used to vaporize the liquid below $\eta = 0$. The thermal non-equilibrium between phases is only observed in the inner zone, as will be seen in the next section.

4.2.2 Inner zone: problem of the order of Γ^{-1}

In a characteristic spatial length scale of the order of Γ^{-1}, the macroscopic viscous effects due to the gas-liquid interaction, as well as the thermal non-equilibrium between gas and solid phases, are observed. In order to capture such variations, a stretching in the spatial coordinate is necessary. This spatial coordinate change corresponds to a boundary-layer expansion near the interface gas-liquid, and is given by $\tilde{\eta} = \Gamma\eta$. As the flow approaches the stagnation-point from above, a decrease in the velocity field is seen, and below the stagnation-point, the velocity field is a result of the low-rate vaporization of the liquid . Hence, in the inner zone, near the interface, a re-scaling in the momentum variable is required and given by $\tilde{f} = \Gamma f$, since in this region the velocity field is of the order of Γ^{-1}. It also must be considered that in the inner zone thermal equilibrium is no longer satisfied, and, hence, a two-equation model for the energy is required to follow the variation of the temperatures.

After performing the spatial stretching, the equations to be solved are given by:

$$\Gamma Pr\tilde{f}''' + \tilde{f}\tilde{f}'' - \Gamma^2\left(\tilde{f}'\right)^2 - \Gamma\varepsilon\beta Pr\tilde{f}' = -\varepsilon Pr\left(1+\beta\Gamma\right), \tag{4.33}$$

$$\Gamma\varepsilon\tilde{\theta}_g'' + \varepsilon\tilde{f}\tilde{\theta}_g' = -\Gamma\ n_g\left(\theta_s - \theta_g\right), \tag{4.34a}$$

$$\Gamma^2(1-\varepsilon)\theta_s'' = \Gamma\ n_g\left(\theta_s - \theta_g\right), \tag{4.34b}$$

in which the prime now denotes differentiation with respect to $\tilde{\eta}$. The solutions are proposed to be expressed as:

$$\left.\begin{aligned} \tilde{f} &= \tilde{f}_{(0)} + \Gamma^{-1}\tilde{f}_{(1)} + O(\Gamma^{-2}), \\ \theta_g &= \theta_{g(0)} + \Gamma^{-1}\theta_{g(1)} + O(\Gamma^{-2}), \\ \theta_s &= \theta_{s(0)} + \Gamma^{-1}\theta_{s(1)} + O(\Gamma^{-2}). \end{aligned}\right\} \tag{4.35}$$

Substituting the momentum solution in Equation (4.33) and collecting the terms

with similar powers, the following set of governing equations are obtained:

$$\tilde{f}'''_{(0)} - \varepsilon\beta\left(\tilde{f}'_{(0)} - 1\right) = 0, \tag{4.36a}$$

$$Pr\,\tilde{f}'''_{(1)} + \tilde{f}_{(0)}\tilde{f}''_{(0)} - \left(\tilde{f}'_{(0)}\right)^2 - \varepsilon\beta Pr\,\tilde{f}'_{(1)} = -\varepsilon Pr, \tag{4.36b}$$

that must be solved with boundary conditions at $\tilde{\eta} = 0$ given by:

$$\tilde{f}_{(0)} = \tilde{f}_0, \quad \tilde{f}_{(1)} = 0, \tag{4.37}$$

$$\left.\frac{d\tilde{f}_{(0)}}{d\tilde{\eta}}\right|_{\tilde{\eta}=0} = \left.\frac{d\tilde{f}_{(1)}}{d\tilde{\eta}}\right|_{\tilde{\eta}=0} = 0 \tag{4.38}$$

The utilization of the boundary-layer expansion near the interface imposes that the solutions from the inner zone must obey a matching flux condition with the solutions from the outer zone. So, in addition to the boundary conditions presented before, the solutions of Equations (4.36a) and (4.36b) must obey a matching condition with the outer zone as:

$$\left.\frac{d\tilde{f}_{(0)}}{d\tilde{\eta}}\right|_{\tilde{\eta}\to+\infty} = \left.\frac{df_{(0)}}{d\eta}\right|_{\eta=0}, \quad \left.\frac{d\tilde{f}_{(1)}}{d\tilde{\eta}}\right|_{\tilde{\eta}\to+\infty} = \left.\frac{df_{(1)}}{d\eta}\right|_{\eta=0}. \tag{4.39}$$

When Equations (4.36a) and (4.36b) are solved with the boundary and matching conditions given by Equations (4.37) - (4.39), the momentum in the inner zone is obtained as:

$$\begin{aligned}\tilde{f}(\tilde{\eta}) = \tilde{f}_0 + \tilde{\eta} + \frac{1}{\sqrt{\varepsilon\beta}}\left(e^{-\sqrt{\varepsilon\beta}\tilde{\eta}} - 1\right) + \frac{\Gamma^{-1}}{8\varepsilon\beta Pr}\left[\frac{7}{\sqrt{\varepsilon\beta}}\left(e^{-\sqrt{\varepsilon\beta}\tilde{\eta}} - 1\right) - 6\tilde{\eta}\;e^{-\sqrt{\varepsilon\beta}\tilde{\eta}} - \right.\\ 8(1-\varepsilon Pr)\tilde{\eta} - 2\left(\frac{1}{\sqrt{\varepsilon\beta}} + \tilde{f}_0\right)(3 + 2\sqrt{\varepsilon\beta}\tilde{\eta})\;e^{-\sqrt{\varepsilon\beta}\tilde{\eta}} + 6\left(\frac{1}{\sqrt{\varepsilon\beta}} + \tilde{f}_0\right) - \\ \left. 2\sqrt{\varepsilon\beta}\tilde{\eta}^2\;e^{-\sqrt{\varepsilon\beta}\tilde{\eta}} - \frac{1}{\sqrt{\varepsilon\beta}}\left(7 - 8\varepsilon Pr - \sqrt{\varepsilon\beta}\tilde{f}_0\right)\left(1 - e^{-\sqrt{\varepsilon\beta}\tilde{\eta}}\right)\right] + O(\Gamma^{-2})\end{aligned} \tag{4.40}$$

The horizontal component of the velocity may be calculated by deriving Equation (4.40) with respect to $\tilde{\eta}$. Note that, at the interface, the horizontal component of the velocity is zero, since near $\tilde{\eta} = 0$ the velocity field is a result of the liquid fuel vaporization, and this process is characterized by an abrupt phase change, with the

expanding gas having only normal component.

The behavior pointed by Equation (4.40) is observed in Figure (4.3). The vaporization rate, to be obtained in Section (4.5), is exhibited in Figure (4.3).

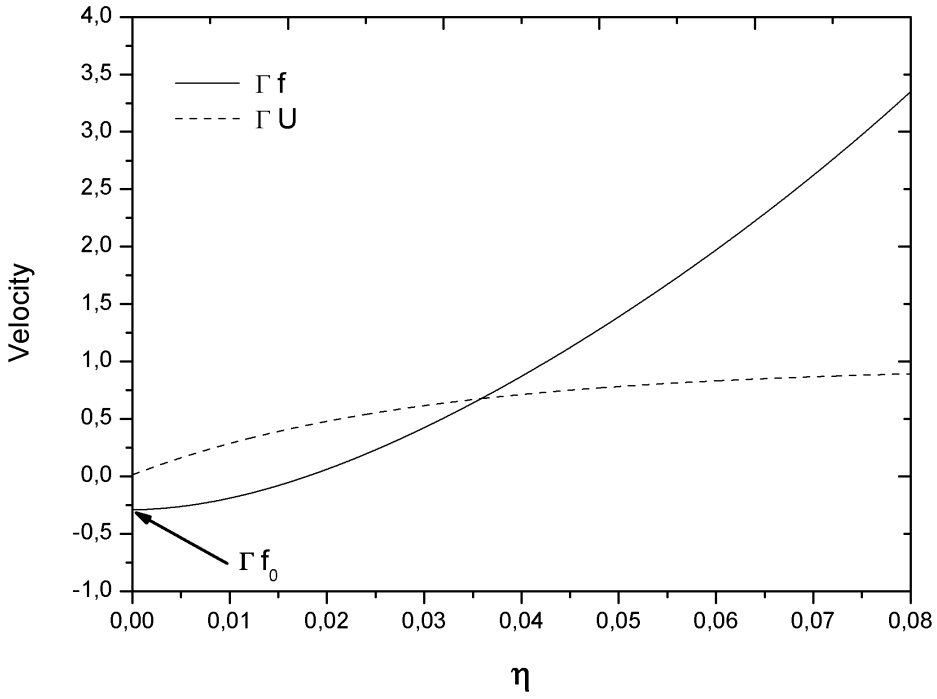

Figure 4.3 - Velocity in the inner zone, $\tilde{f}_0 \simeq -0.29$, $\varepsilon = 0.3$, $\beta = Pr = 1.0$, $\Gamma = 60.0$.

It is possible to visualize that the macroscopic viscous effects are only observed in the inner zone.

Substituting the solutions for the temperatures given in (4.35) in Equations (4.34a) and (4.34b), two sets of governing equations are obtained:

$$(1-\varepsilon)\theta''_{s(0)} = 0, \tag{4.41a}$$

$$(1-\varepsilon)\theta''_{s(1)} = n_g\left(\theta_{s(0)} - \theta_{g(0)}\right), \tag{4.41b}$$

which must satisfy boundary conditions at $\tilde{\eta} = 0$ given by:

$$\theta_{s(0)} - \theta_{s0} = \theta_{s(1)} = 0, \tag{4.42}$$

and matching flux condition with the outer zone:

$$\left.\frac{d\theta_{s(0)}}{d\tilde{\eta}}\right|_{+\infty} = 0, \quad \left.\frac{d\theta_{s(1)}}{d\tilde{\eta}}\right|_{+\infty} = \left.\frac{d\theta_{(0)}}{d\eta}\right|_{0}. \tag{4.43}$$

The solutions of Equations (4.41a) and (4.41b) with the boundary and matching conditions given in Equations (4.46) and (4.47) provide the solid phase temperature profile in the inner zone as:

$$\theta_s(\tilde{\eta}) = \theta_{s0} + \Gamma^{-1}\left[(1-\theta_{s0})\sqrt{\frac{2}{\pi\gamma}}\,\tilde{\eta} + \frac{(\theta_{s0}-\theta_B)}{\gamma\; n_g}\left(e^{-\sqrt{n_g/\varepsilon}\;\tilde{\eta}} - 1\right)\right] + O(\Gamma^{-2}) \tag{4.44}$$

Note that, in the inner zone, the solid phase temperature is constant in its leading order, at the value of θ_{s0}, then, variations in the solid matrix temperature occur only at orders of Γ^{-1} and higher. The difference between solid phase temperature and gas phase temperature at the interface, θ_{s0} and θ_B, respectively, is of the order Γ^{-1}. To exhibit that, it is recalled that the both temperatures are equal in the outer zone and the thermal non-equilibrium is found in the inner zone, with a thickness of order of the Γ^{-1}. And since there are no sink or source heat terms, the difference between the gas and solid temperatures must be of the order of Γ^{-1}.

For the gas phase in the inner zone, the following set of governing equations are valid:

$$\varepsilon\theta''_{g(0)} = -n_g\left(\theta_{s(0)} - \theta_{g(0)}\right), \tag{4.45a}$$

$$\varepsilon\theta''_{g(1)} + \varepsilon\tilde{f}_{(0)}\theta'_{g(0)} = -n_g\left(\theta_{s(1)} - \theta_{g(1)}\right), \tag{4.45b}$$

in which the boundary conditions at the interface, $\tilde{\eta} = 0$, are given by:

$$\theta_{g(0)} - \theta_B = \theta_{g(1)} = 0, \tag{4.46}$$

and the matching flux condition with the outer zone imposes that:

$$\left.\frac{d\theta_{g(0)}}{d\tilde{\eta}}\right|_{\tilde{\eta}\to+\infty} = 0, \quad \left.\frac{d\theta_{g(1)}}{d\tilde{\eta}}\right|_{\tilde{\eta}\to+\infty} = \left.\frac{d\theta_{(0)}}{d\eta}\right|_{\eta=0}. \tag{4.47}$$

Solving Equations (4.45a) and (4.45b) with the boundary and matching conditions given by Equations (4.46) and (4.47), the gas phase temperature in the inner zone is obtained as:

$$\theta_g(\tilde{\eta}) = \theta_{s0} - (\theta_{s0} - \theta_B)\, e^{-\sqrt{n_g/\varepsilon}\tilde{\eta}} + \Gamma^{-1}\left\{(1-\theta_{s0})\sqrt{\frac{2}{\pi\gamma}}\,\tilde{\eta} + \right.$$

$$\frac{(\theta_{s0}-\theta_B)}{\gamma\, n_g}\left(e^{-\sqrt{n_g/\varepsilon}\tilde{\eta}} - 1\right) + \frac{(\theta_{s0}-\theta_B)}{4}\sqrt{\frac{\varepsilon}{n_g}}\,\tilde{\eta}\, e^{-\sqrt{n_g/\varepsilon}\tilde{\eta}}\left[1 + \frac{2}{1-\varepsilon} + \right.$$

$$\left.\sqrt{\frac{n_g}{\varepsilon}}\left(2\tilde{f}_0 - \frac{1}{\sqrt{\varepsilon\beta}} + 1\right)\right] - \sqrt{\frac{n_g}{\varepsilon}}\frac{(\theta_{s0}-\theta_B)}{\varepsilon\beta}\left(\frac{1}{2\sqrt{n_g/\varepsilon} + \sqrt{\varepsilon\beta}}\right) \times$$

$$\left. e^{-\sqrt{n_g/\varepsilon}\tilde{\eta}}\left(e^{-\sqrt{\varepsilon\beta}\tilde{\eta}} - 1\right)\right\} + O(\Gamma^{-2}) \tag{4.48}$$

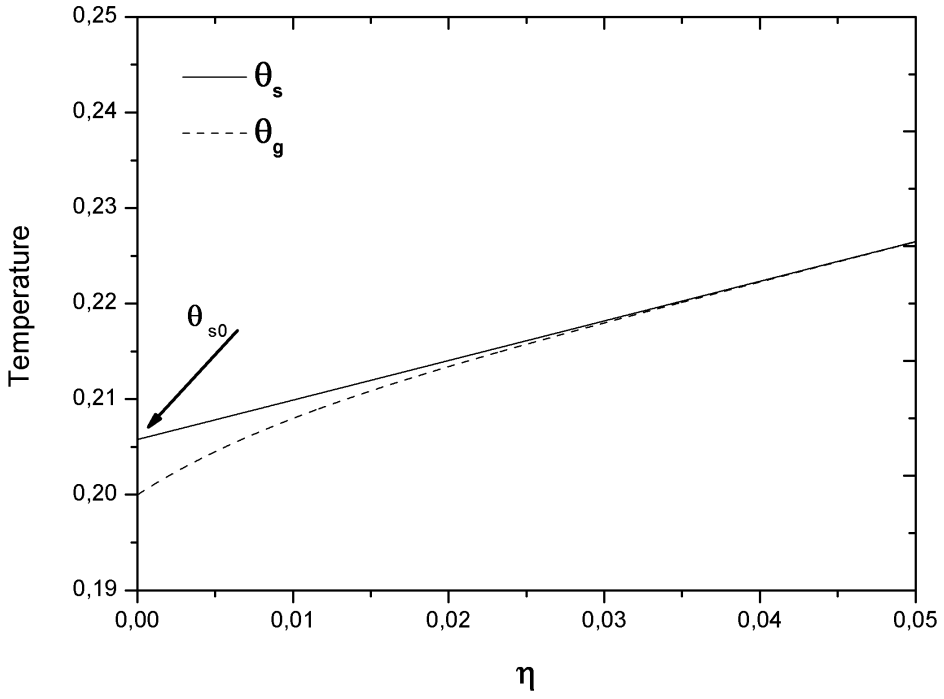

Figure 4.4 - Temperatures in the outer zone, $\theta_B = 0.2$, $\theta_{s0} \simeq 0.206$, $\varepsilon = 0.3$, $n_g = \beta = 1.0$, $\Gamma = 60.0$.

The temperature profiles for gas and solid phases are presented in Figure (4.4). The solid phase temperature up to this point is an unknown value, because θ_{s0} will be determined at the end of Section (4.5). However that result is used here for sake of exhibiting the behavior of the gas and solid temperatures and the effect of the heat transfer between the phases (non-equilibrium condition).

4.3 Liquid-solid region

In the liquid solid region, $\eta < 0$, the solid matrix is filled by the liquid fuel. The liquid flow obeys a simple configuration in this region, and the analysis will focus on the thermal interactions between the phases. Like the gas-solid region, two zones also exist. In most part of the liquid-solid region liquid fuel and solid matrix are in thermal equilibrium because of the long contact time, then a one-equation model is enough for describing the temperature profile. As the liquid flow approaches the interface, liquid and solid temperatures become different. In a length scale of order Γ^{-1} near the interface, the liquid fuel remains at an almost constant temperature, its boiling temperature, and all the heat provided to the liquid phase is used in phase change. The solid phase, on the other hand, does not have such physical constraint, and its temperature continues to raise as result of the heat flux coming from the gas-solid region. The thermal description for the boiling zone is made employing the two-equation model.

4.3.1 Equilibrium zone: problem of the order of unity

In a region of the order of unity below the interface, thermal equilibrium between solid and liquid phases is found, and a single equation for the energy conservation is required. Summing Equations (4.22) and (4.23) and considering $\theta_s = \theta_l = \theta$, as a result of the thermal equilibrium, the following governing equation is obtained:

$$\left(\frac{J+\gamma}{M}\right)\frac{d^2\theta}{dz^2} - \frac{d\theta}{dz} = 0 \tag{4.49}$$

and the boundary conditions far below the interface are given by $\theta = \theta_{-\infty}$ for $z \to -\infty$, and $\theta = \theta_{s0}$ at $z = 0$. Solving Equation (4.49) with the boundary conditions given above, the temperature profile in the equilibrium zone is obtained as:

$$\theta(z) = (\theta_{s0} - \theta_{-\infty})\, e^{zM/(J+\gamma)} + \theta_{-\infty} \tag{4.50}$$

It must be remembered that the vaporization rate parameter, M, is directly related with the vaporization rate, $\dot{m}$, thus $M \sim \Gamma^{-1}$. Therefore, only at a large distance from the interface the exponential behavior of the temperature is noted. Such behavior may be observed in Figure (4.5).

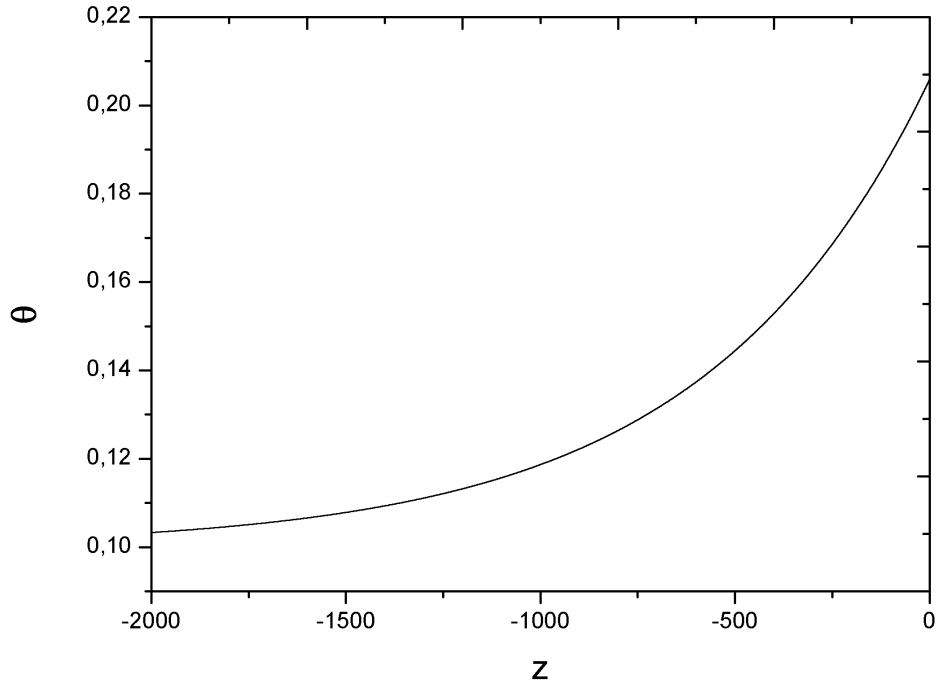

Figure 4.5 - Temperature in the equilibrium zone, $\theta_{s0} \simeq 0.206$, $\theta_{-\infty} = 0.1$, $J = 1.0$, $\varepsilon = 0.3$, $M \simeq 0.005$.

The parameter M is related with the vaporization rate through $M = -\Gamma^{-1} a^{1/2} (c_l/c_p) \tilde{f}_0$. As in previous sections, the vaporization rate and the solid phase temperature at the interface, used to plot Figure (4.5), are calculated in Section (4.5).

As the liquid flow approaches the interface, a detachment between solid and liquid temperatures becomes measurable. This zone is called boiling zone. The difference between the temperatures is due to the fact that the liquid fuel has a limiting value for its temperature, namely, the boiling temperature. When the liquid-solid system approaches this boiling temperature, the liquid fuel ceases to increase its

temperature, and all heat provided to it goes to phase change. The solid matrix, on the other hand, does not have such physical constraint, and its temperature increases in the boiling zone. The result is that at the interface, the solid phase has a higher temperature than the liquid fuel. It will be seen forward that in the boiling zone the heat exchange between solid and liquid phases is the main responsible for providing the necessary heat to vaporize the liquid fuel.

4.3.2 Boiling zone: problem of the order of Γ^{-1}

In a characteristic spatial length scale of the order of Γ^{-1} below the interface, thermal non-equilibrium is observed between phases. In order to capture such variations, a stretching in the spatial coordinate change is necessary and given by $\tilde{z} = \Gamma z$. A two-equation model must be employed, so both Equations (4.22) and (4.23) must be used. The temperature solutions are expressed as:

$$\left.\begin{aligned} \theta_l(\tilde{z}) &= \theta_B + \Gamma^{-1}\theta_{l(1)} + O(\Gamma^{-2}), \\ \theta_s(\tilde{z}) &= \theta_{s(0)} + \Gamma^{-1}\theta_{s(1)} + O(\Gamma^{-2}). \end{aligned}\right\} \tag{4.51}$$

It must be noted that in the boiling zone the liquid is at an almost constant temperature, the boiling temperature, hence, the leading order expansion of θ_l is a constant value and variations occur only in its higher order terms. Substituting Equation (4.51) in Equations (4.22) and (4.23), after performing the stretching in the spatial coordinate and collecting equal powers, the following equations are found:

$$\varepsilon J \frac{d^2\theta_{l(1)}}{d\tilde{z}^2} = -n_l(\theta_{s(1)} - \theta_{l(1)}) \tag{4.52a}$$

$$(1-\varepsilon)\frac{d^2\theta_{s(0)}}{d\tilde{z}^2} = n_l(\theta_{s(0)} - \theta_B) \tag{4.52b}$$

$$(1-\varepsilon)\frac{d^2\theta_{s(1)}}{d\tilde{z}^2} = n_l(\theta_{s(1)} - \theta_{l(1)}) \tag{4.52c}$$

The above set of equations must obey boundary conditions at the interface, $\tilde{z} = 0$, given by:

$$\theta_{s(0)} - \theta_{s0} = \theta_{s(1)} = \theta_{l(1)} = 0, \tag{4.53}$$

and matching condition with the equilibrium zone giving:

$$\left.\frac{d\theta_{s(0)}}{d\tilde{z}}\right|_{\tilde{z}\to-\infty} = 0, \quad \left.\frac{d\theta_{s(1)}}{d\tilde{z}}\right|_{\tilde{z}\to-\infty} = \left.\frac{d\theta_{l(1)}}{d\tilde{z}}\right|_{\tilde{z}\to-\infty} = \left.\frac{d\theta}{dz}\right|_{z=0^-}. \tag{4.54}$$

Solving Equations (4.52a), (4.52b) and (4.52c) with the boundary and matching conditions given by Equations (4.53) and (4.54), the temperature solutions for the boiling zone are obtained, and expressed as:

$$\theta_l(\tilde{z}) = \theta_B + \Gamma^{-1}\left(\frac{M}{J+\gamma}(\theta_{s0} - \theta_{-\infty})\tilde{z}\right) + O(\Gamma^{-2}), \tag{4.55a}$$

$$\begin{aligned}\theta_s(\tilde{z}) = \theta_B + (\theta_{s0} - \theta_B)\ \ e^{\sqrt{n_l/(1-\varepsilon)}\tilde{z}} + \\ \Gamma^{-1}\left(\frac{M}{J+\gamma}(\theta_{s0} - \theta_{-\infty})\tilde{z}\right) + O(\Gamma^{-2}),\end{aligned} \tag{4.55b}$$

It must be pointed out that the terms M and $(\theta_{s0} - \theta_B)$ are of the order of Γ^{-1}, as mentioned previously. In the boiling zone, the liquid is at an almost constant temperature, the boiling temperature θ_B, and the variations in the liquid temperature are observed only in the terms of order Γ^{-1} and higher.

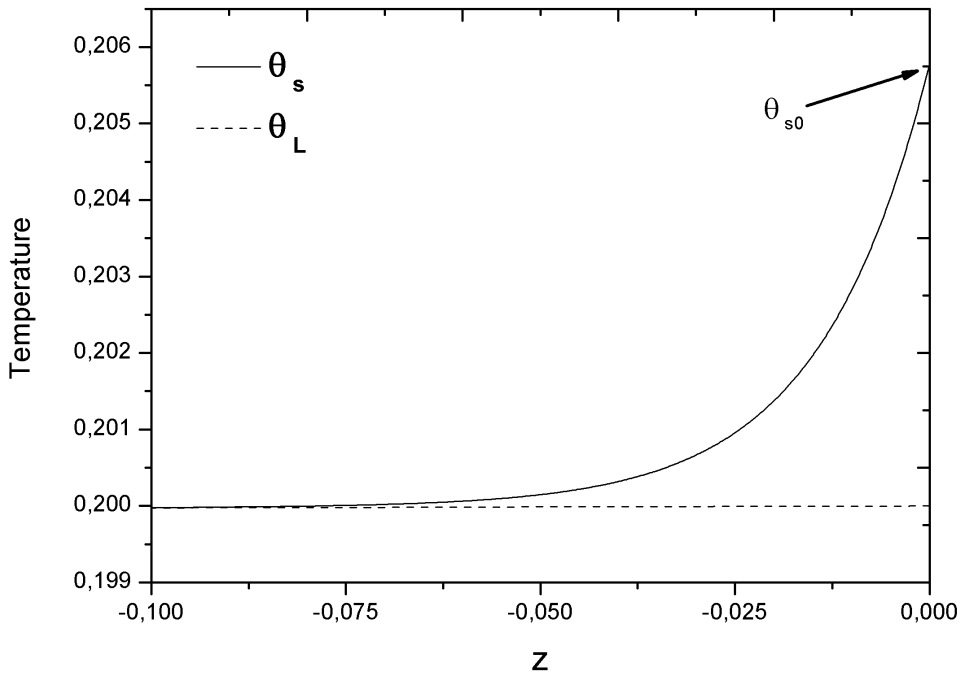

Figure 4.6 - Temperatures in the boiling zone, $\theta_{s0} \simeq 0.206$, $\theta_B = 0.2$, $\theta_{-\infty} = 0.1$, $\varepsilon = 0.3$, $J = n_l = 1.0$, $M \simeq 0.005$, $\Gamma = 60.0$.

The temperature profiles for solid phase and liquid fuel in the boiling zone are presented in Figure (4.6).

The solid matrix conducts heat from the gas-solid region to the liquid-solid region. The large contact area between liquid and solid provides an intense interphase heat transfer, enhancing the vaporization regime. In the next section this heat exchange and its effect on the vaporization rate is quantified, through the energy conservation at the interface.

The difference between solid and liquid phases temperature in the boiling zone is the main responsible for providing the heat necessary to phase change of the low-volatile fuel, as will be seen in the next sections.

4.4 Fuel mass fraction

In a small region above the interface the flow field is a result from the convection of gaseous fuel, that arises from the liquid fuel phase change occurring in the boiling zone. The fuel mass fraction is governed by Equation (4.16), with the following boundary conditions:

$$y_F(\eta \to +\infty) = 0, \quad y_F(\eta = 0) = y_{F0}. \tag{4.56}$$

Also, at the interface, mass conservation is given by:

$$\frac{1}{\Gamma}\frac{1}{Le_F}\left.\frac{dy_F}{d\eta}\right|_{\eta=0^+} = (1 - y_{F0})\, f|_0\,. \tag{4.57}$$

The mass fraction at the interface, y_{F0}, is unknown, but it must be small, since the fuel is considered to be low volatile. Fuel mass transport occurs in two regimes: convection and diffusion. The convection process is due to the velocity field of the gas flow. So, as in the momentum solution, the fuel mass fraction must be solved in the outer zone and in the inner zone. However, an intermediary zone is required for the fuel mass fraction solution, as will be seen in the following.

4.4.1 Outer zone: problem of the order of unity

The equation to be solved for the fuel mass fraction is given by:

$$\frac{1}{\Gamma}\frac{d^2 y_f}{d\eta^2} + Le_F f \frac{dy_f}{d\eta} = 0. \tag{4.58}$$

The boundary condition to be obeyed is:

$$y_F(\eta \to +\infty) = 0. \tag{4.59}$$

The solution of Equation (4.58) is expressed as:

$$y_F = y_{F(0)} + \Gamma^{-1} y_{F(1)} + O(\Gamma^-2) \tag{4.60}$$

Substituting Equation (4.60) in Equation (4.58), collecting the terms of similar order of magnitude and solving the resulting set of equations with the boundary condition given in Equation (4.59), it is found that in the outer zone, the fuel mass fraction is null for every η:

$$y_F(\eta) = 0. \tag{4.61}$$

Since the fuel is considered to be low volatile ($l = O(\Gamma)$), the vaporization regime is low (as observed in the last section), and as a result, no fuel is observed in the outer zone, as pointed by Equation (4.61).

In order to observe the fuel mass fraction, the analysis must be made in the inner zone. The spatial coordinate must then be stretched as $\tilde{\eta} = \Gamma\eta$, and Equation (4.58) must be analyzed in this new coordinate. However, the matching procedure is not achievable between outer and inner zone for the fuel mass fraction variable. This demands an analysis in an intermediary zone, of the order of $\Gamma^{1/2}$, between outer and inner zone, in order that the matching flux between zones is obeyed.

4.4.2 Intermediary zone: problem of the order of $\Gamma^{-1/2}$

The intermediary zone, necessary only for the fuel mass fraction variable, is analyzed by a stretching in the spatial coordinate, given by $\hat{\eta} = \Gamma^{1/2}\eta$, in Equation (4.58). The momentum in this zone is also re-scaled as $\hat{f} = \Gamma^{1/2} f$, and a quick inspection in Equation (4.15) reveals that the momentum in the intermediary zone will be similar to the profile in the outer zone, as given in Equation (4.32a), but with the independent variable being $\hat{\eta}$ instead of η.

The fuel mass fraction conservation in the intermediary zone follows:

$$\frac{d^2\hat{y}_f}{d\hat{\eta}^2} + Le_F \hat{f} \frac{d\hat{y}_f}{d\hat{\eta}} = 0, \tag{4.62}$$

in which the "hat" notation in the fuel mass fraction variable is only to distinguish between zones. The solution of Equation (4.62) is expressed as:

$$\hat{y}_F = \hat{y}_{(0)} + O(\Gamma^{-1}). \tag{4.63}$$

Inserting Equation (4.63) in Equation (4.62), the following equation is found for the leading order term:

$$\frac{d^2\hat{y}_{F(0)}}{d\hat{\eta}^2} + Le_F\hat{f}_{(0)}\frac{d\hat{y}_{F(0)}}{d\hat{\eta}} = 0, \tag{4.64}$$

Boundary and matching conditions are given respectively by:

$$\hat{y}_{F(0)}(0) = y_{F0}, \quad \left.\frac{d\hat{y}_{F(0)}}{d\hat{\eta}}\right|_{\hat{\eta}\to+\infty} = 0. \tag{4.65}$$

The leading order term of the fuel mass fraction in the intermediary zone is given by the solution of Equation (4.64) with the boundary and matching conditions given by Equations (4.65):

$$\hat{y}_F(\hat{\eta}) = y_{F0}\ erfc\left(\hat{\eta}\sqrt{\frac{Le_F}{2}}\right) + O(\Gamma^{-1}). \tag{4.66}$$

The higher order terms are not necessary and shall not be obtained.

4.4.3 Inner zone: problem of the order of Γ^{-1}

The fuel mass fraction in the inner zone is obtained from the stretching of the spatial coordinate given by $\tilde{\eta} = \Gamma^{1/2}\hat{\eta}$. Performing this stretching in Equation (4.62), the following equation is obtained (and also re-scaling the momentum as $\tilde{f} = \Gamma^{1/2}\hat{f}$):

$$\Gamma\frac{d^2\tilde{y}_F}{d\tilde{\eta}^2} + Le_F\tilde{f}\frac{d\tilde{y}_F}{d\tilde{\eta}} = 0, \tag{4.67}$$

And such equation must obey the following boundary and matching conditions respectively:

$$\tilde{y}_F(0) = y_{F0}, \quad \Gamma\left.\frac{d\tilde{y}_F}{d\tilde{\eta}}\right|_{+\infty} = \Gamma^{1/2}\left.\frac{d\hat{y}_F}{d\hat{\eta}}\right|_0. \tag{4.68}$$

The solution of Equation (4.67) is expressed as:

$$\tilde{y}_F = \tilde{y}_{F(0)} + \Gamma^{-1/2}\tilde{y}_{F(1/2)} + O(\Gamma^{-1}) \tag{4.69}$$

Substituting the solution in Equation (4.69) in Equation (4.67), the following set of equations for the first two terms is found:

$$\frac{d^2\tilde{y}_{F(0)}}{d\tilde{\eta}^2} = 0, \tag{4.70a}$$

$$\frac{d^2\tilde{y}_{F(1/2)}}{d\tilde{\eta}^2} = 0. \tag{4.70b}$$

And the boundary and matching conditions are given respectively by:

$$\tilde{y}_{F(0)}(0) - y_{F0} = \tilde{y}_{F(1/2)}(0) = 0, \tag{4.71a}$$

$$\Gamma \left.\frac{d\tilde{y}_{F(0)}}{d\tilde{\eta}}\right|_{\tilde{\eta}\to+\infty} = 0, \quad \Gamma \left.\frac{d\tilde{y}_{F(1/2)}}{d\tilde{\eta}}\right|_{\tilde{\eta}\to+\infty} = \Gamma^{1/2} \left.\frac{d\hat{y}_{F(0)}}{d\hat{\eta}}\right|_{e\hat{t}a=0}. \tag{4.71b}$$

Solving Equations (4.70a) and (4.70b) with conditions given in Equations (4.71a) and (4.71b), the fuel mass fraction in the inner zone is obtained as:

$$\tilde{y}_F(\tilde{\eta}) = y_{F0} - \Gamma^{-1/2} y_{F0} \sqrt{\frac{2}{\pi} Le_F}\ \tilde{\eta} + O(\Gamma^{-1}). \tag{4.72}$$

4.5 Determination of the unknowns of the problem: y_{F0}, $\tilde{f}_0$ and θ_{s0}

The mass conservation at the interface is given by:

$$\left.\frac{d\tilde{y}_F}{d\tilde{\eta}}\right|_{\tilde{\eta}=0^+} = \Gamma^{-1}(1 - y_{F0})\tilde{f}_0. \tag{4.73}$$

Solving Equation (4.73), the fuel mass fraction at the interface, y_{F0}, is obtained as:

$$y_{F0} = \frac{\tilde{f}_0}{\tilde{f}_0 - \Gamma^{1/2}\sqrt{2\ Le_F/\pi}}. \tag{4.74}$$

The performed analysis assumes a low-volatile liquid fuel. So, the non-dimensional latent heat of the liquid fuel is re-written as $\tilde{l} = \Gamma\tilde{l}$, in which $\tilde{l}$ is a unitary order parameter that determines the type of fuel analyzed. Re-writing Equation (4.25b)

in terms of $\tilde{l}$, $\tilde{\eta}$ and $\tilde{z}$, the energy conservation at the interface is given by:

$$\varepsilon \left.\frac{d\tilde{\theta}_g}{d\tilde{\eta}}\right|_{0^+} = -\tilde{l}\tilde{f}_0 + \Gamma\varepsilon\frac{J}{a^{1/2}}\left.\frac{d\theta_l}{d\tilde{z}}\right|_{-\infty} - \Gamma\frac{n_l}{a^{1/2}}\int_{-\infty}^{0}(\theta_s - \theta_l)d\tilde{z} \tag{4.75}$$

Substituting Equations (4.48), (4.55b) and (4.55a) into Equation (4.75), the vaporization rate $\tilde{f}_0$ is obtained by collecting the leading order terms in Equation (4.75):

$$\tilde{f}_0 = -\Gamma\sqrt{\frac{n_l}{a}}\,\frac{(\theta_{s0} - \theta_B)}{\tilde{l}}\,(1-\varepsilon)^{1/2} \tag{4.76}$$

At a first glance, it may seen that the magnitude order argument have been violated in the process of obtaining the vaporization rate expression, since in the above expressions the parameter Γ appears. However, it must remembered that the term $(\theta_{s0} - \theta_B)$ is of the order of Γ^{-1}, hence, the expression (4.76) is of the order of unity.

The results pointed out by Equation (4.76) exhibits that the main responsible for providing the heat necessary for the phase change of the liquid fuel is the solid matrix, that transport conductively heat to the boiling zone, while the gas-liquid heat exchange have a minor role in such process. This can be seen from the fact that $\tilde{f}_0$ was obtained from the heat exchange between solid and liquid phases.

The solid phase temperature at the interface, θ_{s0} is obtained from the continuity of the solid phase heat flux at the interface:

$$\Gamma \left.\frac{d\theta_s}{d\tilde{\eta}}\right|_{0^+} = \Gamma \left.\frac{d\theta_s}{d\tilde{z}}\right|_{0^-}. \tag{4.77}$$

The leading order term of the solid phase temperature in the inner zone is a constant value, namely, θ_{s0}. Hence, the solid phase heat flux reaching the interface from the inner zone, at $\tilde{\eta} = 0^+$, is given by the higher order term:

$$\Gamma \left.\frac{d\theta_s}{d\tilde{\eta}}\right|_{0^+} = \left.\frac{d\theta_{s(1)}}{d\tilde{\eta}}\right|_{0^+} = (1-\theta_{s0})\sqrt{\frac{2}{\pi\gamma}} - \sqrt{\frac{n_g}{\varepsilon}}\frac{(\theta_{s0} - \theta_B)}{\gamma n_g} \tag{4.78}$$

in which one must impose the continuity of such expression with the solid phase heat flux below the interface, in the boiling zone.

Expanding Equation (4.77) and collecting the leading order terms, the solid phase

temperature at the interface is obtained as:

$$\theta_{s0} = \left(\theta_B + \Gamma^{-1}\sqrt{\frac{2\varepsilon}{\pi\ n_l}}\right)\left(\frac{\sqrt{\pi\ n_l}}{\sqrt{\pi\ n_l} + \Gamma^{-1}\sqrt{2\varepsilon}}\right), \tag{4.79}$$

Since $\Gamma^{-1} \ll 1$, the solid phase temperature at the interface can be estimated to be:

$$\theta_{s0} \sim \theta_B + \Gamma^{-1}\sqrt{\frac{2\varepsilon}{\pi\ n_l}}, \tag{4.80}$$

a expression that confirms the assumption that $(\theta_{s0} - \theta_B) = O(\Gamma^{-1})$.

Since it is known that $(\theta_{s0} - \theta_B) = O(\Gamma^{-1})$, the continuity of the solid phase heat flux at the interface can only be obeyed if $(1 - \theta_{s0}) = O(1)$. This restrain emerges from the fact that the liquid fuel is considered to be low-volatile, such that it is hard to vaporize such liquid, as pointed by the low-vaporization regime observed. The obtained restrain shows that, in order to vaporize the liquid fuel, the injection temperature must be one order of magnitude higher than the boiling temperature of the liquid fuel (remember that $\theta_{s0} \sim \theta_B$ and that the temperatures were re-scaled by the injection temperature, T_∞).

The plots in the previous sections are calculated utilizing the values of $\tilde{f}_0$ and θ_{s0} given by expressions (4.76) and (4.79), respectively. The parameters and properties of gas and liquid phases utilized are the following:

$$c_l/c_p = n_g = Pr = a = Le_F = 1.0, \quad \Gamma \equiv \bar{\lambda}_s/\bar{\lambda}_g = 60.0,$$

$$n_l = \tilde{l} = 1.0, \quad J \equiv \bar{\lambda}_l/\bar{\lambda}_s = 1.0,$$

The properties of the solid matrix are given by:

$$\varepsilon = 0.3, \quad \beta = 1.0$$

in which the porosity, ε, was chosen according to the usual value of porosity observed in oil reservoirs.

The oxidant stream temperature is five times greater than the boiling temperature of the liquid fuel, thus, $\theta_B = 0.2$, and ten times the temperature of the liquid reservoir,

thus, $\theta_{-\infty} = 0.1$.

Using such values, the vaporization rate, the solid phase temperature at the interface and the fuel mass fraction at the interface, obtained from expressions (4.76), (4.79) and (4.74) are given by:

$$\tilde{f}_0 = -0.290394, \quad \theta_{s0} = 0.205785, \quad y_{F0} = 0.738115.$$

As expected, the difference between the solid phase temperature at the interface and the liquid fuel boiling temperature is of the order of Γ^{-1}. The vaporization rate is low, as expected also. The fuel mass fraction is of the order of $\Gamma^{-1/2}$, as a result of the low volatile fuel.

4.6 Conclusions

A low vaporization regime inside a porous medium has been analyzed in the present chapter. A stream of hot oxidant impinging over a pool of a low-volatile liquid fuel was the studied geometry. Under the assumptions of a low porosity medium and of high rates of interphase heat transfer (gas-solid and liquid-solid) profiles of momentum and temperature were obtained for the different spatial length scales. A matched asymptotic expansion method was conducted in order to capture both thermal and viscous boundary layer effects.

In the gas-solid region, two distinct zones were analyzed, the outer zone, in which thermal equilibrium was observed and the macroscopic viscous effects were not observed, and the inner zone, in which gas and solid phases present a thermal non-equilibrium and the macroscopic viscous effects due to the gas-liquid interaction were observed. In the liquid-solid region, two regions were also observed, an equilibrium zone, in which liquid and solid are in thermal equilibrium, due to the high rates of interphase heat transfer, and a boiling zone, near the interface, in which the liquid fuel is at an almost constant temperature, its boiling temperature. In this zone, all heat provided to the liquid fuel goes to phase change.

Imposing the continuity of the solid phase heat flux at the interface, it was observed that in order to obtain this vaporization regime, the oxidant must be injected at temperatures higher than the boiling temperature of the liquid fuel by one order of magnitude. This restrain arises from the fact that the liquid fuel considered is a low-

volatile one. Such feature is also the responsible for the fact that the vaporization regime is low.

From the energy conservation at the interface, it is observed that the solid matrix is the main responsible for the vaporization of the liquid fuel, that "carries" the heat from above the interface to the liquid-solid region. Due to the intense interphase heat transfer between liquid and solid, the obtained vaporization regime is more efficient than an impinging flow in free conditions, as such regime is governed by the gas-liquid heat exchange. The role of the porous matrix is to enhance the vaporization process of the liquid fuel.

5 COMBUSTION OF LOW-VOLATILE LIQUID FUEL IN A LOW POROSITY MEDIUM

In the present chapter, the combustion of a heavy liquid fuel in a porous medium is analyzed. A pool of liquid fuel subjected to a stream of hot oxidant is considered to be immersed inside an infinite low porosity medium, such that the permeability of the medium is also low. High rates of interphase heat transfer are also considered. Unitary Lewis number is considered for both oxidant and fuel gas phase.

The analysis proposed in this chapter is the conclusion of the development performed in Chapter (3) and (4).

5.1 Mathematical formulation

The mathematical formulation of the proposed problem follows the previous analysis. However, in the present case, the reaction-rate term must be taken into account as a heat source and as a mass sink for the reactant species. A single-step global reaction is considered, such that the chemical reaction is generically expressed as:

$$F + sO \rightarrow (1+s)P + Q \tag{5.1}$$

in which is considered the stoichiometric reaction of fuel (F) and oxidant (O) (s is the stoichiometric coefficient), generating the combustion products (P) and releasing an amount of heat Q.

The geometry analyzed in the present chapter is an impinging-flow configuration inside a porous medium. A stream of hot oxidant is injected and it impinges on the surface of a pool of a low-volatile liquid fuel. A low-vaporization regime is initiated, and after ignition conditions are achieved, a diffusion flame is established.

A schematic geometry of the proposed problem is given in Figure (5.1).

Following the same assumptions made in previous chapters, the following governing equations are valid in the gas-solid region (the same presented in Chapter (2)) :

$$\rho\frac{\partial\bar{u}}{\partial\bar{x}} + \rho\frac{\partial\bar{v}}{\partial\bar{z}} = 0, \tag{5.2}$$

$$\rho\bar{u}\frac{\partial\bar{u}}{\partial\bar{x}} + \rho\bar{v}\frac{\partial\bar{u}}{\partial\bar{z}} = -\varepsilon\frac{\partial\bar{p}}{\partial\bar{x}} + \bar{\mu}\frac{\partial^2\bar{u}}{\partial\bar{z}^2} - \varepsilon\bar{\mu}\frac{\bar{u}}{K}, \tag{5.3}$$

$$\varepsilon\rho\bar{v}\frac{\partial Y_F}{\partial \bar{z}} = \varepsilon\rho\bar{D}_F\frac{\partial^2 Y_F}{\partial \bar{z}^2} - \varepsilon\bar{w}_F, \tag{5.4}$$

$$\varepsilon\rho\bar{v}\frac{\partial Y_O}{\partial \bar{z}} = \varepsilon\rho\bar{D}_O\frac{\partial^2 Y_O}{\partial \bar{z}^2} - \varepsilon s\bar{w}_F, \tag{5.5}$$

$$\varepsilon\rho\bar{v}c_p\frac{\partial T_g}{\partial \bar{z}} = \varepsilon\bar{\lambda}_g\frac{\partial^2 T_g}{\partial \bar{z}^2} + \varepsilon Q\bar{w}_F + h_v(T_s - T_g), \tag{5.6}$$

$$0 = (1-\varepsilon)\bar{\lambda}_s\frac{d^2 T_s}{d\bar{z}^2} - h_v(T_s - T_g). \tag{5.7}$$

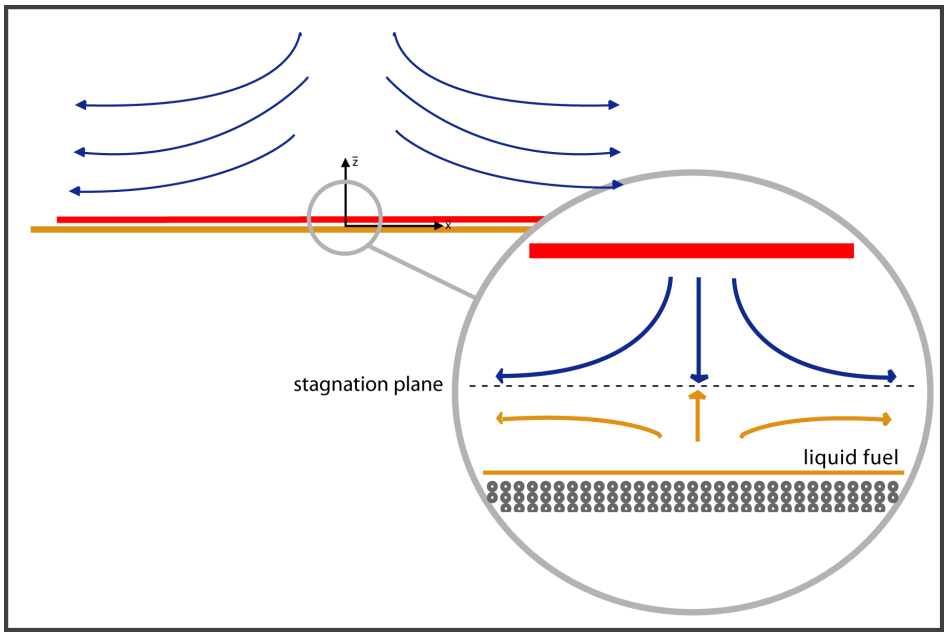

Figure 5.1 - Diffusion flame established inside a porous medium

In Equations (5.4), (5.5) and (5.6) the term $\bar{w}_F$ is the strong non-linear Arrhenius reaction term. The two phases (gas and solid) are connected thermally by the heat transfer between them (in which h_v is the interphase heat exchange coefficient), and mechanically by the resistance created by the tortuous channels of the porous medium (represented by the Darcy term in Equation (5.3)). The heat released due to the exothermic nature of the combustion is quantified by the Q that appears in Equation (5.6).

The injection conditions ($\bar{z} \to \infty$) for the above set of equations are given by:

$$\bar{v} = \bar{v}_\infty, \quad \bar{u} = \bar{x} \left.\frac{d\bar{u}}{d\bar{x}}\right|_\infty, \quad T_g = T_s = T_\infty, \quad Y_O = Y_{O0}, \quad Y_F = 0. \tag{5.8}$$

At the liquid-gas interface, the following conditions must be obeyed:

$$\bar{v} = \bar{v}_0, \quad T_g = T_0, \quad Y_F - Y_{F0} = 0. \tag{5.9}$$

The gas-liquid interface divides liquid fuel, at $\bar{z} = 0^-$, and gaseous fuel, at $\bar{z} = 0^+$. At the interface, liquid and gaseous fuel are approximately in equilibrium at the boiling temperature, T_B. Thus, the gas phase temperature at the liquid surface, T_0, is equal to the boiling temperature.

The velocity of the gaseous fuel at the liquid surface, $\bar{v}_{0^+}$, is related to the vaporization rate, $\dot{\bar{m}}$, through:

$$\rho.\bar{v}_{0^+} = \rho_l.\bar{v}_{l0^-} = \dot{\bar{m}}, \tag{5.10}$$

in which $\bar{v}_{l0^-}$ and $\bar{v}_{0^+}$ stand for the velocities of the liquid fuel and vapor fuel at the interface, respectively.

Mass and energy balance at the interface yield:

$$\rho \bar{D}_F \left.\frac{\partial Y_F}{\partial \bar{z}}\right|_{\bar{z}=0} = -(1 - Y_{F0})\, \rho\bar{v}|_{\bar{z}=0^+}, \tag{5.11a}$$

$$\varepsilon\, \bar{\lambda}_g \left.\frac{\partial T_g}{\partial \bar{z}}\right|_{\bar{z}=0^+} = \rho\bar{v}|_{\bar{z}=0^+} L + \varepsilon\, \bar{\lambda}_l \left.\frac{\partial T_l}{\partial \bar{z}}\right|_{\bar{z}=-\bar{z}_b} - h_l \int_{-\bar{z}_b}^{0^-} (T_s - T_l) d\bar{z} \tag{5.11b}$$

The conditions at the flame ($\bar{z}_f$) are given by:

$$T_g = T_f, \quad Y_F = Y_O = 0. \tag{5.12}$$

in which it is considered complete consumption of species at the flame, known as the Burke-Schumann limit.

In the liquid-solid region, $\bar{z} < 0$, the mass and energy conservation lead to the set

of equations given by (the same as the obtained in Chapter (4)):

$$\rho_l \bar{v}_l = \dot{\bar{m}} \tag{5.13}$$

$$\varepsilon \rho_l \bar{v}_l c_l \frac{dT_l}{d\bar{z}} = \varepsilon \bar{\lambda}_l \frac{d^2 T_l}{d\bar{z}^2} + h_l (T_s - T_l) \tag{5.14}$$

$$0 = (1-\varepsilon) \bar{\lambda}_s \frac{d^2 T_s}{d\bar{z}^2} - h_l (T_s - T_l) \tag{5.15}$$

Equation (5.13) provides the condition for imposing a standing gas-liquid interface at $\bar{z} = 0$. The injection conditions ($\bar{z} \to -\infty$)for the liquid fuel are given by:

$$T_l = T_s = T_{-\infty}, \quad \bar{v}_l = \bar{v}_{l-\infty}. \tag{5.16}$$

5.1.1 Non-dimensional formulation

The governing equations are made non-dimensional and are transformed by means of the non-dimensional variables and transformations defined in Chapter (2).

Under such modifications, the governing equations of the gas phase, Equations (5.2) to (5.7), become:

$$U = \frac{df}{d\eta}, \tag{5.17}$$

$$\frac{Pr}{\Gamma} \frac{d^3 f}{d\eta^3} + f \frac{df^2}{d\eta^2} - \left(\frac{df}{d\eta} \right)^2 - \Gamma \varepsilon \beta Pr \frac{df}{d\eta} = -\varepsilon Pr \left(1 + \beta \Gamma \right), \tag{5.18}$$

$$\frac{1}{\Gamma} \frac{d^2 y_f}{d\eta^2} + Le_F f \frac{dy_f}{d\eta} = Le_F \frac{w_F}{a}, \tag{5.19}$$

$$\frac{1}{\Gamma} \frac{d^2 y_O}{d\eta^2} + Le_O f \frac{dy_O}{d\eta} = S \; Le_F \frac{w_F}{a}, \tag{5.20}$$

$$0 = \frac{\varepsilon}{\Gamma} \frac{d^2 \theta_g}{d\eta^2} + \varepsilon f \frac{d\theta_g}{d\eta} + \varepsilon q \frac{w_F}{a} + \Gamma n_g (\theta_s - \theta_g), \tag{5.21}$$

$$0 = (1-\varepsilon) \frac{d^2 \theta_s}{d\eta^2} - \Gamma n_g (\theta_s - \theta_g), \tag{5.22}$$

in which Le_i is the i-species Lewis number, defined as $Le_i \equiv \alpha_i / D_i$, the ratio between the thermal and mass diffusivities. The stoichiometric coefficient S is defined as $S \equiv (s/Y_{O\infty}) Le_O / Le_F$, w_F is the non-dimensional reaction rate, defined by $w_F \equiv \bar{w}_F \left(z_s / \rho_\infty \bar{v}_\infty \right)$ and the non-dimensional heat released is defined as $q \equiv Q / c_p T_\infty$.

The non-dimensional injection conditions ($\eta \to \infty$) are given by:

$$\left.\frac{df}{d\eta}\right|_{\eta\to+\infty} = U_\infty, \quad \theta_g = \theta_s = 1, \quad y_F = y_O - 1 = 0. \tag{5.23}$$

in which, as previously, U_∞ is the horizontal component velocity far from the gas-liquid interface.

The following non-dimensional boundary conditions at $\eta = 0$ must be satisfied by Equations (5.17) to (5.22):

$$f - f|_0 = \left.\frac{df}{d\eta}\right|_{\eta=0} = 0, \quad \theta_g - \theta_B = \theta_s - \theta_{s0} = 0, \quad y_F - y_{F0} = y_O = 0. \tag{5.24}$$

The vaporization rate, $\dot{m}$, is related with $f|_0$ through:

$$-\, a^{1/2}\, f|_0 = \dot{m} \tag{5.25}$$

The consideration of a low volatile liquid fuel will lead to a low-vaporization rate, as in Chapter (4).

Mass and energy must be conserved at the interface following:

$$\frac{1}{\Gamma}\frac{1}{Le_F}\left.\frac{dy_F}{d\eta}\right|_{\eta=0^+} = (1 - y_{F0})\, f|_0\,, \tag{5.26a}$$

$$\frac{\varepsilon}{\Gamma}\left.\frac{d\theta_g}{d\eta}\right|_{\eta=0^+} = -l\, f|_0 + \varepsilon\frac{J}{a^{1/2}}\left.\frac{d\theta_l}{dz}\right|_{z=-z_b} - \frac{N_l}{a^{1/2}}\int_{-z_b}^{0}(\theta_s - \theta_l)dz. \tag{5.26b}$$

In the present problem, it is considered a low volatile liquid fuel, such that $l = O(\Gamma)$.

The conditions at the flame (η_f) are given by:

$$\theta_g - \theta_f = y_F = y_O = 0. \tag{5.27}$$

Below the gas-liquid interface the following governing equations are valid:

$$\varrho_l v_l = \dot{m}, \tag{5.28}$$

$$\varepsilon J \frac{d^2\theta_l}{dz^2} - \varepsilon M \frac{d\theta_l}{dz} = -N_l(\theta_s - \theta_l), \tag{5.29}$$

$$(1-\varepsilon)\frac{d^2\theta_s}{dz^2} = N_l(\theta_s - \theta_l), \tag{5.30}$$

in which $\dot{m} \equiv \bar{\dot{m}}/\left(\rho_\infty \bar{v}_\infty\right)$, $M \equiv \dot{m}(c_l/c_p)$ and $J \equiv \bar{\lambda}_l/\bar{\lambda}_s$. The parameter M is related to $f|_0$ through (5.25). And, hence, it is obtained that $M = O(\Gamma^{-1})$.

The injection boundary conditions ($z \to -\infty$) are given by:

$$\theta_l - \theta_{-\infty} = \theta_s - \theta_{-\infty} = y_F - 1 = y_O = 0. \tag{5.31}$$

The solution of the liquid-solid problem is the same as the presented in Chapter (4).

The gas-solid problem will take into account a heat source term and mass sink terms in the governing equations. The exothermic reaction of fuel and oxidant at the flame region provide an additional heat to the flow field and to the solid matrix. Boundary layers also emerges from this problem, similarly to the previous cases analyzed. However, due to the low-vaporization regime, the flame is not localized in the inner zone (recalling that the inner zone is a region of order Γ^{-1} close to the liquid-gas interface), but in a region of order $\Gamma^{-1/2}$ close to the liquid-gas interface, denoted as the flame zone. Since the vaporization rate is low, the fuel mass flux to the flame is also low. In order to sustain the stoichiometric fuel/oxidant flux to the flame, oxidant must be injected at a low velocity. Under such conditions, a diffusion flame must be established outside the inner zone, in the flame zone.

It must be pointed that in the present problem the Burke-Schumann regime is considered, such that the reaction rate is infinitely fast and the flame is confined into an infinitely thin region. The problems of extinction and stability of the flame are not considered in the present work.

In the next sections, the two regions (gas-solid and liquid-solid) will be analyzed separately. In each analysis, a boundary expansion will be performed in order to capture the different physical process in each zone (outer, flame and inner for the gas-solid region, and equilibrium and boiling for the liquid-solid region). However, differently from the analysis in Chapter (4), the vaporization rate and the solid phase temperature at the interface are considered to be existent only in its leading order term (mathematically, it will be considered that $\tilde{f}_1 = \theta_{s1} = 0$).

5.2 Gas-solid region

In the gas-solid region, in which an impinging flow configuration is observed, the Schvab-Zel'dovich formulation is applied (FACHINI, 2007; FACHINI, 1999; LIÑAN; WILLIAMS, 1993) in order to eliminate the strong non-linear reaction rate term from Equations (5.19) - (5.21). Such formulation utilizes new functions, denoted as mixture fraction, Z, and excess enthalpy, H. Combining Equations (5.19) - (5.21) conveniently, the following set of governing equations is found:

$$\frac{1}{\Gamma}\frac{d^2Z}{d\eta^2} + fLe(Z)\frac{dZ}{d\eta} = 0, \tag{5.32}$$

$$\frac{\varepsilon}{\Gamma}\frac{d^2H}{d\eta^2} + \varepsilon f\left[\frac{dH}{d\eta} + N_H(Z)\frac{dZ}{d\eta}\right] + \Gamma n_g\frac{(\theta_s-\theta_g)Le_F(S+1)}{q} = 0, \tag{5.33}$$

in which $Z \equiv Sy_F - y_O + 1$ and $H \equiv (S+1)\theta_g/q + y_F + y_O$. Note that:

$$N_H(Z) \equiv \begin{cases} (Le_F - 1)/S, & \text{for } Z > 1 \\ (1 - Le_O), & \text{for } Z < 1 \end{cases} \tag{5.34a}$$

$$Le(Z) \equiv \begin{cases} Le_F, & \text{for } Z > 1 \\ Le_O, & \text{for } Z < 1 \end{cases} \tag{5.34b}$$

According to the definition of Z: $Z = 1$ at the flame, $Z > 1$ on the fuel side and $Z < 1$ on the oxidant side.

In the present work, it will be considered that the Lewis number for fuel and oxidant are equal unity, and, hence, Equations (5.32) and (5.33) simplifies to:

$$\frac{1}{\Gamma}\frac{d^2Z}{d\eta^2} + f\frac{dZ}{d\eta} = 0 \tag{5.35}$$

$$\frac{\varepsilon}{\Gamma}\frac{d^2H}{d\eta^2} + \varepsilon f\frac{dH}{d\eta} + \Gamma n_g(\theta_s-\theta_g)\frac{(S+1)}{q} = 0 \tag{5.36}$$

The consideration of unitary Lewis number for oxidant and fuel avoids the discontinuities in the second derivatives of the functions H and Z, simplifying the mathematical formulation. Physically, a unitary Lewis number represents equal heat and mass diffusivities.

The boundary conditions to be imposed are given by:

$$Z(0) = Sy_{F0} + 1, \quad Z(\infty) = 0, \quad Z(\eta_f) = 1, \tag{5.37}$$

$$H(0) = \frac{(S+1)}{q}\theta_B + y_{F0}, \quad H(\infty) = \frac{(S+1)}{q} + 1, \quad H(\eta_f) = \frac{(S+1)}{q}\theta_f. \tag{5.38}$$

in which the flame temperature and position (respectively, θ_f and η_f) are unknown values of the problem.

The problem in the gas-solid region presents three different length scales: an outer zone (of the order of unity), a flame zone (of the order of $\Gamma^{-1/2}$) and an inner zone (of the order of Γ^{-1}). Each zone will be solved in its appropriate length scale and the matching condition between the solutions is imposed in order to obtain the complete solution of the problem. Note that under the assumption of negligible thermal expansion, variations in the temperature field does not affect the gas velocity field. And, hence, the momentum analysis in the present problem is equal to the analysis performed in Chapter (4).

5.2.1 Outer zone: problem of the order of unity

In the outer zone, of spatial length scale of the order of unity, the momentum profile is the same as that obtained in Chapter (4) and given by:

$$f(\eta) = \eta - \Gamma^{-1}\frac{1 - \varepsilon Pr}{\varepsilon\beta Pr}\eta + O(\Gamma^{-2}), \tag{5.39}$$

in which no macroscopic viscous effects are present.

The behavior of the mixture fraction in the outer zone is determined by:

$$\frac{1}{\Gamma}\frac{d^2Z}{d\eta^2} + f\frac{dZ}{d\eta} = 0. \tag{5.40}$$

The existence of the large parameter Γ ($\equiv \bar{\lambda}_s/\bar{\lambda}_g \gg 1$) motivates to seek a solution in the form:

$$Z = Z_{(0)} + \Gamma^{-1}Z_{(1)} + O(\Gamma^{-2}). \tag{5.41}$$

The boundary condition imposed to Equation (5.40) for $\eta \to \infty$ is $Z = 0$. The condition at $\eta = 0$ is not obeyed by the outer zone solutions. This condition is

obeyed by the inner zone solutions. And the flame zone solutions matches with its neighbor zones (outer, from above, and inner, from below) solutions.

After substituting the expression for Z given by Equation (5.41) in Equation (5.40), equal powers of Γ are collected in order to obtain a set of governing equations for the mixture fraction. Solving such equations, with the boundary condition $Z(\eta \rightarrow \infty) = 0$, the solution of Equation (5.40) is:

$$Z(\eta) = 0 \tag{5.42}$$

From the definition of the mixture fraction and from Equation (5.42), it is seen that the outer zone contains only oxidant.

The excess enthalpy function in the outer zone is described by:

$$\frac{\varepsilon}{\Gamma}\frac{d^2H}{d\eta^2} + \varepsilon f\frac{dH}{d\eta} + \Gamma n_g(\theta_s - \theta_g)\frac{(S+1)}{q} = 0 \tag{5.43}$$

A magnitude order analysis of Equation (5.43) shows three terms with three different magnitude orders. The first term is of order Γ^{-1}, the second one is of the order of unity and the third term is of the order of Γ. Then, in a first approximation the condition $\theta_s \sim \theta_g$ prevails. And hence, in the outer zone, thermal equilibrium between phases is considered.

The interphase heat transfer term in Equation (5.43) can be eliminated combining Equation (5.43) with Equation (5.22). The resulting equation is given by:

$$\frac{\varepsilon}{\Gamma}\frac{d^2H}{d\eta^2} + \varepsilon f\frac{dH}{d\eta} + (1-\varepsilon)\frac{d^2H}{d\eta^2} = 0, \tag{5.44}$$

in which $\theta_s = \theta_g = \theta$ is expressed in terms of the H function.

Equation (5.44) must be solved with the following boundary conditions:

$$H(0) = (S+1)\theta_m/q + 1, \quad H(\infty) = (S+1)/q + 1 \tag{5.45}$$

in which θ_m is a temperature observed from the outer zone when the flow approaches the flame zone. Such temperature is justified by the existence of the thermal bound-

ary layers (flame zone and inner zone).

Like the mixture fraction, a solution for the excess enthalpy is proposed to be expressed as:

$$H = H_{(0)} + O(\Gamma^{-1}), \tag{5.46}$$

Substituting Equation (5.46) in Equation (5.44) and collecting equal powers of Γ, it is found for the leading order:

$$\gamma \frac{d^2 H_{(0)}}{d\eta^2} + f_{(0)} \frac{dH_{(0)}}{d\eta} = 0, \tag{5.47}$$

in which it was defined $\gamma = (1 - \varepsilon)/\varepsilon$, and from Equation (5.39), $f_{(0)} = \eta$.

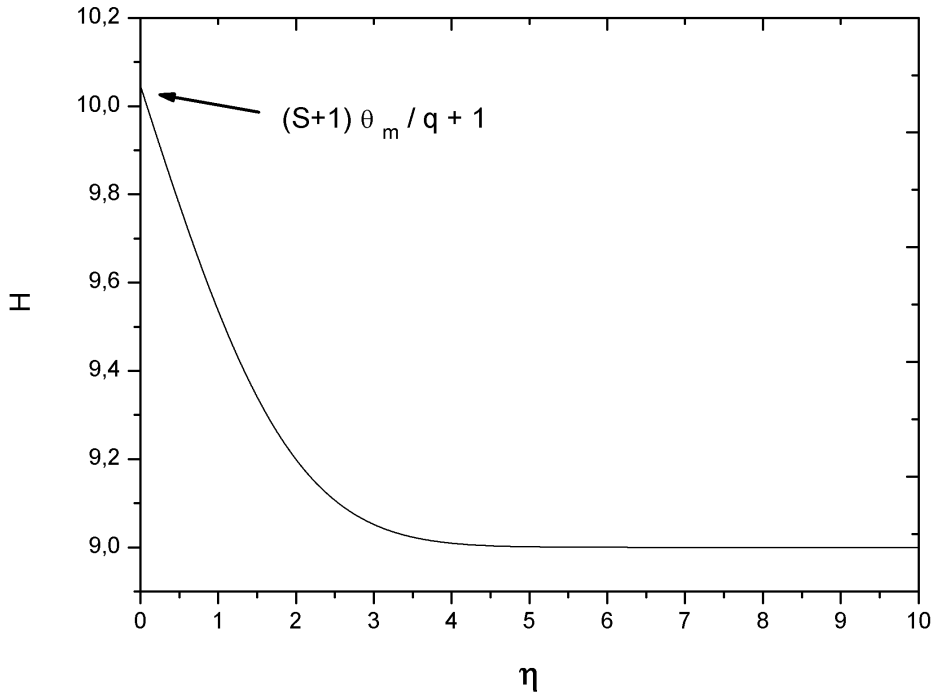

Figure 5.2 - Excess enthalpy in the outer zone, $\theta_m = 1.13$, $S = 15.0$, $q = 2$, $\varepsilon = 0.3$.

The boundary conditions for Equation (5.47) are given by:

$$H_{(0)}(0) = (S+1)\theta_m/q + 1, \quad H_{(0)}(\eta \to \infty) = (S+1)/q + 1. \tag{5.48}$$

The solution of Equation (5.47) with the boundary conditions given by Equation (5.48) gives the leading order term for the excess enthalpy function as:

$$H_{(0)}(\eta) = 1 + \frac{(S+1)}{q}\left[\theta_m - (\theta_m - 1)\ erf\left(\frac{\eta}{\sqrt{2\gamma}}\right)\right]. \tag{5.49}$$

The excess enthalpy profile in the outer zone is presented in Figure (5.2).

It can be seen that as the flow approaches the flame zone, the excess enthalpy increases, due to the existence of the exothermic reaction, and hence, increasing the oxidant temperature in the outer zone.

From the definition of H in the outer zone, the leading order term for the temperature in the outer zone may be expressed as:

$$\theta_{(0)}(\eta) = \theta_m - (\theta_m - 1)\ erf\left(\eta/\sqrt{2\gamma}\right). \tag{5.50}$$

The temperature profile in the outer zone is presented in Figure (5.3).

The characteristic of the outer zone is thermal equilibrium between the gas and solid phases. It is anticipated that this thermal equilibrium prevails up to the flame zone, which has a thickness of order $\Gamma^{-1/2}$, and it is a result from the intense inter-phase heat transfer. The thermal non-equilibrium is only found in the inner zone, of thickness of order Γ^{-1}.

It will be seen from the flame zone analysis, that the temperature observed from the outer zone, θ_m, is equal to the flame temperature, θ_f, and this temperature will be obtained in Section (5.4).

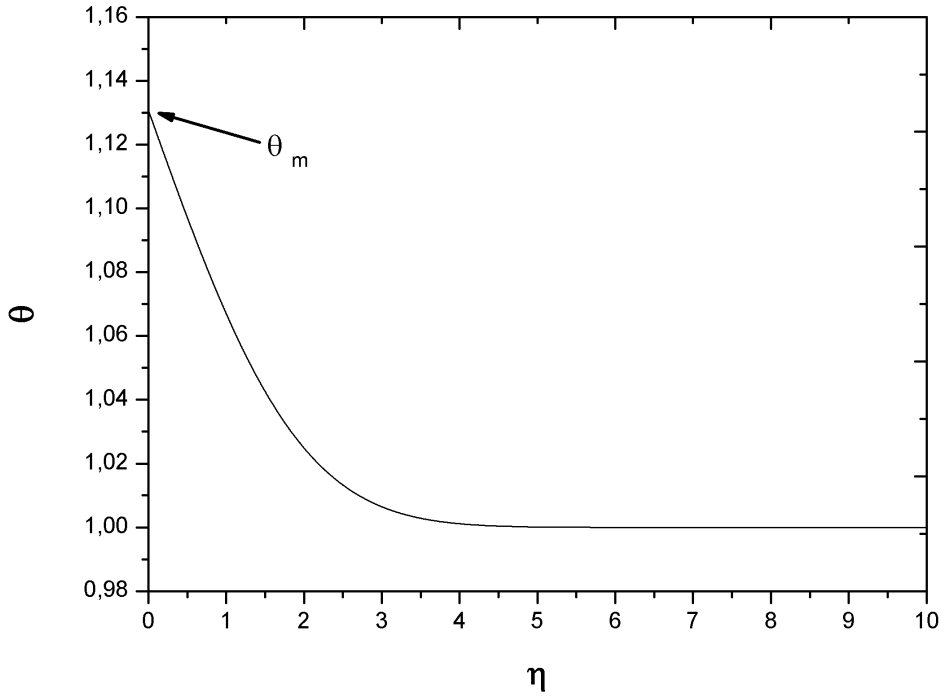

Figure 5.3 - Temperature in the outer zone, $\theta_m = 1.13$, $\varepsilon = 0.3$.

5.2.2 Flame zone: problem of the order of $\Gamma^{-1/2}$

When the flow reaches a region of the order of $\Gamma^{-1/2}$ from the gas-liquid interface, it enters the flame zone. There, the exothermic chemical reaction takes place, and oxidant and fuel are consumed stoichiometrically. The heat flux towards the inner zone is the flux that reaches the gas-liquid interface and controls the liquid fuel vaporization.

The flame zone is divided in two distinct regions: one above the flame ($\eta > \eta_f$, in which η_f is the flame position) and one below the flame. Above the flame, the gas flow is composed by oxidant and combustion products. Hence, below the flame, the gas flow is composed by fuel and products. The flame is located in the position in which the mass fluxes are in a stoichiometric proportion.

In order to analyze the flame zone, a stretching in the spatial variable is necessary and given by $\hat{\eta} = \Gamma^{1/2}\eta$. The momentum variable must be re-scaled also as $\hat{f} = \Gamma^{1/2} f$, in order to keep it as a unitary order variable.

It can be noted that this intermediary zone is of the same order of magnitude than the intermediary zone that appears in Chapter (4) when obtaining the fuel mass fraction. Hence, the same argument made previously concerning the momentum solution in this zone applies in the present discussion.

So, the momentum in the flame zone is given by:

$$\hat{f}(\hat{\eta}) = \hat{\eta} - \Gamma^{-1}\frac{1-\varepsilon Pr}{\varepsilon\beta Pr}\hat{\eta} + O(\Gamma^{-2}) \tag{5.51}$$

Like Equation (5.39), Equation (5.51) does not present the macroscopic viscous effects. This indicates that the inner zone property, i.e., vaporization rate $f_0 = f(0)$, is not yet observed from the flame zone.

In order to obtain the mixture fraction in the flame zone, the following differential equation must be solved:

$$\frac{d^2\hat{Z}}{d\hat{\eta}^2} + \hat{f}\frac{d\hat{Z}}{d\hat{\eta}} = 0 \tag{5.52}$$

in which the "hat" notation is only to distinguish between zones profiles.

The boundary conditions for Equation (5.52) are given by:

$$\hat{Z}(\hat{\eta}\to\infty) = 0, \quad \hat{Z}(\hat{\eta}_f) = 1, \quad \hat{Z}(\hat{\eta}=0) = Sy_{F0} + 1. \tag{5.53}$$

in which y_{F0} is the gaseous fuel mass fraction at the gas-liquid interface.

The solution of Equation (5.52) is expressed as:

$$\hat{Z}(\hat{\eta}) = \hat{Z}_{(0)} + \Gamma^{-1/2}\hat{Z}_{(1/2)} + \Gamma^{-1}\hat{Z}_{(1)} + \Gamma^{-3/2}\hat{Z}_{(3/2)} + O(\Gamma^{-2}). \tag{5.54}$$

Substituting Equation (5.54) in Equation (5.52) and collecting equal powers of Γ, the governing equation for the leading order term of the mixture fraction in the flame zone is found as:

$$\frac{d^2\hat{Z}_{(0)}}{d\hat{\eta}^2} + \hat{f}_{(0)}\frac{d\hat{Z}_{(0)}}{d\hat{\eta}} = 0 \tag{5.55}$$

Recalling, in the flame zone the solutions for the mixture fraction and excess enthalpy function must be found for before ($\hat{Z} < 1$) and after ($\hat{Z} > 1$) the flame, which represents the oxidant and the fuel sides, respectively.

Equation (5.55) must be solved with the following boundary conditions:

$$\hat{Z}_{(0)}(\hat{\eta} \to \infty) = 0, \quad \hat{Z}_{(0)}(\hat{\eta}_f) = 1, \tag{5.56}$$

and Equation (5.55) also must obey the continuity of its first derivative at the flame:

$$\left.\frac{d\hat{Z}_{(0)}}{d\hat{\eta}}\right|_{\hat{\eta}_f^+} = \left.\frac{d\hat{Z}_{(0)}}{d\hat{\eta}}\right|_{\hat{\eta}_f^-} \tag{5.57}$$

Solving Equation (5.55) with the boundary conditions from above and with the continuity of the first derivative at the flame, the leading order solution is found as:

$$\hat{Z}_{(0)}(\hat{\eta}) = \begin{cases} 1 - \left(erf\left(\hat{\eta}/\sqrt{2}\right) - erf\left(\hat{\eta}_f/\sqrt{2}\right)\right)/erfc\left(\hat{\eta}_f/\sqrt{2}\right), & \text{for } \hat{Z} > 1, \\ \\ erfc\left(\hat{\eta}/\sqrt{2}\right)/erfc\left(\hat{\eta}_f/\sqrt{2}\right), & \text{for } \hat{Z} < 1. \end{cases} \tag{5.58}$$

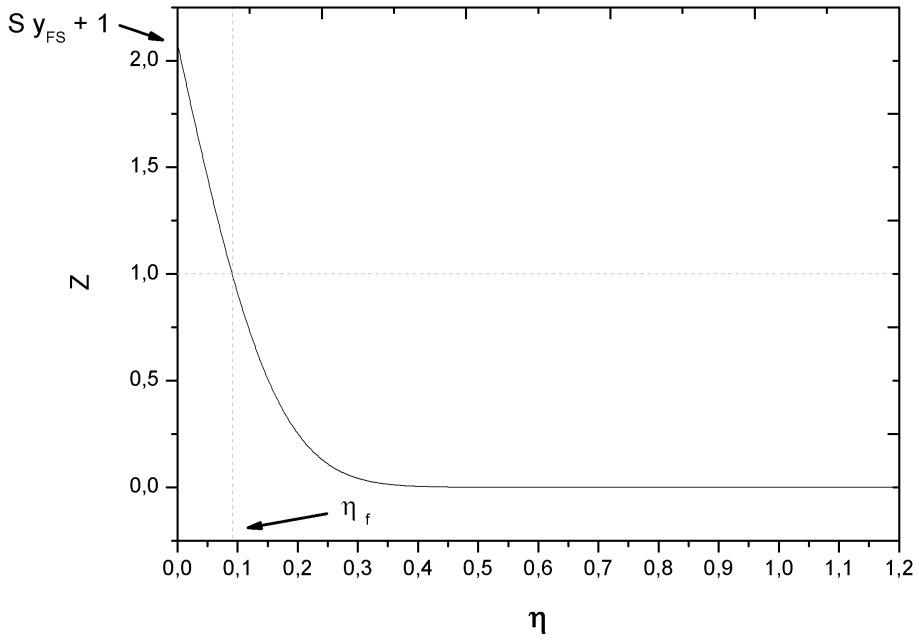

Figure 5.4 - Mixture fraction in the flame zone, $\hat{\eta}_f = 0.7$, $S = 15.0$, $y_{F0} = 0.07$.

Analyzing the expression of the mixture fraction on the fuel side, a relation between the flame position, $\hat{\eta}_f$, and the fuel mass fraction in interface, y_{F0}, is specified:

$$erf\left(\frac{\hat{\eta}_f}{\sqrt{2}}\right) = \frac{Sy_{F0}}{Sy_{F0}+1}. \tag{5.59}$$

This relation is obtained by taking the leading order solution to the gas-liquid interface, imposing that $\hat{Z}_{(0)}(0) = S\ y_{F0} + 1$.

The mixture fraction in the flame zone is presented in Figure (5.4), and the flame is located in the position in which $\hat{Z} = 1$, as can be seen from Figure (5.4).

Performing the stretching in the spatial variable ($\hat{\eta} = \Gamma^{1/2}\eta$), the governing equation for the excess enthalpy in the flame zone is given by:

$$\varepsilon\frac{d^2\hat{H}}{d\hat{\eta}^2} + \varepsilon\hat{f}\frac{d\hat{H}}{d\hat{\eta}} + \Gamma n_g(\hat{\theta}_s - \hat{\theta}_g)\frac{(S+1)}{q} = 0. \tag{5.60}$$

It is possible to observe that the thermal equilibrium between solid and gas phases is still observed in the flame zone, as pointed previously. Re-writing Equation (5.60) with $\hat{\theta}_s = \hat{\theta}_g = \hat{\theta}$, and adding it to Equation (5.22), one finds:

$$\varepsilon\frac{d^2\hat{H}}{d\hat{\eta}^2} + \varepsilon\hat{f}\frac{d\hat{H}}{d\hat{\eta}} + \Gamma\frac{(S+1)}{q}(1-\varepsilon)\frac{d^2\hat{\theta}}{d\hat{\eta}^2} = 0. \tag{5.61}$$

The solutions are expressed as:

$$\left\{\begin{array}{c} \hat{H} = \hat{H}_{(0)} + \Gamma^{-1/2}\hat{H}_{(1/2)} + \Gamma^{-1}\hat{H}_{(1)} + O(\Gamma^{-3/2}), \\ \hat{\theta} = \hat{\theta}_{(0)} + \Gamma^{-1/2}\hat{\theta}_{(1/2)} + \Gamma^{-1}\hat{\theta}_{(1)} + O(\Gamma^{-3/2}). \end{array}\right\} \tag{5.62}$$

In a first approximation, Equation (5.61) results:

$$\frac{d^2\hat{\theta}_{(0)}}{d\hat{\eta}^2} = 0. \tag{5.63}$$

It must be pointed that the solutions must be expressed before and after the flame, $\hat{\eta}_f$. In the oxidant side, $\hat{\theta}_{(0)} = q/(S+1)\left(\hat{H}_{(0)} + \hat{Z}_{(0)} - 1\right)$, and in the fuel side,

$\hat{\theta}_{(0)} = q/(S+1)\left(\hat{H}_{(0)} + (1-\hat{Z}_{(0)})/S\right)$. Then Equation (5.63) is written as:

$$\frac{d^2}{d\hat{\eta}^2}\begin{cases} \left(\hat{H}_{(0)} - \frac{\hat{Z}_{(0)}}{S}\right) = 0, & \text{for } \hat{Z} > 1, \\ \left(\hat{H}_{(0)} + \hat{Z}_{(0)}\right) = 0, & \text{for } \hat{Z} < 1. \end{cases} \tag{5.64}$$

The boundary condition obeyed by Equation (5.64) is the condition at the flame, given by:

$$\hat{H}_{(0)}(\hat{\eta}_f) = (S+1)\theta_f/q. \tag{5.65}$$

Also, Equation (5.64) must match with the excess enthalpy in the outer zone as:

$$\hat{H}_{(0)}(\hat{\eta} \to \infty) = H_{(0)}(\eta = 0) = 1 + \frac{(S+1)}{q}\theta_m \ , \quad \left.\frac{d\hat{H}_{(0)}}{d\hat{\eta}}\right|_{\hat{\eta}\to+\infty} = 0. \tag{5.66}$$

The continuity of the first derivative at the flame must also be obeyed:

$$\left.\frac{d\hat{H}_{(0)}}{d\hat{\eta}}\right|_{\hat{\eta}=\hat{\eta}_f^+} = \left.\frac{d\hat{H}_{(0)}}{d\hat{\eta}}\right|_{\hat{\eta}=\hat{\eta}_f^-} \tag{5.67}$$

Solving Equation (5.64) with boundary, matching and continuity conditions given by Equations (5.65) - (5.67), the leading order term of the excess enthalpy function in the flame zone is found as:

$$\hat{H}_{(0)}(\hat{\eta}) = \begin{cases} (S+1)\theta_f/q + \sqrt{2/\pi}e^{-\hat{\eta}_f^2}(S+1)\left(\hat{\eta}-\hat{\eta}_f\right) / \left(S\ erfc\left(\hat{\eta}_f/\sqrt{2}\right)\right) - \\ \left(erf\left(\hat{\eta}/\sqrt{2}\right) - erf\left(\hat{\eta}_f/\sqrt{2}\right)\right)/S\ erfc\left(\hat{\eta}_f/\sqrt{2}\right), & \text{for } \hat{Z} > 1 \\ 1 + (S+1)\theta_m/q - erfc\left(\hat{\eta}/\sqrt{2}\right)/erfc\left(\hat{\eta}_f/\sqrt{2}\right), & \text{for } \hat{Z} < 1. \end{cases} \tag{5.68}$$

Applying the conditions at the flame, is found that $\theta_m = \theta_f$. The unknown temperature observed from the outer zone to the flame zone is the flame temperature itself. The excess enthalpy in the flame zone is presented in Figure (5.5).

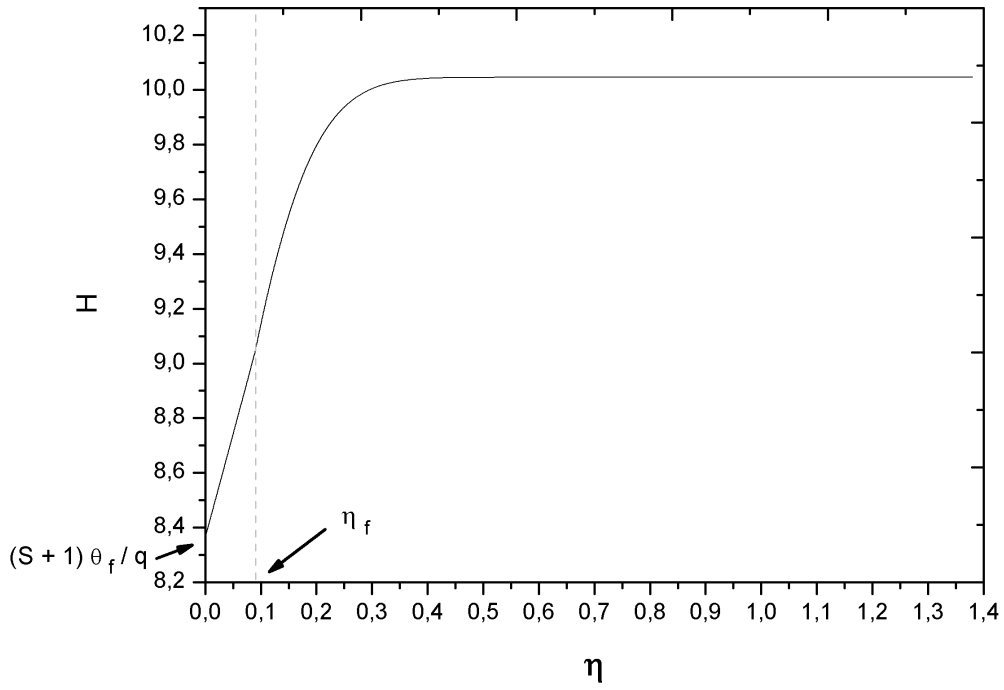

Figure 5.5 - Excess enthalpy in the flame zone, $\theta_f = 1.13$, $\hat{\eta}_f = 0.7$, $S = 15.0$, $q = 2.0$.

In the flame zone, gas and solid are yet in thermal equilibrium. Their profile is obtained by the solution of Equation (5.61), with the following boundary and matching conditions:

$$\hat{\theta}(\hat{\eta}_f) = \theta_f, \quad \hat{\theta}(0) = \theta_{s0}, \quad \Gamma^{1/2} \left. \frac{d\hat{\theta}}{d\hat{\eta}} \right|_{\hat{\eta} \to +\infty} = \left. \frac{d\theta}{d\eta} \right|_{\eta=0}. \tag{5.69}$$

Note that when the inner zone is observed from the flame zone, the solid phase temperature at the gas-liquid interface is observed. This is due to the asymptotic behavior of the temperature, and from the fact that the solid phase heat flux is conductive, resulting in a linear decrease.

The solution of Equation (5.61) is expressed as:

$$\hat{\theta}(\hat{\eta}) = \hat{\theta}_{(0)} + O(\Gamma^{-1/2}) \tag{5.70}$$

Substituting Equation (5.70) in Equation (5.61), the leading order term of the tem-

perature profile in the flame zone is given by the solution of the following differential equation:

$$\frac{d^2\hat{\theta}_{(0)}}{d\hat{\eta}^2} = 0, \tag{5.71}$$

that must be solved with the following boundary and matching conditions:

$$\hat{\theta}_{(0)}(\hat{\eta}_f) = \theta_f, \quad \hat{\theta}_{(0)}(0) = \theta_{s0}, \quad \left.\frac{d\hat{\theta}_{(0)}}{d\hat{\eta}}\right|_{\hat{\eta}\to+\infty} = 0. \tag{5.72}$$

Hence, the leading order term of the temperature in the flame zone is given by:

$$\hat{\theta}_{(0)}(\hat{\eta}) = \begin{cases} \theta_{s0} + (\theta_f - \theta_{s0})\hat{\eta}/\hat{\eta}_f, & \text{for} \quad \hat{\eta} < \hat{\eta}_f \ (Z > 1) \\ \\ \theta_f, & \text{for} \ \ \hat{\eta} > \hat{\eta}_f \ (Z < 1). \end{cases} \tag{5.73}$$

It must be pointed that $(\theta_f - \theta_{s0}) = O(1)$. This result is mandatory when the continuity of the solid heat flux from above and below the interface is imposed. The temperature profile in the flame zone is presented in Figure (5.6).

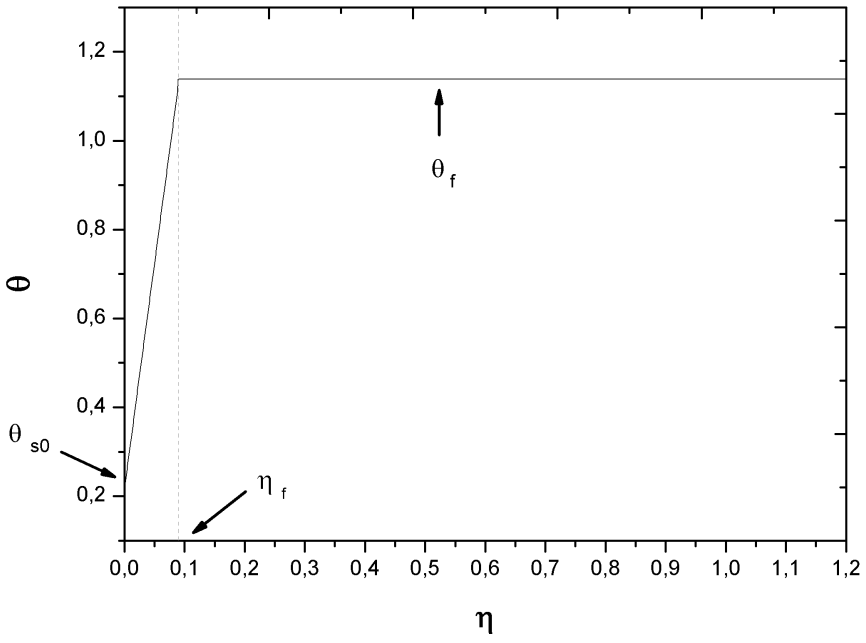

Figure 5.6 - Temperature in the flame zone, $\theta_{s0} = 0.22$, $\theta_f = 1.13$, $\hat{\eta}_f = 0.7$.

The flame position exhibited in Figure (5.6) is located in the point in which the temperature presents a discontinuity in its derivative.

Unlike in free flame conditions, the heat released at the flame is transported to both sides by conduction and convection in the gas phase, and additionally by conduction in the solid phase. This additional process increases the heat transfer from the flame to the liquid surface, $\hat{\eta} = 0$, and, consequently, augments the vaporization rate: phase change.

The thermal equilibrium between phases depends on the characteristic flow time, τ_f, compared with the characteristic heat exchange time, τ_h, and both are approximately given by:

$$\begin{cases} \tau_f \simeq X/\vartheta, \\ \tau_h \simeq \rho c_p/h_g. \end{cases} \tag{5.74}$$

in which X and ϑ are, respectively, a characteristic length scale and a characteristic velocity. When the characteristic flow time is higher than the characteristic heat exchange time, the non-equilibrium is observed, and when both are of the same order, or if the characteristic heat exchange time is higher than the characteristic flow time, thermal equilibrium is observed.

In the present problem, the non-dimensional characteristic velocity is always of unitary order (in each zone it is re-scaled), but the non-dimensional characteristic length scale decreases ($X_{oz} > X_{fz} > Xiz$), as the spatial variable is stretched in each zone. Hence, the characteristic flow time in each zone follows the relation:

$$\tau_{f_{oz}} = \Gamma^{-1/2}\tau_{f_{fz}} = \Gamma^{-1}\tau_{f_{iz}}. \tag{5.75}$$

And the ratio between the characteristic flow time and the characteristic heat exchange time in each zone follows:

$$\frac{\tau_f}{\tau_h} = \begin{cases} O(\Gamma), & \text{Outer zone}, \\ O(\Gamma^{1/2}), & \text{Flame zone}, \\ O(1). & \text{Inner zone}. \end{cases} \tag{5.76}$$

From Equation (5.76) it is concluded that the thermal equilibrium between solid and gas phases is observed in the outer and in the flame zone, while in the inner zone the non-equilibrium prevails.

5.2.3 Inner zone: problem of the order of Γ^{-1}

As the flow reaches a region of the order Γ^{-1} from the gas-liquid interface, it enters the inner zone. In this zone, the macroscopic viscous effect become relevant, due to the interface, and the low-vaporization regime is described. Also, thermal equilibrium is no longer satisfied. Hence, the two-energy model must be solved for determining the properties of the gas and solid phases.

In order to analyze the the problem in this small region, a boundary layer expansion must be performed. The spatial coordinate is stretched as $\tilde{\eta} = \Gamma^{1/2}\hat{\eta}$. The momentum also must be re-scaled in the inner zone according to $\tilde{f} = \Gamma^{1/2}\hat{f}$.

The momentum profile is the same as the one calculated in Chapter (4), but considering $\tilde{f}_1 = 0$, because the thermal expansion for the gas phase is negligible, and hence, the heat source (flame) does not influence the flow field. The momentum in the inner zone is then given by:

$$\tilde{f}(\tilde{\eta}) = \tilde{f}_0 + \tilde{\eta} + \frac{1}{\sqrt{\varepsilon\beta}}\left(e^{-\sqrt{\varepsilon\beta}\tilde{\eta}} - 1\right) + \frac{\Gamma^{-1}}{8\varepsilon\beta Pr}\left[\frac{7}{\sqrt{\varepsilon\beta}}\left(1 - e^{-\sqrt{\varepsilon\beta}\tilde{\eta}}\right) - 6\tilde{\eta}\ e^{-\sqrt{\varepsilon\beta}\tilde{\eta}} - \right.$$
$$8(1-\varepsilon Pr)\tilde{\eta} - 2\left(\frac{1}{\sqrt{\varepsilon\beta}} + \tilde{f}_0\right)\left(3 + 2\sqrt{\varepsilon\beta}\tilde{\eta}\right)\ e^{-\sqrt{\varepsilon\beta}\tilde{\eta}} + 6\left(\frac{1}{\sqrt{\varepsilon\beta}} + \tilde{f}_0\right) -$$
$$\left. 2\sqrt{\varepsilon\beta}\tilde{\eta}^2\ e^{-\sqrt{\varepsilon\beta}\tilde{\eta}} - \frac{1}{\sqrt{\varepsilon\beta}}\left(7 - 8\varepsilon Pr - \sqrt{\varepsilon\beta}\tilde{f}_0\right)\left(1 - e^{-\sqrt{\varepsilon\beta}\tilde{\eta}}\right)\right] + O(\Gamma^{-2}) \qquad (5.77)$$

Re-scaling the spatial coordinate in Equation (5.52) leads to:

$$\Gamma\frac{d^2\tilde{Z}}{d\tilde{\eta}^2} + \tilde{f}\frac{d\tilde{Z}}{d\tilde{\eta}} = 0 \qquad (5.78)$$

in which the tilde in the Z variable is only to distinguish between zones profiles.

Boundary and matching conditions of Equation (5.78) are given by:

$$\tilde{Z}(0) = Sy_{F0} + 1, \quad \Gamma\left.\frac{d\tilde{Z}}{d\tilde{\eta}}\right|_{+\infty} = \Gamma^{1/2}\left.\frac{d\hat{Z}}{d\hat{\eta}}\right|_{0}. \qquad (5.79)$$

Solution to Equation (5.78) are expressed as:

$$\tilde{Z} = \tilde{Z}_0 + \Gamma^{-1/2}\tilde{Z}_{(1/2)} + O(\Gamma^{-1}\tilde{Z}_{(1)}), \qquad (5.80)$$

in which $\tilde{Z}_0$ is constant and given by $\tilde{Z}_0 = Sy_{F0} + 1$ (arises from matching and boundary conditions).

Substituting Equation (5.80) in Equation (5.78) and collecting the higher order terms, the following differential equation is found:

$$\frac{d^2\tilde{Z}_{(1/2)}}{d\tilde{\eta}^2} = 0, \tag{5.81}$$

which must satisfy boundary and matching conditions given by:

$$\tilde{Z}_{(1/2)}(0) = 0, \quad \left.\frac{d\tilde{Z}_{(1/2)}}{d\tilde{\eta}}\right|_{\tilde{\eta}\to+\infty} = \left.\frac{d\hat{Z}_{(0)}}{d\hat{\eta}}\right|_{\hat{\eta}=0}. \tag{5.82}$$

The solution of Equation (5.81) with boundary and matching conditions given by Equations (5.81) provides the mixture fraction in the inner zone:

$$\tilde{Z}(\tilde{\eta}) = (S\ y_{F0} + 1) - \Gamma^{-1/2}\sqrt{\frac{2}{\pi}}\ \frac{\tilde{\eta}}{erfc\left(\hat{\eta}_f/\sqrt{2}\right)} + O(\Gamma^{-1}). \tag{5.83}$$

The profile of the mixture fraction in the inner zone is presented in Figure (5.7).

In the inner zone, the thermal equilibrium between solid and gas phases is no longer observed. In order to analyze the thermal problem in this zone, the two-equation model must be solved. Equations (5.21) and (5.22) in the inner variables are expressed as:

$$0 = \Gamma\varepsilon\frac{d^2\theta_g}{d\tilde{\eta}^2} + \varepsilon\tilde{f}\frac{d\theta_g}{d\tilde{\eta}} + \Gamma n_g(\theta_s - \theta_g), \tag{5.84}$$

$$0 = \Gamma^2(1-\varepsilon)\frac{d^2\theta_s}{d\tilde{\eta}^2} - \Gamma n_g(\theta_s - \theta_g). \tag{5.85}$$

The above equations must obey boundary and matching conditions given by:

$$\theta_s(0) = \theta_{s0}, \quad \theta_g(0) = \theta_B, \quad \Gamma^{1/2}\left.\frac{d\theta_{s,g}}{d\eta}\right|_{+\infty} = \left.\frac{d\hat{\theta}}{d\hat{\eta}}\right|_0 \tag{5.86}$$

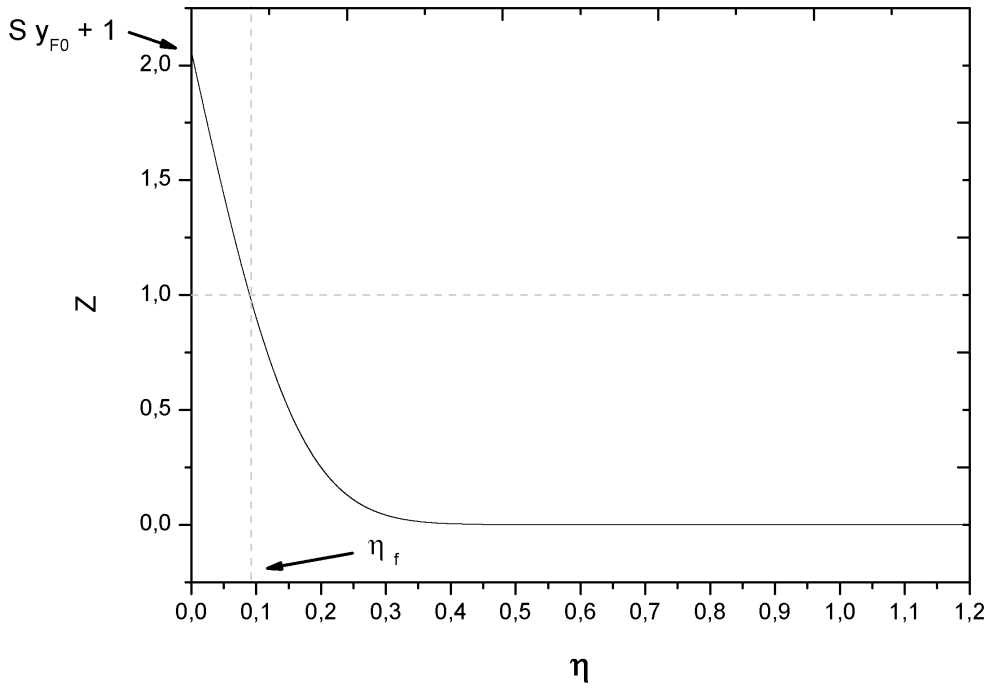

Figure 5.7 - Mixture fraction in the inner zone, $y_{F0} = 0.07$, $\hat{\eta}_f = 0.70$, $S = 15.0$.

The solutions of Equations (5.84) and (5.85) are expressed as:

$$\left\{ \begin{array}{l} \theta_s = \theta_{s(0)} + \Gamma^{-1/2}\theta_{s(1/2)} + O(\Gamma^{-1}), \\ \theta_g = \theta_{g(0)} + \Gamma^{-1/2}\theta_{g(1/2)} + O(\Gamma^{-1}). \end{array} \right\} \tag{5.87}$$

Substituting Equations (5.87) into Equations (5.84) and (5.85) and collecting equal powers of Γ, the following set of equations is found:

$$\frac{d\theta_{s(0)}}{d\tilde{\eta}} = 0, \tag{5.88a}$$

$$\frac{d\theta_{s(1/2)}}{d\tilde{\eta}} = 0, \tag{5.88b}$$

$$\varepsilon \frac{d^2\theta_{g(0)}}{d\tilde{\eta}^2} + n_g(\theta_{s(0)} - \theta_{g(0)}) = 0, \tag{5.88c}$$

$$\varepsilon \frac{d^2\tilde{\theta}_{g(1/2)}}{d\tilde{\eta}^2} + n_g(\theta_{s(1/2)} - \theta_{g(1/2)}) = 0. \tag{5.88d}$$

The above set of equations must be solved with the following boundary and matching conditions:

$$\theta_{s(0)}(0) - \theta_{s0} = \theta_{s(1/2)}(0) = 0, \quad \theta_{g(0)}(0) - \theta_B = \theta_{g(1/2)}(0) = 0, \tag{5.89a}$$

$$\left.\frac{d\theta_{s(0)}}{d\tilde{\eta}}\right|_{+\infty} = \left.\frac{d\theta_{s(1/2)}}{d\tilde{\eta}}\right|_{+\infty} - \left.\frac{d\hat{\theta}_{(0)}}{d\hat{\eta}}\right|_{0} = 0, \quad \left.\frac{d\theta_{g(0)}}{d\tilde{\eta}}\right|_{+\infty} = \left.\frac{d\theta_{g(1/2)}}{d\tilde{\eta}}\right|_{+\infty} - \left.\frac{d\hat{\theta}_{(0)}}{d\hat{\eta}}\right|_{0} = 0 \tag{5.89b}$$

In a rigorous way, the conditions $\theta_{s(1/2)}(0) = \theta_{g(1/2)}(0) = 0$ should be replaced by $\theta_{s(1/2)}(0) = \theta_{s1/2}$ and $\theta_{g(1/2)}(0) = \theta_{B1/2}$, in order to capture minor temperature fluctuations (as considered in Chapter (4)). However, these fluctuations have been neglected in order to simplify the calculations in this chapter.

Solving Equations (5.88a) - (5.88d) with boundary and matching conditions given by Equations (5.89a) and (5.89b), the profiles for gas and solid phase temperatures in the inner zone are obtained as:

$$\theta_s(\tilde{\eta}) = \theta_{s0} + \Gamma^{-1/2}\frac{(\theta_f - \theta_{s0})}{\hat{\eta}_f}\tilde{\eta} + O(\Gamma^{-1}), \tag{5.90}$$

$$\theta_g(\tilde{\eta}) = \theta_{s0} - (\theta_{s0} - \theta_B)e^{-\sqrt{n_g/\varepsilon}\tilde{\eta}} + \Gamma^{-1/2}\frac{(\theta_f - \theta_{s0})}{\hat{\eta}_f}\tilde{\eta} + O(\Gamma^{-1}). \tag{5.91}$$

Through the inner zone, practically all the heat released in the flame zone goes to the liquid surface. From there, the heat is partially used to change the liquid fuel to vapor of fuel. The other part of the heat goes to the thermal equilibrium, liquid-solid region. The temperatures profiles in the inner zone are presented in Figure (5.8).

As seen in Figure (5.8), the temperatures decouple only at the inner zone. However, their difference is not large, since the inner zone is very small. Precisely, the difference between the gas and solid phases is of the order of the inner zone thickness, $(\theta_{s0} - \theta_B) = O(\Gamma^{-1})$. Although this result is the same as the result obtained in Chapter (4), the solid phase temperature at the interface in the present case will be larger, as a consequence of the existence of the flame.

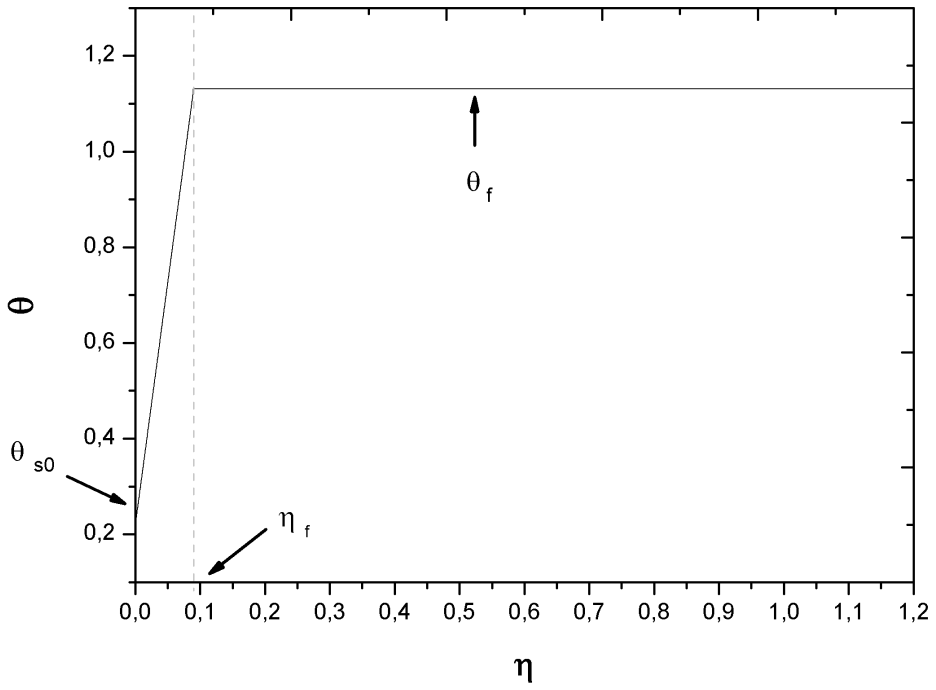

Figure 5.8 - Temperatures in the inner zone, $\theta_{s0} = 0.22$, $\theta_f = 1.13$, $\theta_B = 0.2$, $\hat{\eta}_f = 0.7$, $n_g = 1.0$, $\varepsilon = 0.3$.

The excess enthalpy function, that accounts for the chemical and thermal enthalpy, may be obtained directly from its definition. Then, its leading order term is given by:

$$\tilde{H}_{(0)}(\tilde{\eta}) = \frac{(S+1)}{q}\left[\theta_{s0} - (\theta_{s0} - \theta_B)\; e^{-\sqrt{n_g/\varepsilon}\tilde{\eta}}\right] + y_{F0} \tag{5.92}$$

The enthalpy variation in the inner zone is caused by the fuel vaporization at the gas-liquid interface (chemical enthalpy) and by the heating of the gaseous fuel (thermal enthalpy). The excess enthalpy function, $\tilde{H}$, is presented in Figure (5.9).

From the analysis presented in this section, five unknown values have emerged: flame temperature (θ_f), flame position ($\hat{\eta}_f = \Gamma^{-1/2}\eta_f$), vaporization rate ($\tilde{f}_0$), solid phase temperature at the interface (θ_{s0}) and fuel mass fraction at the interface (y_{F0}). These values will be specified through continuity conditions and energy conservation at the interface, as will be seen subsequently.

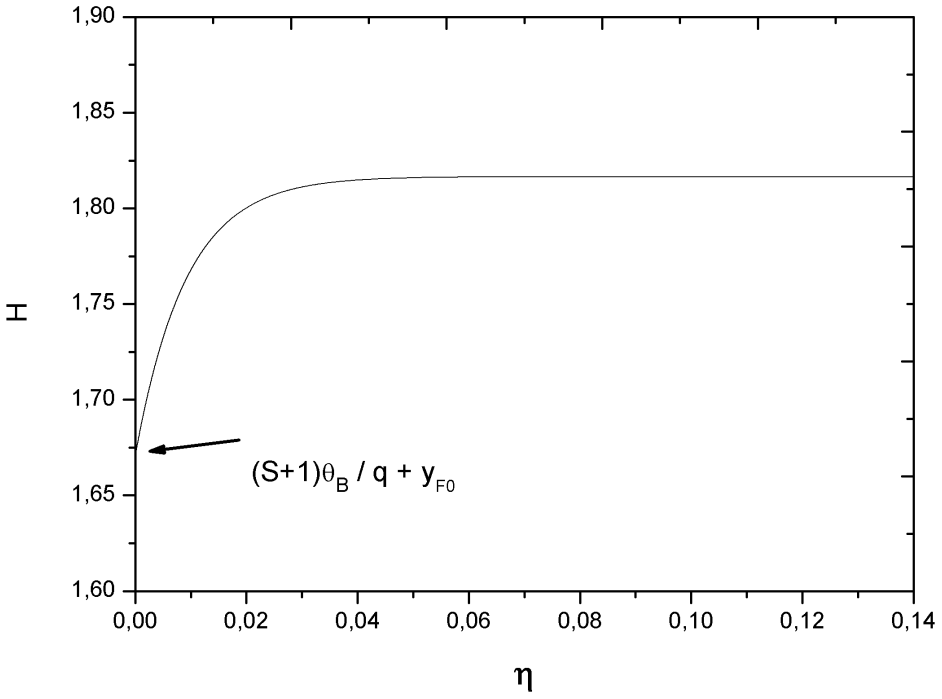

Figure 5.9 - Excess enthalpy in the inner zone, $\theta_{s0} = 0.22$, $\theta_B = 0.2$, $y_{F0} = 0.07$, $S = 15.0$, $q = 2.0$, $n_g = 1.0$, $\varepsilon = 0.3$.

5.3 Liquid-solid region

Recalling, in the region below the gas-liquid interface, $\tilde{\eta} < 0$, the solid matrix is filled by the liquid fuel and it is defined as liquid-solid region. In this region, two distinct zones are observed. Own to the high rate of heat transfer between liquid and solid phases ($N_l = O(\Gamma^2)$), the thermal equilibrium condition is found in most part of the liquid-solid region. The thermal equilibrium permits imposing the simplification $\theta_s = \theta_l = \theta$, and a one-equation model is enough for describing the temperature profile. By approaching the liquid surface from below, the detachment of the temperature profiles is observed. In a length scale of order Γ^{-1} near the interface, the liquid fuel remains at an almost constant temperature, its boiling temperature, and all the heat provided to the liquid phase in this zone by the solid phase is used in phase change. The solid phase, on the other hand, does not have such physical constraint, and its temperature continues to increase as an effect of the heat flux coming from the gas-solid region, above the interface. Then, a detachment between the temperature

profiles is seen, and the two-equation model is required in this zone o determine the liquid and solid phases temperatures.

The liquid-solid problem detailed in the present chapter is the equal to the liquid-solid problem detailed in Chapter (4).

5.3.1 Equilibrium zone: problem of the order of unity

In a region of order of unity below the interface, thermal equilibrium between solid and liquid phases is assumed, thus $\theta_s = \theta_l = \theta$. Following the procedure presented in Chapter (4), the differential equation that must be solved for determining the temperature profile in the equilibrium zone is given by:

$$\left(\frac{J+\gamma}{M}\right)\frac{d^2\theta}{dz^2} - \frac{d\theta}{dz} = 0. \tag{5.93}$$

The boundary conditions for Equation (5.93) are given by $\theta = \theta_{-\infty}$ for $z \to -\infty$, and $\theta = \theta_{s0}$ at $z = 0$. Solving Equation (5.93) with these boundary conditions, the temperature profile is expressed by:

$$\theta(z) = (\theta_{s0} - \theta_{-\infty})\, e^{zM/(J+\gamma)} + \theta_{-\infty}. \tag{5.94}$$

It must be remembered that the parameter M is directly related with the vaporization rate, in such a way that $M \sim f_0 = O(\Gamma^{-1})$ according to Equation (5.25), as a result of the low-vaporization regime. Only at a large distance of the interface the exponential behavior of the temperature in the equilibrium zone is observed, as exhibited by Figure (5.10). The difference between Equation (5.94) and Equation (4.50) is the value of the solid phase temperature at the interface, θ_{s0}. In the present problem, it is higher than the problem presented in Chapter (4), due to the existence of the flame.

As the flow approaches the interface from below, a thermal decoupling between phases is observed in a small region near the interface, the boiling zone. In this zone, the liquid fuel is at an almost constant temperature, its boiling temperature, and almost all heat provided to the liquid fuel goes to change its phase.

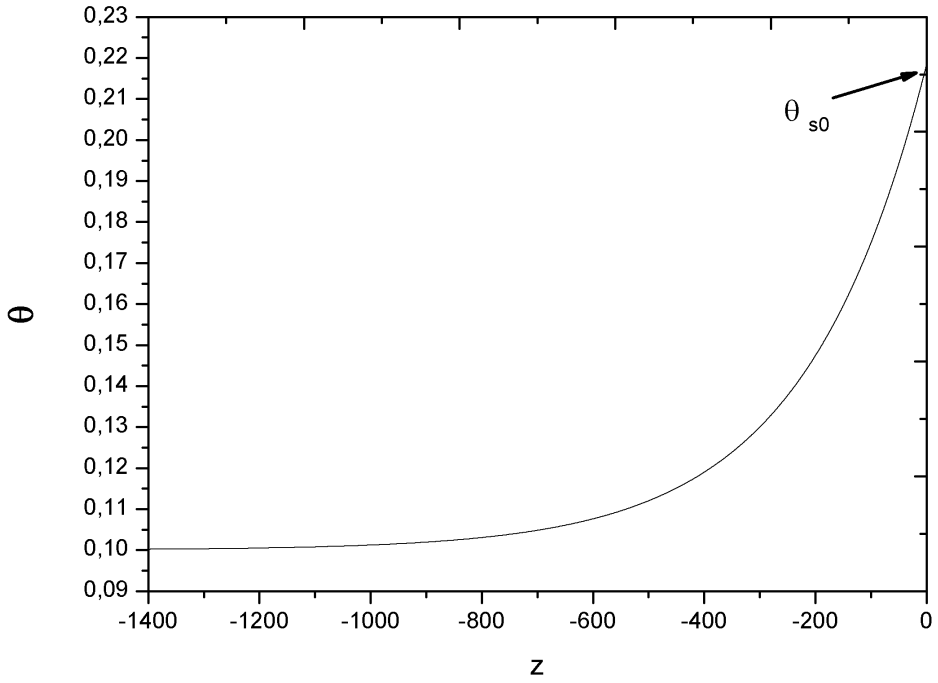

Figure 5.10 - Temperature in the equilibrium zone, $\theta_{s0} = 0.22$, $\theta_{-\infty} = 0.1$, $M = 0.015$, $J = 1.0$, $\varepsilon = 0.3$.

5.3.2 Boiling zone: problem of the order of Γ^{-1}

In a spatial length scale of order Γ^{-1} below the interface, thermal non-equilibrium is observed between phases. In order to capture the temperature variations, a stretch in the spatial coordinate is necessary and given by $\tilde{z} = \Gamma z$. This coordinate change must be performed in Equations (5.29) and (5.30), and their solutions follows the same procedure as the one performed in Chapter (4). The difference, as said previously, is that in the present chapter it is being considered that $\theta_{s1} = 0$, hence, the temperature profiles for the boiling zone in the present chapter can be directed obtained from setting $\theta_{s1} = 0$ in Equations (4.55a) and (4.55b):

Hence, the solid and liquid phase temperatures in the boiling zone are expressed by:

$$\theta_l(\tilde{z}) = \theta_B + \Gamma^{-1}\left(M\frac{\theta_{s0} - \theta_{-\infty}}{J+\gamma}\right)\tilde{z} + O(\Gamma^{-2}), \tag{5.95a}$$

$$\theta_s(\tilde{z}) = \theta_B + (\theta_{s0} - \theta_B)\ exp\left(\sqrt{\frac{n_l}{1-\varepsilon}}\tilde{z}\right) + \Gamma^{-1}\left(M\frac{\theta_{s0} - \theta_{-\infty}}{J+\gamma}\right)\tilde{z} + O(\Gamma^{-2}). \quad (5.95b)$$

As mentioned before, and to be proved in the next section, the terms M and $(\theta_{s0} - \theta_B)$ are of the order of Γ^{-1}. Based on this, it is seen that the temperature variation of the liquid phase is of the order of Γ^{-2}. The solid phase temperature in a first approximation is also constant and equal to the boiling temperature, and its variation is of the order of Γ^{-1} (even though the leading order term for the solid phase temperature it is a constant, the fact that $(\theta_{s0} - \theta_B) = O(\Gamma^{-1})$ leads the leading order variations to the order of Γ^{-1}). Hence, the solid-liquid heat exchange term in Equation (5.26b) is of the order of unity ($N_l = O(\Gamma^2)$ and $\bar{z}_b = O(\Gamma^{-1})$), the same order of the vaporization term, lf ($l = O(\Gamma)$ and $f = O(\Gamma^{-1})$). The temperature profiles in the boiling zone are presented in Figure (5.11).

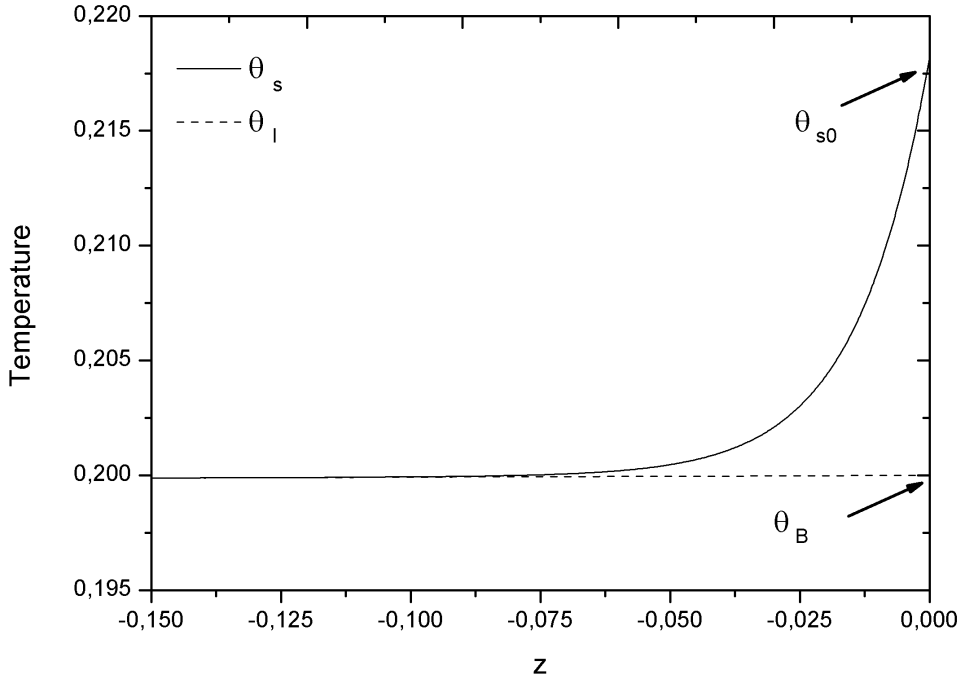

Figure 5.11 - Temperatures in the boiling zone, $\theta_{s0} = 0.22$, $M = 0.015$, $\theta_B = 0.2$. $\theta_{-\infty} = 0.1$, $J = n_l = 1.0$, $\varepsilon = 0.3$.

Although the obtained profiles in the present chapter for the boiling zone are similar

to the temperature profiles obtained in Chapter (4), the solid phase temperature at the interface in the present case is higher. This is a consequence of the existence of the flame, which provides additional heat to the system, hence, increasing the solid matrix temperature and the vaporization rate.

In the next section, the continuity of the solid phase heat flux and the energy conservation at the interface will be used in order to obtain the five unknown values of the problem.

5.4 Determination of the unknowns of the problem: $\hat{\eta}_f$, θ_f, $\tilde{f}_0$, θ_{s0} and y_{F0}

Five unknowns characterize the problem: flame position ($\hat{\eta}_f$), flame temperature (θ_f), vaporization rate ($\tilde{f}_0$), solid phase temperature at the interface (θ_{s0}) and fuel mass fraction at the interface (y_{F0}). They are determined through two conditions: continuity of the solid phase heat flux at the interface and the energy conservation at the interface.

From Equation (5.26b), the energy conservation at the interface is given by:

$$\varepsilon \frac{d\theta_g}{d\tilde{\eta}}\bigg|_{\tilde{\eta}=0^+} = -\tilde{l}\tilde{f}_0 + \Gamma\varepsilon \frac{J}{a^{1/2}} \frac{d\theta_l}{d\tilde{z}}\bigg|_{\tilde{z}\to-\infty} - \Gamma \frac{n_l}{a^{1/2}} \int_{-\infty}^{0} (\theta_s - \theta_l) d\tilde{z}. \tag{5.96}$$

in which the latent heat of vaporization have been re-scaled by $\tilde{l} = \Gamma\ l$ (following the low-volatile fuel hypothesis), $\tilde{f}_0 = \Gamma f_0$ and $N_l = n_l \Gamma^2$.

In the energy conservation equation at the interface, the leading order terms are correspondent to the vaporization rate and to the heat exchange between solid and liquid phases in the boiling zone. Then, balancing these two terms and using Equations (5.95a) and (5.95b) to determine the integral term, the vaporization rate is specified by:

$$\tilde{f}_0 = -\Gamma \left(\frac{n_l}{a}\right)^{1/2} \frac{(\theta_{s0} - \theta_B)}{\tilde{l}} (1-\varepsilon)^{1/2}. \tag{5.97}$$

This expression is equal to the vaporization rate obtained in Chapter (4), and given by Equation (4.76), when we set $\tilde{f}_1 = 0$. However, in the present problem, the solid phase temperature at the interface, θ_{s0}, is higher, as a consequence of the heat source due to the exothermic reaction in the flame zone.

If the higher order terms of the energy conservation at the interface are collected,

the following relation is found:

$$\left.\frac{d\tilde{\theta}_{g(0)}}{d\tilde{\eta}}\right|_{0^+} = \frac{J}{a^{1/2}} \left.\frac{d\theta_{l(1)}}{d\tilde{z}}\right|_{-\infty} \tag{5.98}$$

Evaluating Equation (5.98), it is obtained:

$$\sqrt{\frac{n_g}{\varepsilon}}(\theta_{s0} - \theta_B) = \frac{M}{J+\gamma}(\theta_{s0} - \theta_{-\infty}). \tag{5.99}$$

The parameter M is related to the vaporization rate through $M \equiv -\Gamma^{-1}\,(c_l/c_p)\,a^{1/2}\tilde{f}_0$, as seen in Equation (5.25). If the vaporization rate, $\tilde{f}_0$, given by Equation (5.97), is utilized in the definition for M, and inserted in Equation (5.99), the solid phase temperature at the interface is obtained as:

$$\theta_{s0} = \theta_{-\infty}\left(\frac{c_p}{c_l}\right)\sqrt{\frac{n_g}{n_l}}\frac{\tilde{l}}{\sqrt{\varepsilon(1-\varepsilon)}} \tag{5.100}$$

If the continuity of the solid phase heat flux at the interface is imposed, the following equality must be true:

$$\Gamma^{1/2}\left.\frac{d\tilde{\theta}_s}{d\tilde{\eta}}\right|_{0^+} = \Gamma\left.\frac{d\theta_s}{d\tilde{z}}\right|_{0^-}, \tag{5.101}$$

in which the re-scaling in the gas phase is performed through the flame zone, since it is in this zone that the heat source is located.

Since the leading order term for the solid phase in the inner zone is a constant value, the continuity of the heat flux is expressed through:

$$\left.\frac{d\tilde{\theta}_{s(1/2)}}{d\tilde{\eta}}\right|_{0^+} = \Gamma\left.\frac{d\theta_{s(0)}}{d\tilde{z}}\right|_{0^-}. \tag{5.102}$$

Equation (5.102) is a valid expression even with the Γ multiplying the right side. The solution for this apparent incongruence is that the leading order term for the solid temperature, $\theta_{s(0)}$, is formed by a constant term and a term that appears as a function of $(\theta_{s0} - \theta_B) = O(\Gamma^{-1})$, which is the same order of $d\tilde{\theta}_{s(1/2)}/d\tilde{\eta}$. Evaluating Equation (5.102), the flame temperature is obtained as a function of the flame

position and of the solid phase temperature at the interface:

$$\theta_f = \theta_{s0} + \Gamma(\theta_{s0} - \theta_B)\sqrt{\frac{n_l}{1-\varepsilon}}\,\hat{\eta}_f. \tag{5.103}$$

Since $(\theta_{s0} - \theta_B) = O(\Gamma^{-1})$, according to Equation (5.99), the flame temperature, θ_f, is one order of magnitude higher than the solid temperature at the interface, θ_{s0}. Otherwise, the model would be non-valid, since the matching would not be accomplished.

The flame position, $\hat{\eta}_f$, is found from the mixture fraction expression in the flame zone, when the leading order term is taken to $\hat{\eta} \to 0$. Performing this condition in Equation (5.58) for the mixture fraction in the fuel side, gives:

$$erf\left(\frac{\hat{\eta}_f}{\sqrt{2}}\right) = \frac{Sy_{F0}}{Sy_{F0}+1}, \tag{5.104}$$

which can be approximated by to give the flame position as:

$$\hat{\eta}_f \sim \sqrt{\frac{2}{\pi}}\,\frac{Sy_{F0}}{Sy_{F0}+1}. \tag{5.105}$$

Mass conservation at the interface, expressed in terms of the mixture fraction, is given by:

$$\left.\frac{d\tilde{Z}}{d\tilde{\eta}}\right|_{\tilde{\eta}=0} = \frac{S}{\Gamma}(1-y_{F0})\tilde{f}_0. \tag{5.106}$$

From Equations (5.83) and (5.102), the fuel mass fraction at the liquid surface is determined:

$$y_{F0} = \frac{\left(\Gamma^{-1/2}\tilde{f}_0\sqrt{\pi/2} + 1/S\right)}{\left(\Gamma^{-1/2}\tilde{f}_0\sqrt{\pi/2} - 1\right)}. \tag{5.107}$$

Analyzing the order of magnitude of Equation (5.107), it is possible to observe that the stoichiometric coefficient must obey the following constraint:

$$S > \frac{\Gamma^{1/2}}{\tilde{f}_0}\sqrt{\frac{2}{\pi}} \tag{5.108}$$

in such a way that $y_{F0} \sim \Gamma^{-1/2}$.

The magnitude order of S given by (5.108) is physically justified by the fact that a low-volatile (heavy) liquid fuel is being considered.

The problem unknowns are calculated using the following properties:

$$c_p/c_l = n_g = n_l = 1.0, \quad q = 2.0,$$

$$\theta_{-\infty} = 0.1, \quad \theta_B = 0.2$$

$$\Gamma = 60.0, \quad a = J = 1.0,$$

$$\varepsilon = 0.3, \quad \tilde{l} = 1, \quad S = 15.0$$

Which lead to:

$$\theta_{s0} = 0.2182, \quad \tilde{f}_0 = -0.9145, \quad y_{F0} = 0.0708, \quad \hat{\eta}_f = 0.6985, \quad \theta_f = 1.1308 \quad (5.109)$$

These values were used in the evaluation of the profiles presented in all parts of the present chapter.

As seen, the flame temperature is close to the injection temperature of the oxidant. However, this does not means a flame at low temperature. Instead, leads to the conclusion that in order to the diffusion flame regime is established, the oxidant injection temperature must be high, close to the flame temperature. This fact arises due to the low vaporization regime.

5.5 Conclusions

In this chapter, the burning of a low-volatile liquid fuel inside a low porosity medium have been analyzed. A stream of hot oxidant impinging against the liquid surface has been considered.

Different spatial length scales arise in the present problem due to physical processes that occurs in different length scales. Differently from the problem presented in Chapter (4), three, not two, zones emerged from the analysis in the gas-solid region. As previously, an outer and an inner zone were observed, of length scales of the order of unity and of the order of Γ^{-1}, respectively. However, in a length scale of the order of $\Gamma^{-1/2}$, a flame zone emerged. In this zone, the diffusion flame is established, and consumption of oxidant and fuel occurs. Since the heat transfer between gas and solid phases is considered to be intense, the two phases are in thermal equilibrium

in the most part of the gas-solid region. This equilibrium is justified by the analysis of characteristic times given in Equation (5.76).

The diffusion flame in the flame zone is sustained by the vaporized fuel. The solid phase enhances the vaporization rate through heat conduction, transporting the heat from the inner zone (a region of the order of Γ^{-1} above the interface) to the boiling zone (a region of the order of Γ^{-1} below the interface). The heat flux in the inner zone is originated in the flame zone. Through the intense heat transfer between solid and liquid phases in the boiling zone, heat is provided to the liquid fuel such that it goes through phase change.

The results obtained also points to an injection temperatures close to the flame temperature (high), in order to the diffusion flame regime is established. This is a consequence of the fact that the considered fuel is a low-volatile one.

It is important to emphasize that a Burke-Schumann limit was imposed in the present study. This imposition leads to a existing and established flame. In order to study ignition and stability (that may lead to the extinction regime) of the flame, the large activation energy procedure could be employed (LIÑAN, 1974).

6 CONCLUSIONS AND FUTURE WORKS

The present work analyzed the burning of a low-volatile liquid fuel inside a low porosity medium, subjected to an impinging stream of hot oxidant. The combustion process was studied under the scope of the fluid-dynamical aspects of the system. High rates of heat transfer between phases were assumed, by considering $N_g = O(\Gamma)$ and $N_l = O(\Gamma^2)$.

In order to perform a detailed physical analysis, the problem was divided in three parts.

In the first, a Hiemenz flow with heat transfer was considered (Chapter (3)). A stagnation-point flow was analyzed and profiles for momentum and temperatures of solid and gas phases were obtained. Two spatial length scales were recognized: an outer zone, in which the flow was governed by the Darcy equation with minor corrections, and in which thermal equilibrium between phases was observed, and an inner zone, a region of the order of Γ^{-1} from the solid wall, in macroscopic which viscous effects (to distinguish from the viscous effects that arises from the fluid-to-pore interaction) and thermal decoupling were observed. However, the thermal non-equilibrium is balanced by the low velocity of the flow, in such a way that the resident time of the flow was high enough to the gas phase reach an almost thermal equilibrium with the solid phase. Then, the thermal non-equilibrium was only observed in the higher order terms.

In the second part, an impinging flow against a pool of low-volatile liquid fuel was considered (Chapter (4)). The system was divided in two regions: the region in which the semi-infinite porous matrix was filled with the gas flow, gas-solid region, and the region in which the semi-infinite porous matrix was filled with the liquid fuel, liquid-solid region. In the gas-solid region, two spatial length scales were recognized. An outer zone, in which gas and solid were in thermal equilibrium due to the intense heat transfer, and in which the macroscopic viscous effects were not observed. And an inner zone, in which the thermal decoupling was observed and the low-vaporization regime, due to the fact that the fuel was low-volatile, was observed. In the liquid-solid region, two zones were also observed. In most part of the domain, liquid fuel and solid matrix were in thermal equilibrium due to the intense heat transfer between them. This zone was denoted as the equilibrium zone. In a region of the order of Γ^{-1} below the gas-liquid interface, the liquid fuel temperature remained at an almost

constant value, its boiling temperature, while the solid phase temperature increased towards the interface. In this zone, the boiling zone, all heat provided to the liquid fuel goes to phase change. From the energy balance at the interface, the vaporization rate was obtained. From this interface analysis, the vaporization was demonstrated to be a result of the heat exchanged between the solid phase and the liquid phase in the boiling zone. The porous matrix is the responsible for transporting the heat provided by the hot oxidant stream to inside the boiling zone. It was also shown that the injected oxidant should be one magnitude order higher than the liquid fuel boiling temperature. If a lower injection temperature was considered, the heavy fuel would not evaporate.

The third and conclusive part, was to consider the flame regime (Chapter (5)). As before, different spatial length scales arose. However, due to the low-vaporization regime, the flame have established in a region of the order of $\Gamma^{-1/2}$ away from the interface (the flame zone). It was concluded that the injection temperature should be close to the flame temperature, due to the fact that the low-vaporization regime imposes a small fuel mass flux to the flame, imposing injection of oxidant at high temperatures.

The study of the original problem in three steps offered a fertile ground for studies. The analytical expressions obtained in the development of the problem offered a comprehensive analysis of the physical aspects of each problem (heat transfer, heat transfer + phase change, heat transfer + phase change + chemical reaction).

6.1 Future works

Some extensions of the present problem can be suggested as future works:

- Consider a wider range of values for porosity and heat transfer, for example, $N_v = N_l = O(1)$ and $1/\kappa = O(1)$;
- Consider the thermal expansion for the gas. This will lead to variations in the gas phase density, and hence, a state equation will be required.
- Consider the limit of large activation energies for the flame in order to study ignition and extinction conditions for the diffusion flame;
- Consider the effect of capillarity of the liquid fuel in the porous medium.

REFERENCES

AKKUTLU, I. Y.; YORTSOS, Y. C. The dynamics of in-situ combustion fronts in porous media. **Comb. Flame**, v. 134, p. 229–247, 2003. 6

ALAZMI, B.; VAFAI, K. Constant wall heat flux boundary conditions in porous media under local thermal non-equilibriumm conditions. **Int. J. Heat Mass Transfer**, v. 45, p. 3071–3087, 2002. 23

ALKIDAS, A.; DURBETAKI, P. Ignition of a gaseous mixture by a heated surface. **Comb. Sci. Tech.**, v. 7, p. 135–140, 1973. 8

ARNOLD, F. A physical model for two-phase flow in steam injection wells. **J. Petroleum Sci. & Eng.**, v. 3, p. 173–183, 1989. 6

ATTIA, H. On the effectiveness of porosity on stagnation point flow with heat transfer over a permeable surface. **J. Porous Media**, v. 10, p. 625–631, 2007. 22

BABADAGLI, T.; AL-BEMANI, A. Investigations on matrix recovery during steam injection into heavy-oil containing carbonate rocks. **J. Petroleum Sci. & Eng.**, v. 58, p. 259–274, 2007. 6

BARRA, A.; ELLZEY, J. Heat recirculation and heat transfer in porous burners. **Comb. Flame**, v. 137, p. 230–241, 2004. 2

BEAR, J. **Dynamics of fluids in porous media**. New York: American Elsevier, 1988. 1-19 p. 1, 21

_____. _____. New York: American Elsevier, 1988. 90-113 p. 13

BERNECKER, R. R.; PRICE, D. Burning to detonation transition in porous beds of a high-energy propellants. **Comb. Flame**, v. 48, p. 219–231, 1982. 3

BRANCH, M. C. In-situ combustion retorting of oil shale. **Prog. Energy Comb. Sci.**, v. 5, p. 193–206, 1979. 3

BRINKMAN, H. A calculation of the viscous force exerted by a flowing fluid in a dense swarm of particles. **Applied Sci. Res. A**, v. 1, p. 27–34, 1947. 22

BUTLER, P.; LEMBECK, M.; KRIER, H. Modeling of shock development and transition to detonation initiated by burning in porous propellant bedsstar, open. **Comb. Flame**, v. 46, p. 75–93, 1982. 3

CASTANIER, L. M.; BRIGHAM, W. E. Upgrading of crude oil via in-situ combustion. **J. Petroleum Sci. & Eng.**, v. 39, p. 125–136, 2003. 5, 6

CHAO, B.; WANG, H.; CHENG, P. Stagnation point flow of a chemically reactive fluid in a catalytic porous bed. **Int. J. Heat Mass Transfer**, v. 39, p. 3003–3019, 1996. 8

DóREA, F.; LEMOS, M. de. Simulation of laminar impinging jet on a porous medium with a thermal non-equilibriumm model. **Int. J. Heat Mass Transfer**, v. 53, p. 5089–5101, 2010. 23

FACHINI, F. An analytical solution for the quasi-steady droplet combustion. **Comb. Flame**, v. 116, p. 302–306, 1999. 14, 15, 79

FACHINI, F. F. Extended schvab-zel'dovich formulation for multicomponent-fuel diffusion flames. **Int. J. of Heat and Mass Transf.**, v. 50, p. 1038–1045, 2007. 14, 15, 17, 79

GOTTFRIED, B. Combustion of crude oil in a porous medium. **Comb. Flame**, v. 12, p. 5–13, 1968. 3

HANAMURA, K.; ECHIGO, R.; ZHDANOK, S. Superadiabatic combustion in a porous-medium. **Int. J. Heat Mass Transfer**, v. 36, p. 3201–3209, 1993. 1, 2

HIEMENZ, K. Die grenzschicht an einem in den gleichförmigen flüessegkeitsstrom engetauchten geraden kreiszylinder. **Dinglers Polytechnisches Journal**, v. 326, p. 321, 1911. 9, 12, 17, 18

HOLMES, M. **Introduction to perturbation methods**. New York: Springer-Verlag, 1995. 47-153 p. 19, 53

HOWELL, J. R.; HALL, M. J.; ELLZEY, J. L. Combustion of hydrocarbons fuels within porous inert media. **Progr. Energy Comb. Sci.**, v. 22, p. 121–145, 1996. 1

JABBOUR, C.; QUINTARD, M.; BERTIN, H.; ROBIN, M. Oil recovery by steam injection: three-phase flow effects. **J. Petroleum Sci. & Eng.**, v. 16, p. 109–130, 1996. 6

JENG, T.; TZENG, S. Numerical study of confined slot jet impinging on porous metallic foam heat sink. **Int. J. Heat Mass Transfer**, v. 48, p. 4685–4694, 2005. 23

JIANG, P.; LU, X. Numerical simulation and theoretical analysis of thermal boundary characteristics of convection heat transfer in porous media. **Int. J. Heat Fluid Flow**, v. 28, p. 1144–1156, 2007. 22

JIANG, P.; REN, Z. Numerical investigation of forced convection heat transfer in porous media using a thermal non-equilibriumm model. **Int. J. Heat Fluid Flow**, v. 22, p. 102–110, 2001. 22

JUGJAI, S.; PONGSAI, C. Liquid fuels-fired porous burner. **Comb. Sci. Tech**, v. 179, p. 1823–1840, 2007. 3

KAVIANY, M.; SINGH, B. Radiative heat transfer in porous media. **Advances in heat transfer**, v. 23, p. 133–186, 1993. 15

KRIER, H.; KEZERLE, J. A. A separated two-phase flow analysis to study deflagration-to-detonation transition (ddt) in granulated propellant. In: **INTERNATIONAL SYMPOSOSIUM ON COMBUSTION, 1979, Pittisburgh**. Pittisburgh: The Combustion Institute, 1979, 1979. 3

KRISHNAMURTHY, L. On gas-phase ignition of diffusion flame in the stagnation-point boundary layer. **Acta Astronautica**, v. 3, p. 935–942, 1976. 8

KUMARAN, V.; TAMIZHARASI, R.; VAJRAVELO, K. Approximate analytic solutions of stagnation point flow in a porous medium. **Commun. Nonlinear Sci Numer. Simulat.**, v. 14, p. 2677–2688, 2009. 22

LEE, D.; VAFAI, K. Analytical characterization and conceptual assessment of solid and fluid temperature differentials in porous media. **Int. J. Heat Mass Transfer**, v. 42, p. 423–435, 1999. 23

LIBBY, P.; WILLIAMS, F. Structure of laminar flamelets in premixed turbulent flames. **Comb. Flame**, v. 44, p. 287–303, 1982. 7

LIÑAN, A. The asymptotic structure of counterflow diffusion flames for large activation energies. **Acta Astronautica**, v. 1, p. 1007–1039, 1974. 7, 105

_____. **El Papel de la mecanica dos fluidos en los processos de combustion**. 1991. Discurso en la Real Academia de Ciencias Exactas, Fisicas e Naturales. 11

LIÑAN, A.; WILLIAMS, F. **Fundamental aspects of combustion**. New York: Oxford University Press, 1993. 111-150 p. 14, 15, 79

LLOYD, S.; WEINBERG, F. A burner for mixtures of very low heat content. **Nature**, v. 251, p. 47–49, 1974. 2

MUJEEBU, M.; ABDULLAH, M.; BAKAR, M. A. Applications of porous media combustion technology - a review. **Applied Energy**, v. 86, p. 1365–1375, 2009. 3

MUJEEBU, M. A.; ABDULLAH, M. Z.; BAKAR, M. Z. A.; MOHAMAD, A. A.; MUHAD, R. M. N.; ABDULLAH, M. K. Combustion in porous media and its applications - a comprehensive survey. **J. of Environ. Manag.**, v. 2, p. 1–26, 2008. 3

MUJEEBU, M. A.; ABDULLAH, M. Z.; BAKAR, M. Z. A.; MOHAMAD, A. A.; ABDULLAH, M. K. A review of investigations on liquid fuel combustion in porous inert media. **Progr. Energy Comb. Sci.**, v. 35, p. 216–230, 2009. 3

NAYFEH, A. **Introduction to Perturbation Techniques**. New York: John Wiley & Sons, 1981. 257-303 p. 19, 53

NIIOKA, T.; WILLIAMS, F. Ignition of a reactive solid in a hot stagnation-point flow. **Comb. Flame**, v. 29, p. 43–54, 1977. 8

OLIVEIRA, A.; KAVIANY, M. Non-equilibrium in the transport of heat and reactants in combustion in porous media. **Prog. Energy Comb. Sci.**, v. 27, p. 523–545, 2001. 3, 21

PEREIRA, F.; OLIVEIRA, A.; FACHINI, F. Asymptotic analysis of stationary adiabatic premixed flames in porous inert media. **Comb. Flame**, v. 156, p. 152–165, 2009. 3, 24, 34

_____. Theoretical analysis of ultra-lean premixed flames in porous inert media. **J. Fluid Mech.**, v. 657, p. 285–307, 2010. 2, 24, 34

PETERS, N. Laminar diffusion flamelet models in non-premixed turbulent combustion. **Prog. Energy Comb. Sci.**, v. 10, p. 319–339, 1984. 7

POINSOT, T.; VEYNANTE, D. **Theoretical and Numerical Combustion**. Philadelphia, PA: R.T. Edwards Inc., 2005. 125-168 p. 7

PRATS, M. Effect of steam injection into two nearby layers. **J. Petroleum Sci. & Eng.**, v. 39, p. 117–124, 2003. 6

SARATHI, P. S. **In-situ combustion handbook - principles and practices**. Tulsa, Oklahoma:, 1998. 3

SCHLICHTING, H. **Boundary-layer theory**. New York: McGraw-Hill, 1968. 81-86 p. 17

SHARMA, O.; SIRIGNANO, W. Ignition of stagnation point flow by a hot body. **Comb. Sci. Tech**, v. 1, p. 95–104, 1969. 8

SIDDIQUI, A.; ZEB, A.; GHORI, Q. Some exact solutions of 2d steady flow of an incompressible viscous fluid through a porous medium. **J. Porous Media**, v. 9, p. 491–502, 2006. 22

SIEGEL, R.; HOWELL, J. **Thermal radiation heat transfer**. Washington, D.C.: Taylor and Francis, 1992. 15

TAKENO, T.; SATO, K. An excess enthalpy flame theory. **Comb. Sci. Tech.**, v. 20, p. 73–84, 1979. 1

TELENGATOR, A. M.; MARGOLIS, S. B.; WILLIAMS, F. A. Stability of quasi-steady deflagrations in confined porous energetic materials. **Comb. Sci. Tech**, v. 160, p. 259–315, 2000. 3

TELENGATOR, A. M.; WILLIAMS, F.; MARGOLIS, S. B. Finite-rate interphase heat-transfer on multiphase burning in confined porous propellants. **Comb. Sci. Tech.**, v. 178, p. 1685–1720, 2006. 3

TIERNEY, C.; WOOD, S.; HARRIS, A. T.; FLETCHER, D. F. Computational fluid dynamics modelling of ultra-lean porous burners. **Prog. Comp. Fluid Dyn.**, v. 10, p. 352–365, 2010. 2

VAFAI, K. **Handbook of porous media**. Boca Raton, FL: CRC Press, 2005. 607-645 p. 1, 2

VAFAI, K.; TIEN, C. Boundary and inertia effects on flow and heat transfer in porous media. **Int. J. Heat Mass Transfer**, v. 24, p. 195–203, 1981. 14

VEYNANTE, D.; VERVISCH, L. Turbulent combustion modelling. **Prog. Energy Comb. Sci.**, v. 28, p. 193–266, 2002. 7

WU, C.; FULTON, P. Experimental simulation of the zones preceding the combustion front of an in-situ combustion process. **SPE Journal**, v. 11, p. 38–46, 1971. 4

WU, Q.; WIENBAUM, S.; ANDREOPOULOS, Y. Stagnation-point flows in a porous medium. **Chemical Engineering Science**, v. 60, p. 123–134, 2005. 22

YUCEL, N.; GUVEN, R. Forced-convection cooling enhancement of heated elements in parallel-plate channels using porous inserts. **Numer. Heat Transfer Part A - Appl.**, v. 51, p. 293–312, 2007. 23

ZHDANOK, S.; KENNEDY, L. A.; KOESTER, G. Superadiabatic combustion of methane-air mixtures under filtration in a packed bed. **Comb. Flame**, v. 100, p. 221–231, 1995. 3

APPENDIX A - THERMAL SOLUTIONS IN THE INNER ZONE FOR THE HIEMENZ FLOW

In this Appendix, the thermal solutions in the inner zone for the gas phase are obtained. The simplified form of Equation (3.41) is treated and justified in this Appendix.

For the thermal solution of the gas phase in the inner zone in the Hiemenz flow problem presented in Chapter (3), the following set of governing equations must be solved:

$$\varepsilon\theta''_{g(1)} = -n_v\left(\theta_{s(1)} - \theta_{g(1)}\right), \tag{A.1}$$

$$\varepsilon\theta''_{g(2)} + \varepsilon\tilde{f}_{i(0)}\theta'_{g(1)} = -n_v\left(\theta_{s(2)} - \theta_{g(2)}\right). \tag{A.2}$$

$$(1-\varepsilon)\theta''_{s(1)} = 0, \tag{A.3}$$

$$(1-\varepsilon)\theta''_{s(2)} = n_v\left(\theta_{s(1)} - \theta_{g(1)}\right) \tag{A.4}$$

The leading order terms are constant at θ_0.

The boundary conditions depends on wether one consider the case of a prescribed wall temperature, or the case of a prescribed wall heat flux. The simplification made in the gas phase energy equations are the same in both cases, and hence, for purpose of exemplification, the constant wall temperature case will be considered. Then, the utilized boundary conditions are given by:

$$\theta_{g(1)} = \theta_{s(1)} = \theta_{g(2)} = \theta_{s(2)} = 0 \tag{A.5}$$

And the matching condition with the outer zone imposes that:

$$\left.\frac{d\theta_{g(1)}}{d\tilde{\eta}}\right|_{+\infty} = \left.\frac{d\theta_{s(1)}}{d\tilde{\eta}}\right|_{+\infty} = \left.\frac{d\theta_{(0)}}{d\eta}\right|_{0} = -\Theta\sqrt{\frac{2}{\pi\gamma}},$$

$$\left.\frac{d\theta_{g(2)}}{d\tilde{\eta}}\right|_{+\infty} = \left.\frac{d\theta_{s(2)}}{d\tilde{\eta}}\right|_{+\infty} = \left.\frac{d\theta_{(1)}}{d\eta}\right|_{0} = \frac{\Theta}{2\gamma}\sqrt{\frac{2}{\pi\gamma}}\left(1 + \frac{1-\varepsilon Pr}{\varepsilon\beta Pr}\gamma\right) \tag{A.6}$$

The solutions of Equations (A.3) and (A.4) with the boundary and matching conditions given by Equations (A.5) and (A.6) provide the solid phase temperature in

the inner zone:

$$\theta_s(\tilde{\eta}) = \theta_0 - \Gamma^{-1}\Theta\sqrt{\frac{2}{\pi\gamma}}\tilde{\eta} + \Gamma^{-2}\frac{\Theta}{2\gamma}\sqrt{\frac{2}{\pi\gamma}}\left(1 + \frac{1-\varepsilon Pr}{\varepsilon\beta Pr}\gamma\right)\tilde{\eta} + O\left(\Gamma^{-3}\right) \tag{A.7}$$

This result is used in Equations (A.1) and (A.2). The solution of Equation (A.1) with the boundary and matching conditions given by Equations (A.5) and (A.6) is straightforward and gives:

$$\theta_{g(1)}(\tilde{\eta}) = -\Gamma^{-1}\Theta\sqrt{\frac{2}{\pi\gamma}}\tilde{\eta} \tag{A.8}$$

Equation (A.2) can be expressed as:

$$\theta''_{g(2)} - \left(\frac{n_v}{\varepsilon}\right)\theta_{g(2)} = -\left(\frac{n_v}{\varepsilon}\right)\theta_{s(2)} - \tilde{f}_{i(0)}\theta'_{g(1)}. \tag{A.9}$$

Evaluating the right-side terms, the following equation is obtained:

$$\theta''_{g(2)} - A\theta_{g(2)} - \frac{B}{C}\left(e^{-C\tilde{\eta}} - 1\right) + B\left(A\ D - 1\right)\tilde{\eta} = 0 \tag{A.10}$$

in which it was defined:

$$A = \frac{n_v}{\varepsilon}, \quad B = \Theta\sqrt{\frac{2}{\pi\gamma}}, \quad C = \sqrt{\varepsilon\beta}, \quad D = \frac{1}{2\gamma}\left(1 + \frac{1-\varepsilon Pr}{\varepsilon\beta Pr}\gamma\right) \tag{A.11}$$

The general solution of Equation (A.10) is given by:

$$\theta_{g(2)}(\tilde{\eta}) = C_1\, exp\left(-\sqrt{A}\tilde{\eta}\right) + C_2\, exp\left(\sqrt{A}\tilde{\eta}\right) + \frac{B}{AC} - \frac{B}{A}\left(1 - AD\right)\tilde{\eta} + \frac{B}{C(C^2 - A)}exp\left(-C\tilde{\eta}\right). \tag{A.12}$$

The boundary and matching conditions for this solution are given by:

$$\theta_{g(2)} = 0, \quad \left.\frac{d\theta_{g(2)}}{d\tilde{\eta}}\right|_{+\infty} = \frac{\Theta}{2\gamma}\sqrt{\frac{2}{\pi\gamma}}\left(1 + \frac{1-\varepsilon Pr}{\varepsilon\beta Pr}\gamma\right) = -\frac{B}{A}(1 - AD) \tag{A.13}$$

The solution given in Equation (A.12) does not obey the matching condition with the outer zone. However, if it is considered that $AD \gg 1$, then, Equation (A.10)

may be written as:

$$\theta''_{g(2)} - A\theta_{g(2)} - \frac{B}{C}\left(e^{-C\tilde{\eta}} - 1\right) + BAD\tilde{\eta} = 0. \tag{A.14}$$

And the general solution of the above equation is given by:

$$\theta_{g(2)} = C_1\ exp\left(-\sqrt{A}\tilde{\eta}\right) + C_2\ exp\left(\sqrt{A}\tilde{\eta}\right) + \frac{B}{AC} + BD\tilde{\eta} + \frac{B}{C(C^2 - A)} exp\left(-C\tilde{\eta}\right). \tag{A.15}$$

And this solution obeys the matching condition promptly.

From the consideration that $AD \gg 1$, utilizing the definitions presented in Equations (A.11), it is obtained that this approximation is valid when the following inequality is obeyed:

$$\frac{n_v}{2\beta Pr}\left(\frac{\beta Pr}{(1-\varepsilon)} + \frac{1}{\varepsilon^2} - \frac{Pr}{\varepsilon}\right) \gg 1 \tag{A.16}$$

This inequality is valid when $\varepsilon \to 0$ or $\varepsilon \to 1$. However, one of the assumptions made in order to construct the model was that the medium was considered of low-porosity ($1/\varepsilon^2 \gg 1$), such that the above inequality must be respected from the beginning.

It is important to note that the term $n_v/(2\beta Pr)$ is of unitary order and when the approximation $\varepsilon \to 0$ is performed, the term $1/\varepsilon^2$ goes faster to infinity than the term Pr/ε, hence, avoiding the expression to be negative-valued.